Combinatorial Cu_xNi_{1-x} alloy thin film catalysts for layer number regulation in CVD grown graphene

A Thesis Presented for the
Master of Science
Degree
The University of Tennessee, Knoxville

Sumeer Khanna
May 2022

Copyright © 2022 by Sumeer Khanna
All rights reserved.

ACKNOWLEDGEMENTS

It is my great pleasure to thank firstly my adviser, Prof. Philip Rack for his constant support and guidance on planning and running the experiments on synthesizing thin film growth of gradient Cu_xNi_{1-x} alloy by RF magnetron sputtering process at the Institute of Advanced Materials and Manufacturing (IAMM) at the University of Tennessee, Knoxville. Additionally, I take this opportunity to extend my gratitude to project collaborator, Dr. Michael Stanford at General Graphene Corporation for his kind assistance with growth of bi-layer graphene by thermal chemical vapor deposition (CVD) process and it's subsequent characterization by optical imaging and Raman spectroscopy techniques for designing a unique process recipe. I appreciate their kind support when access to experimental tools at the Center for Nanophase Materials Science (CNMS), U.S. Department of Energy (DoE), Oak Ridge National Laboratory had been shut down during this Covid-19 coronavirus pandemic shutdown. Furthermore, I'm thankful to Dr. Ivan Vlassiouk at General Graphene for fruitful research discussions on CVD graphene growth and regulation of their layer numbers.

My best gratitude to IAMM at the University of Tennessee, Knoxville for providing access to useful lab facilities such as the RF magnetron sputtering unit for growth of Cu_xNi_{1-x} thin film alloy catalysts on Si/SiO_2 substrates and characterization of CuNi alloy compositions (at.%), analyzing the crystalline lattice structure for obtaining arrangement of atoms in the solid-solution of CuNi alloy, imaging the topographical features by accessing the energy dispersive x-ray spectroscopy (EDS), grazing incidence x-ray diffractometry (GI-XRD) and scanning electron microscopes of EVO and Auriga.

Last but not least, I express my best thanks and support to my parents for their constant support in this perseverance and keeping me motivated for pursuing graduate education during the Covid-19 pandemic.

ABSTRACT

In this work, synthesis of combinatorial library of Cu_xNi_{1-x} (copper nickel) alloy thin films via co-sputtering from Cu (copper) and Ni (nickel) targets as catalysts for chemical vapor deposition (CVD) growth of graphene is reported. The gradient alloy morphology, composition and microstructure were characterized via scanning electron microscopy (SEM), energy dispersive x-ray spectroscopy (EDS), and x-ray diffraction (XRD), respectively. Subsequently, the Cu_xNi_{1-x} alloy thin films were used to grow graphene in a CH_4-Ar-H_2 (methane-argon-hydrogen) ambient in thermal CVD tube furnace. The underlying rationale is to adjust the Cu_xNi_{1-x} alloy carbon solubility at a fixed temperature (~1000 ^oC) to control the graphene layer number as the solubility limit of carbon in Cu is approximately 75 +/- 0.5 ppm and C in Ni is 1.3 at.%.

The energy dispersive x-ray spectroscopy (EDS) analysis revealed that a continuous gradient of Cu_xNi_{1-x} ($25.29\%<x<82.57\%$) was achieved across the 100 mm diameter substrate (~0.86%/mm composition gradient) for a film thickness of ~2 µm. High-resolution SEM imaging revealed the as-deposited grain size enlarged with increasing x and the grain shapes changed from disordered nodular structures to uniform spheres. The XRD spectra confirmed a solid solution was realized and the face centered cubic lattice constant varied from ~3.52 to 3.58 Å, consistent with the measured composition gradient, assuming a Vegard's relationship. Optical microscopy and Raman analysis of the graphene layers suggest single layer growth occurs with $x>68.95\%$, bilayer growth dominates from $47.56\%<x<68.95\%$, and multilayer ($>=3$) growth occurs for $x<47.56\%$. Thus, we have overviewed the Raman analysis of the CVD grown graphene layers.

Finally, we show large area bi-layer graphene can be grown via the thin film catalyst with optimized catalyst composition.

TABLE OF CONTENTS

LIST OF TABLES

LIST OF FIGURES

CHAPTER ONE

INTRODUCTION AND LITERATURE REVIEW

1.1 Introduction to graphene and it's synthesis

Graphene is a distinctive material comprising of few graphitic layer sp^2 covalently bonded 2D carbon allotropes known for its excellent properties of transport (electrical and thermal energy), carrier mobility, high charge carrier density, mechanical robustness and optical behavior. It has found wide applications as electronic and photonic materials [1, 2]. A single layer of graphite forms the fundamental unit of most carbon nanostructures in a hexagonal "honeycomb" lattice. In a 3-dimensional crystal structure of bulk graphite, the layers are held together by van der Waals force along out of plane axis and covalent bonded in hexagonal form for in-plane lattice atoms [1-7].

The varying arrangements of single layer of graphite into various structures can be classified based on their 0-D, 1-D and 2-D types, which are referred in the literature as fullerene (sphere), carbon nanotube (graphitic-layer turned up with respect to its central axis) and graphene (stack of few layers). If the number of graphene layers are in-between 5 to 10, the stack is described as "few-layer" graphene and for layers less than 30 but greater than 20, the stack is termed as multi-layer graphene (nanocrystalline) (Figs. 1.1, 1.2) [1-7].

At the junctions of Brillouin zone, the π and π^* bands converge to a singular position in the Fermi level (E_f), which contribute to the partial-metallic property of very crystalline graphene [8]. Under the application of perpendicular magnetic field to basal plane of graphene, quantization (Landau-level) of energy is observed. This property along with similarity to Dirac spectrum of massless fermions makes graphene a very special material for exploration to the scientists [1, 2]. The meeting of parabolic bands at K and K' points of Brillouin zone in bilayer graphene along with very small band overlap (~0.0016 eV) at greater energies makes it a special semiconducting material [9]. The properties of graphene can be regulated as per the number of graphitic layers. For example, ~97% optical transmission with ~2.2 kΩ/sq. layer resistance has been reported for graphene with single layer. As the no. of layers enlarge, the transmission and sheet resistance has been found to diminish. Accordingly, a transmission value of ~95%, ~92% and ~89% and sheet resistance of 1 kΩ/sq., ~700 kΩ/sq., and 400 kΩ/sq. respectively has been reported for bilayer, tri-layer and 4-layer graphene structures [10]. Graphene is a perfect material for field-effect transistors (FETs) because of their charge carrier mobility of ~15,000 cm^2/Vs and resistivity of ~10^{-6} ohm-cm [7]. Thus, they find good usage in sensors, integrated circuits, electrode material, channel in FET, light emitting diodes, sensors on touch/liquid crystal displays technology because it's optically visible and has

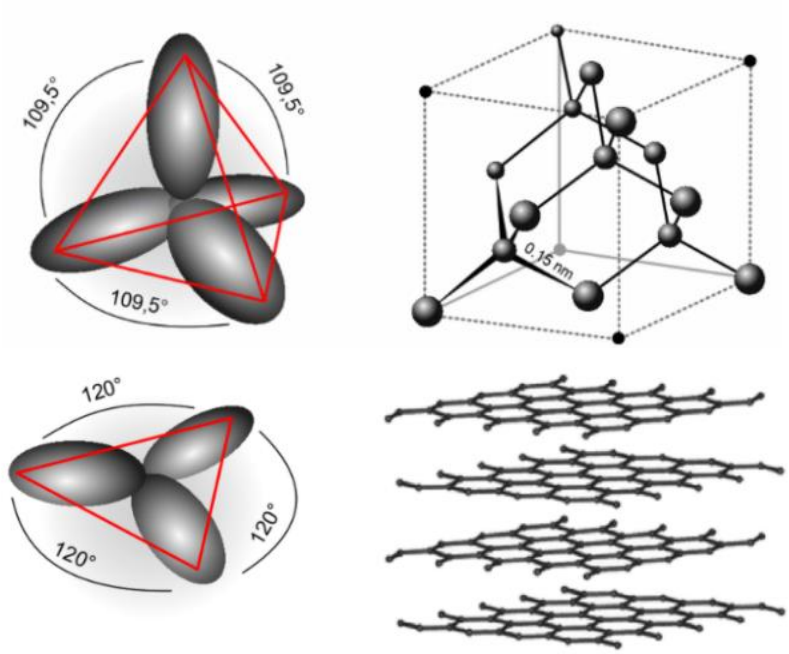

Fig. 1.1 (a) Diamond crystal lattice-sp^3 hybridized (b) Graphite-sp^2 hybridized [1, 2]

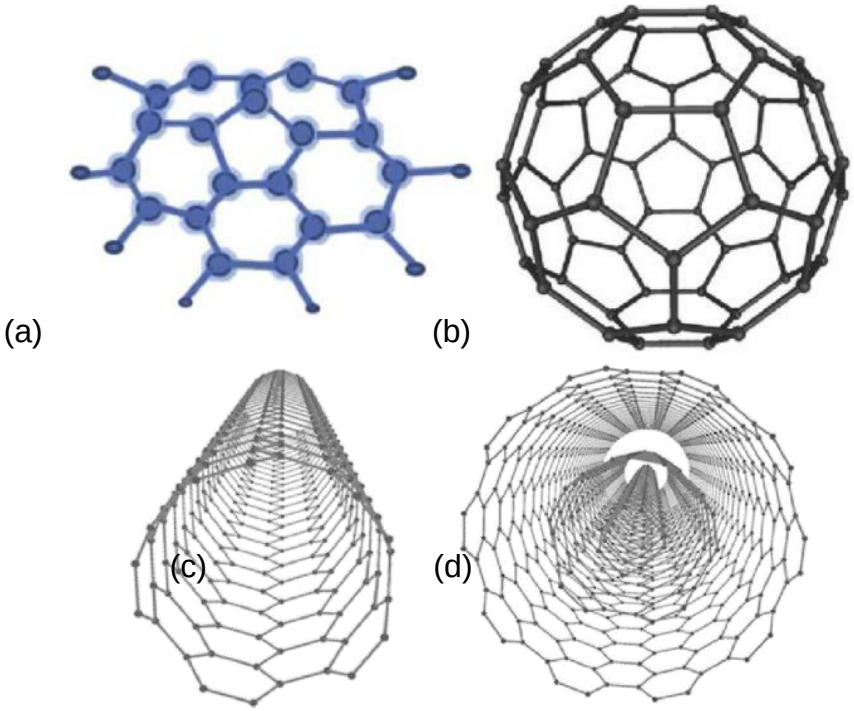

Fig. 1.2 (a) Corannulene structure (b) Buckminsterfullerene C_{60} (c) Single-walled carbon nanotube (SWCNTs) (d) Multiwalled carbon nanotube (MWCNTs) [1, 2]

good electrical conductivity [1, 2]. To make the aforesaid properties available for use, synthesis of mono layer of graphene on a matching substrate material would help in tailoring an effective bandgap for the semiconducting device [7]. Chemical vapor deposition (CVD), surface graphitization (thermal) on SiC, reduction of graphite oxide, breaking bulk graphite crystal into mono- and few-layers are some common methods for growth of graphene layers. Synthesis of large single-crystalline domains and continuous films of electronic-grade graphene prepared by CVD has evolved as an emergent technique [1-7, 11].

CVD growth of graphene can be regulated by employing transition metal catalysts because they provide advantages such as lower stimulation energy for separation of the precursor, graphene nucleation, evolution of the domains and their amalgamation. As conditions necessary for suitable graphene synthesis are widely varying and due to lack of comprehensive knowledge about this process, the selection of appropriate catalyst is difficult. The underlying fundamental principles (assumptions) relating to graphene CVD process are relatively easy to understand although the method for graphene growth appears to be complicated and comprising of use of varying types of catalysts, carbonaceous precursors, and other variables [1-7]. The underlying growth mechanism for CVD graphene can be expected to include dehydrogenation reaction of gaseous source of carbon precursor (CH_4), diffusion of molecules (substrate), dissolution in Cu_xNi_{1-x} alloy solid solution and precipitation of carbon atoms (supersaturation) at defect locations such as grain boundaries on surface (equilibrium graphene growth) upon cooling due to reduced solubility at low temperatures [12].

1.2 Copper (Cu) catalyst

Graphene has become a useful material for research exploration in electronics and spintronics due to its exceptional properties [5-7, 13, 14]. By employing Cu foil, CVD growth of graphene in reduced pressure conditions can be observed to provide with uniform monolayers. The methods for accurately regulating the number of graphene layers [15-17], structural order, boundary shape and identical three-dimensional alignment is necessary. For the synthesis of high-level and good-quality graphene layers, CVD has proven to be an effective method, which is a straightforward process even though it incorporates catalysts of varying types, resources for carbon, and other parameters.

Based on solubility carbon (C) atoms in catalyst material, there are two chemical reactions favored during the growth process. If the solubility is low, for example, C dissolution in C, then surface catalytic reactions [19, 20] are favored. However, for metals such as Ni, which show higher solubility of C, precipitation of C atoms from the bulk on surface during cooling [21, 22] process is favored. The temperature of growth for graphene layers by grain segregation from liquid solution of Cu and C upon cooling is based on Cu-C phase diagram (Fig. 1.3) [18]. By adjusting the growth ratio of graphene, hexagonal graphene flakes

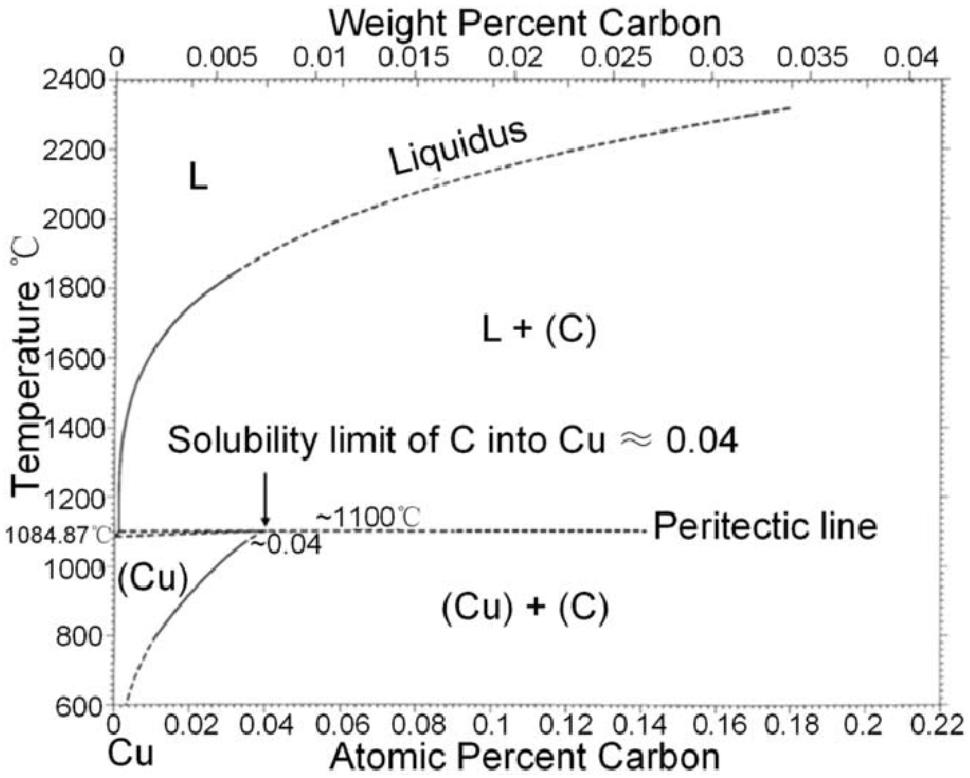

Fig. 1.3 Cu-C phase diagram [18]

(HGFs) of single-crystalline type can be developed with meandering boundaries at normal environmental pressure. The fundamental unit of continuous graphene films is HGF. The gas flow ratio of Ar to H_2 is an important variable which strongly contributes to the regulation of thickness of graphene (number of layers) [5]. Transformation from mixed single/multilayer to single layer based HGFs can be performed by enhancing this ratio [5].

One of the essential steps of the CVD process is surface and bulk catalytic reactions during the cooling process, which involves the nucleation of graphene on a catalyst surface and is further dependent upon parameters such as kind or surface microstructure of catalyst [23, 24], supply of carbon [25], precipitation of carbon from liquid metal-carbon solution [26], record of synthesis, and process variables in CVD synthesis [27-30]. One of the challenges typically observed during synthesis of graphene by CVD process is enhanced dispersion (scattering) of the nucleus (concentration) of Cu & Ni grains from their substrates and subsequent size distribution of graphene domains resulting from this inconsistent nucleation concentration of Cu and Ni grains. Convenient method for producing coherent single-layer graphene films includes low-pressure CVD synthesis of graphene on Cu foil [20].

As per recent report in literature [5], edges of grains oriented in different crystallographic directions of both high-angle and low-angle characteristics severely deteriorate the transport properties (electron, heat) of thin graphene films [31-37]. These boundaries arise by amalgamating small islands of graphene which are randomly oriented and have haphazard shapes leading to creation of bigger islands which are found to be comprising of pentagonal and heptagonal geometries [31-37]. The edges of anisotropic crystal lattice consisting of grains oriented in varying directions are typically points of high thermodynamic energy (surface), which provide impetus to nucleation and growth of HGFs at these highly dynamic locations (non-uniformly dispersed). HGF of dimensions to order of 1-10 µm along oblique path can be ascribed to elevated concentration of graphene source sites and the reduced speed of development of HGFs. Homogeneous, monolayer, self-assembled HGFs (single region) with enhanced dimensions can be obtained by regulation of nucleation method in graphene CVD systems typically achieved by employing liquid Cu as the solution would be identical (no grain boundary) as observed in solid Cu [5]. For example, HGFs with uniform distribution developed on base substrate made of quartz and W with liquid Cu spheres can be demonstrated by aid of scanning electron microscopy (SEM) (Fig. 1.4).

A sizeable intensity ratio I_{2D}/I_G of approximately 2.5-4, full width half maximum (FWHM) of 35-40 cm^{-1} and symmetric 2d peaks positioned at 2698 cm^{-1} from Raman spectroscopy analysis demonstrates features of monolayer graphene type [5]. Furthermore, as per SEM analysis, the latter characteristic property is coherent with the findings from Raman analysis. Predominantly, production of

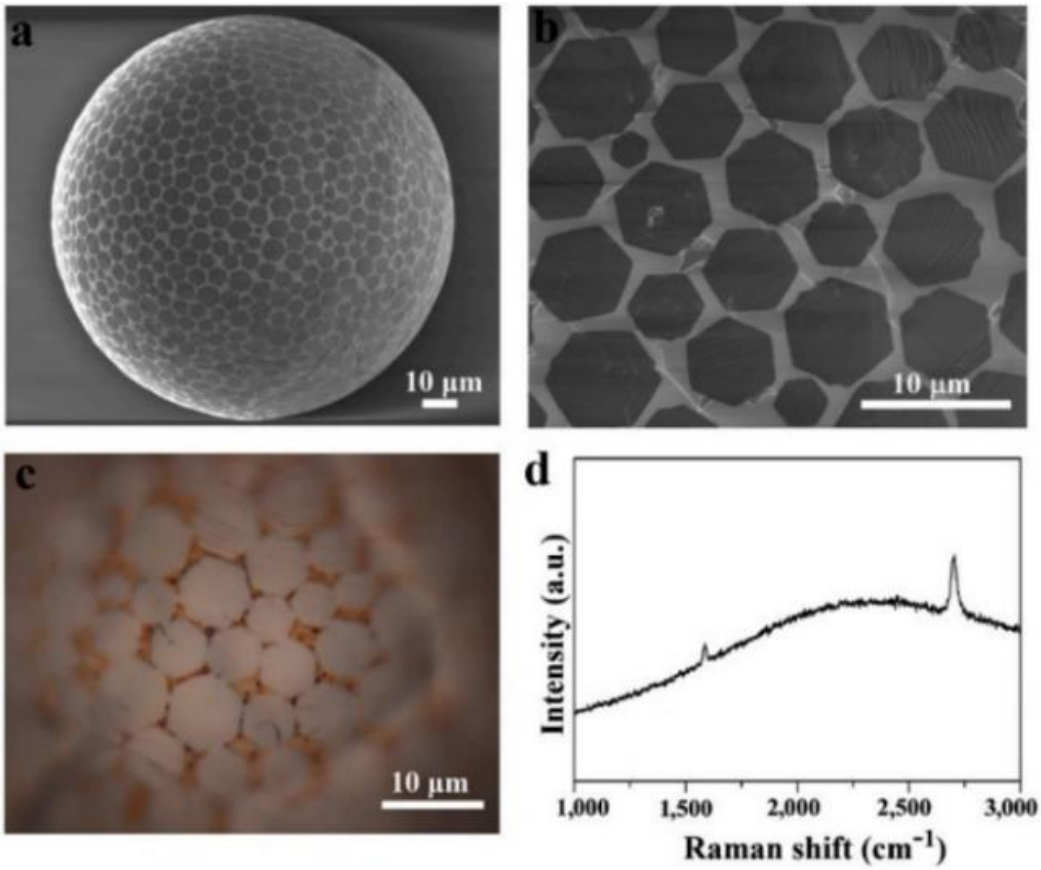

Fig. 1.4 HGFs developed on Cu spheres/quartz substrate (a) uniformly arranged, self-ordered HGFs grown on top of Cu balls at 1080 °C at 10 sccm CH_4/300 sccm H_2 in 20 mins. as illustrated by SEM image, (b) enlarged SEM image respectively, (c) demonstration of HGFs of single-layer on Cu spheres, (d) Raman spectra showing HGFs of single-layer type [5]

monolayer graphene domains is reported [5] with very small no. of bilayer and trilayer regions.

Structures with good spread of HGFs obtained on spherical surface of Cu is reported [5]. An observation of the energetic variations in the concentration and dimension of HGFs on Cu spheres was performed during this study. An evenly distributed layout of the HGFs on Cu spheres was obtained with a typical dimension of HGFs detected as roughly 5 μm and as the time-period for development of graphene was enlarged, the mean gap between HGFs was detected to be diminishing. As demonstrated (Fig. 1.4), the nucleation and mechanism of growth of HGFs on liquid Cu as reported in this study are coherent with the case for growing graphene on solid Cu [5]. Growth of HGFs on Cu spheres is consistent with latter [5].

As demonstrated, HGFs not completely encompassing the surface had no properly defined arrangement link amongst them, and generally, they were found to be nicely distributed [5]. A structure arranged with crystals oriented in varying directions is demonstrated as HGFs concentration on the external Cu surface improved. Thus, HGFs became more self-supported with their orderly arrangement. Additionally, grain boundaries with low-angles were produced due to the edge-to-edge alignment of neighboring HGFs. When the HGFs had an analogous extent, an ideal arrangement of 2D lattice formations of HGFs was demonstrated (Fig. 1.5). An orderly orientation of HGFs can be ascribed to the decrease in total surface/edge energy of HGFs, and the self-alignment of well-arranged constructs of HGFs resulted from the transformation or revolution of HGFs on the exterior of Cu in fluid-state [5]. The continued nucleation and synthesis of HGFs in CVD system leads to development of highly segregated HGFs to closely filled formations and ultimately to constant thin film. As the growth time was significantly increased (40 minutes), uniform monolayer graphene films were obtained, and 1-4 hours produced even better & consistent monolayer films.

Graphene films coherent in nature with large regions resulting from a growth time of about 2 hours are illustrated by the SEM examination [5]. Vanishing of the orderly arrangement and boundaries of HGFs occurred for such films, and the films emerged to be similar to those developed at low pressure. Monolayer nature of graphene films was concluded from the Raman spectroscopy analysis performed at various locations on the film surface. This was matching with the analysis from optical and SEM examinations [4, 5].

The nucleation concentration and growth rate defined the typical size of individual HGFs [4, 5]. A normal size of HGF ~20-30 μm is demonstrated. Additionally, as the temperature of synthesis is enhanced, mean dimensions of HGFs improved to roughly 50 μm, and size of about 120 μm is obtained when the CH_4 flow rates were decreased. Thus, reduced sites of carbon precipitation

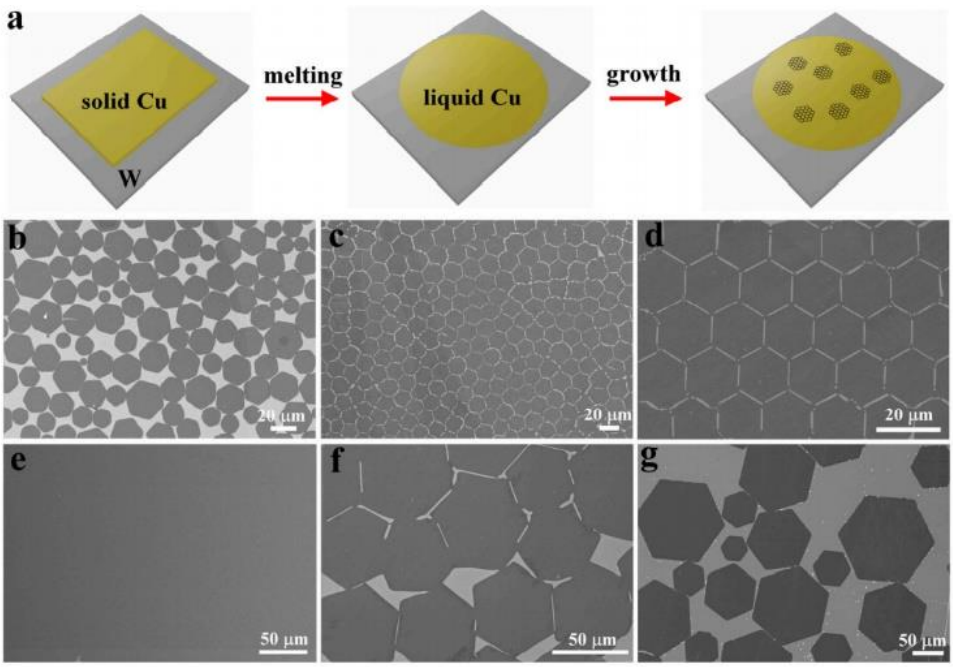

Fig. 1.5 HGFs growth on W substrates with Cu film, liquid state (a) CVD growth process for development of HGFs on exterior of fluidic Cu, (b) incompletely coated and uniformly-distributed HGFs by employing 6 sccm H_2 at 1120 °C for 30 mins shown by SEM image, (c) HGFs and Cu surface represented by the dark and bright regions as densely packed in the SEM image, (d) Equal-sized HGFs showing near-perfect 2d lattice in SEM image, (e) Coherent graphene film grown under 2 hours process time with even contrast, (f & g) analysis of average dimensions of HGFs (bigger in size) show measurements as 50 μm at 1140 °C and 120 μm at 1160 °C [5]

and growth of HGFs in liquid Cu CVD can be ascribed to this greater size [4, 5]. The mean rate of development of HGFs on solid Cu surface is analyzed to be as 0.1-0.2 μm/min is reported to be comparatively much less to that of calculated production rate of 10-50 μm/min for the synthesis of HGFs on relatively horizontal Cu/W surface.

Furthermore, this has significance in providing an efficient method by using liquid Cu surface for synthesis of graphene without any loss of its peculiar structure, and thus, leading to the conclusion that macro-sized HGFs can be obtained [4, 5]. The slower growth rate would not yield such structures. The synthesis of HGFs on liquid and solid Cu surfaces have significant divergences. A blend of several and mono- layered HGFs, reduced dimensions, heterogeneous distribution of atoms across lattice (arbitrary arrangement) is seen for graphene growth on solid Cu surfaces. Whereas the graphene growth on liquid Cu surface produces HGFs with greater dimensions, mono-layer features, uniform arrangement of atoms, and a transparent (consistent distribution) connection amongst varying HGFs [4, 5]. Additionally, the surface characteristics of solid and liquid Cu linked well with these aforesaid respective variations in structural arrangements. Greater size (reduced nucleation concentration) with consistent nucleation on the surface stemming from graphene growth on liquid Cu surface can be related to removal of grain boundary effect as related to growth on solid Cu. Uniformly structured HGFs is shown by the evenly distributed development of C atoms precipitated on surface in form of crystallites of HGF with boundaries along varying crystallographic orientations. However, the solid Cu matrix having varying properties along different crystallographic directions led to development of HGFs which is typically uniformly arranged instead of domains with similar angles [4, 5].

The bigger size of HGFs is ascribed to the rapid evolution of HGFs resulting from larger C atom dispersion rate offered by liquid Cu surface [4, 5]. Additionally, a dense well-arranged structure is obtained from the self-assembly of drifting HGFs on liquid Cu surface. However, for solid Cu surfaces, such arrangement of HGFs is challenging due to the shaky nature of the configuration produced from layer-by-layer growth. Substantial quantities of multilayer HGFs resulting from analogous experimental environments for synthesizing HGFs on solid Cu is demonstrated by SEM analysis as a central dark region. The growth of single-layer HGFs is outstanding. Furthermore, it is contemplated that the eradication of nucleation vacancies avoiding the development of a second layer on same nucleus occurs due high-level movement of Cu atoms in the liquid state. The effect of liquid Cu phase is demonstrated by further analysis [4, 5].

Raman spectroscopy measurements and analysis of the arrangement of atoms across varying crystallographic directions were accomplished by employing poly methyl methacrylate (PMMA) or polysulfone (PSF) for shifting HGFs onto 300 nm SiO_2/Si substrate and chips for analysis by the transmission electron microscopy

(TEM) (Fig. 1.6). Mono-layer nature of the HGFs was demonstrated by the curve-form and its peak location, and fraction of Raman strength of 2D and G crests. SAED images were taken at varying locations of twelve different HGFs of varying size showing single-crystalline nature by six-fold symmetric order of diffraction spots. Diffraction experiments show HGFs with single crystalline behavior and results from electrical characterization (current, I-voltage vs V curves) reveal straight I-V curves (Fig. 1.7).

The development of carbon atoms precipitated on catalyst surface into graphene grains in thermal CVD systems can be regulated by employing liquid Cu, and additionally, it provides constant monolayer films of HGFs which demonstrate similar one-layer, self-assembling, greater dimensions, and distinct islands. Layers with thickness to the order of two and three planes of graphene atoms stacked together were produced comparatively less than that of single plane of graphene atoms [2].

1.3 Nickel (Ni) catalyst

A tunable surface growth reaction (constraining nature) of graphene occurs due to the reduced solubility of carbon in copper lattice [21, 38]. However, carbon re-separation and development of multi-layer graphene upon reducing temperature [39, 40] can occur for materials containing Ni, where C can disperse in the bulk around ~900 °C, as shown by the Ni-C phase diagram (Fig. 1.8) [26]. The evolution of graphene on Cu appears at temperature close to its melting temperature, which leads to direct conversion from solid to gaseous state and coarsening of the surface during the synthesis [41]. The development of numerous areas of graphene with varying directions [42, 43] of crystal growth and distorted domain borders is attributed to the shaky interface amongst graphene and copper, which is inevitable on single crystalline copper substrates.

If the development of multilayer graphene can be precluded by using Ni as a substrate material, then latter would be beneficial for usage over Cu as a catalyst material. Additionally, Ni (111) [26, 38, 39, 44] is known as a metal for its better interface and lattice matching with the graphene [22, 43]. Graphene developed on single crystalline Ni is known to possess single crystalline graphene-domains [26, 46, 47].

Due to merging of graphene domains into a film, there is no existence of tilt-grain boundaries. Large islands of graphene (~10x μm^2) can be developed efficiently by synthesis mechanism occurring on surface at comparatively diminished temperatures of growth (~550 °C), which was reported from the imaging of Low Energy Electron Microscope (LEEM). Consequently, self-ending monolayer can be developed for Cu. By employing ethylene (C_2H_4) as input source of carbon molecules at pressure of 10^{-6} T, synthesis of graphene layers under “ultrahigh vacuum” (UHV) ‘chemical vapor deposition’ (CVD) can be obtained. Auger

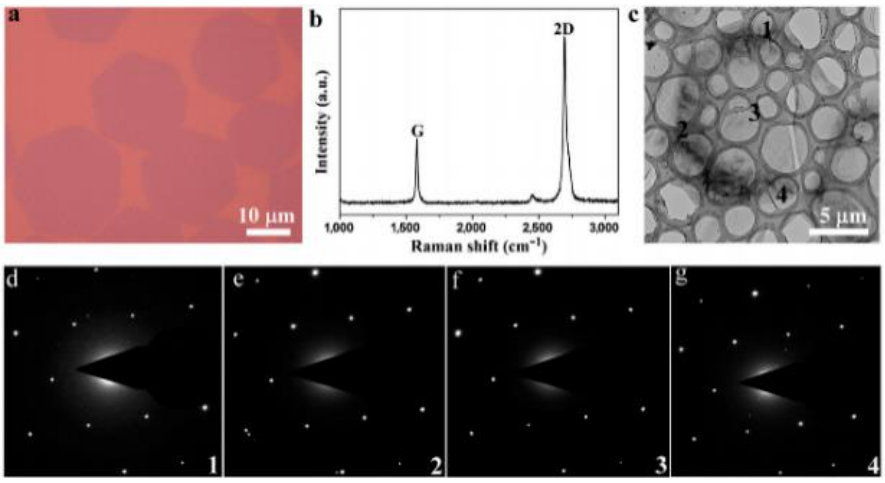

Fig. 1.6 Raman and TEM characterizations, (a) HGFs transferred onto 300 nm shown by optical image, (b) mono-layer HGFs demonstrated by non-appearance of D-band in Raman spectroscopy measurements, (c) different HGFs shown by TEM image at minimal magnification, (d-g) Sixfold symmetry diffraction points demonstrating single crystalline nature as selected area electron diffraction patterns taken at miniature domains marked as 1-4 [5]

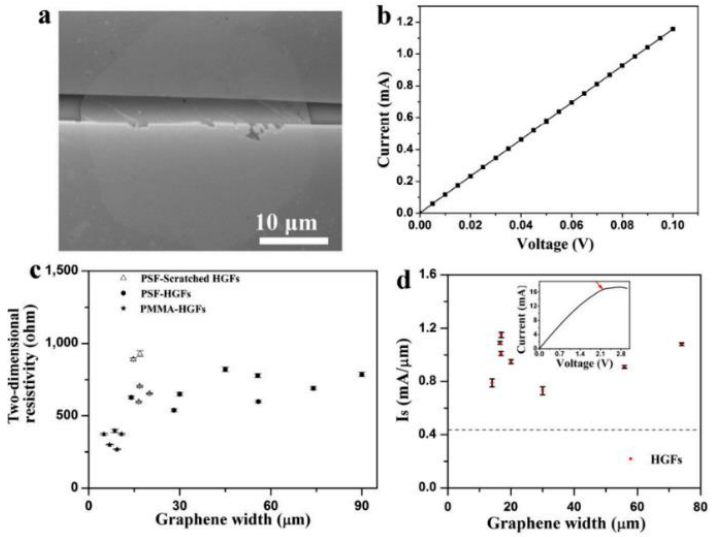

Fig. 1.7 HGFs electrical characterization, (a) SEM image showing 30 nm upper and base electrodes representing device with two stations for specific HGFs, (b) measurement of electrical properties of resistance and resistivity of the device as 87 Ω and 650 Ω-m respectively, (c) HGFs 2D resistivity vs. graphene thickness for several devices, (d) saturation current density (I_S) vs HGF width graph for several devices, I-V curve shown in the inset [5]

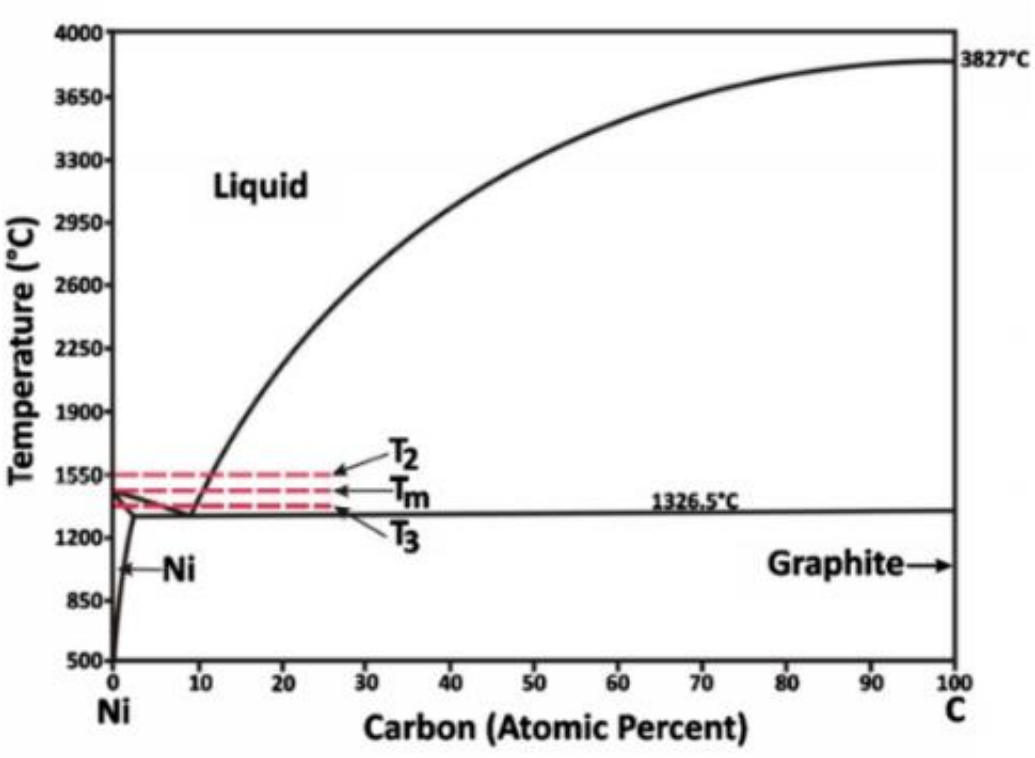

Fig. 1.8 Ni-C phase diagram [26]

electron spectroscopy (AES) was applied for observing the development of graphene films on Ni (111) with help of a mirror analyzer in tubular shape with double pass filters in two distinct UHV systems [26, 38, 39].

The thermal strength of single layers of graphene on Ni (111) was measured from LEEM analysis. A failure of findings with earlier conclusions drawn from electron spectroscopy results are evident at temperatures above 650 °C [43, 46, 47]. Subsequently, a threshold value of temperature for graphene synthesis can be related to this temperature providing a balanced graphene growth (Fig. 1.9).

A surface carbide phase is created at lower temperatures (<400 °C), which is found to be steady at temperature up to ~480 °C as per AES analysis [26, 38]. The nucleation and development of graphene is inhibited by presence of carbide phase. Consequently, growth at heats of 500 °C, 550 °C and 600 °C were carefully chosen for this study, which are situated in between phase strength boundaries of the surface-carbide and graphene [26, 38].

At distinct ethylene introductions around 500 °C, LEEM pictures and AES plots of exterior of top layer are reported (Fig. 1.10). Conversion of fresh Ni (111) surface into varying surface forms for 5-100L disclosures are demonstrated by LEEM. Characterization of this form as well-structured single-layer carbide on surface can be interpreted from the AES measurements. On enhancing the ethylene coverage to 760 L, a first graphene nucleation was demonstrated.

The development of graphene islands at 500 °C takes place at a preliminary level of ~ 5.5 mm/s. No segregation amongst developing graphene grain and Ni_2C segment can be observed from the LEEM movies. Thus, in accordance with results from scanning tunneling microscopy (STM) [26, 38], it's feasible that development of graphene occurs by obvious transformation of the carbide.

The forces acting on the surface are varying at 550 °C. Development of properly labeled carbide signal is not reported in AES [26]. It can be deduced that development of only remote carbide domains or disordered carbide layer occurred based on lower C_{KVV} signal received. Formation of new graphene phase takes place at 600 L. The growth rate of graphene at 550 °C is ~35 nm/s, which is comparatively much higher than that for growth of graphene at 500 °C [26, 38]. Additionally, at the growing graphene head, a region with a width of about 3-4 μm is detected, which is deficient in carbon and coherent with the carbon density drop encircling the varying regions of graphene.

As per this examination, the growth of graphene takes place in a manner analogous to other transition metals by supplementing of carbon to the free surface of graphene [26]. Thus, graphene doesn't touch explicitly with carbon-heavy (carbide) phase at this temperature. Furthermore, the evolution of graphene is dictated by dispersion of atoms on surface and not through carbon

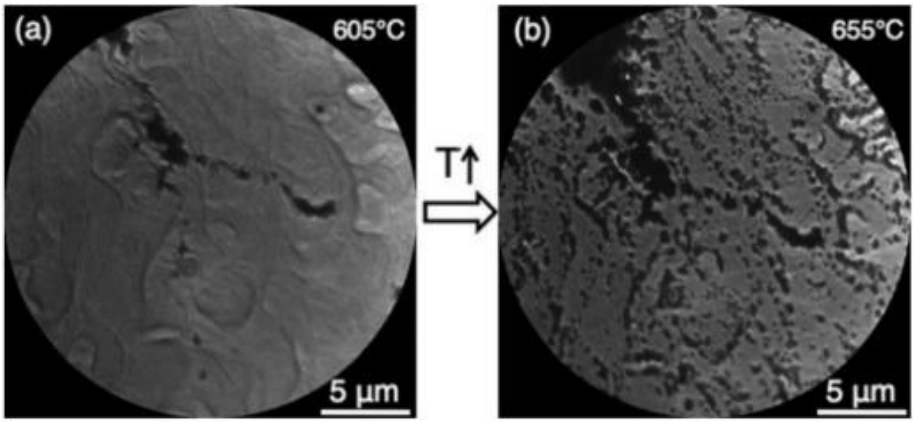

Fig. 1.9 Thermal steadiness of graphene single layer on Ni (111). (a) At 650 °C, Ni (111) surface nearly coated by film of graphene layers (Ni substrate shown by dark regions), (b) Graphene sheet starting to dissolve at higher temperatures of ~655 °C [26]

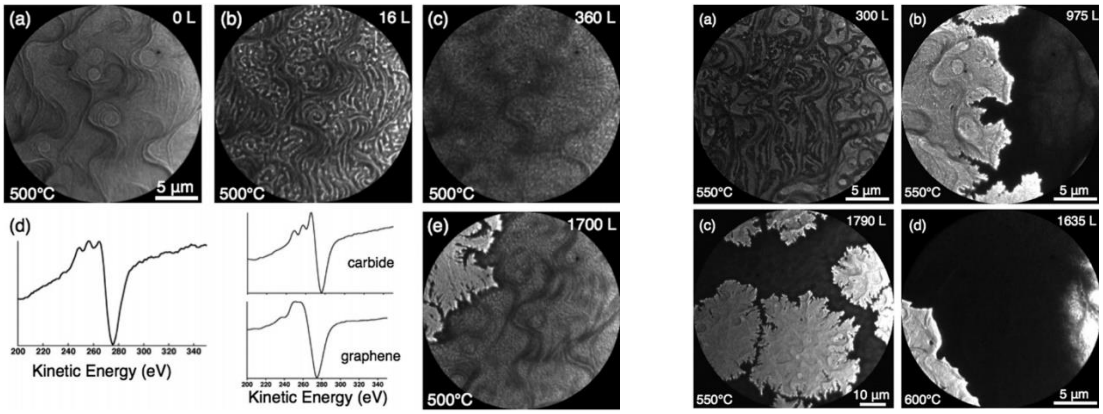

Fig. 1.10 (left) Development of the Ni (111) surface subjected to ethylene at 10^{-6} T, 500 °C, (a) atomic steps on the surface shown by bright lines. Abrasive surface carbide formation on complete surface by introduction of 16 L ethylene, (b) improved microstructure shown by improved disclosure, (c) nucleation of graphene and irregular growth under higher disclosure, (d) carbide and graphene phases as detected by AES, (e) AES plots of phases of pure-carbide and pure-graphene (~400L exposure) lay over together, (right) surface crystal order shown by LEEM images at 550 °C [26]

re-separation in the volume. The rate of evolution of graphene grains reduces when two grains approach each other demonstrates that dispersion of carbon atoms on surface is a limiting mechanism for development of graphene. As per amount of spatial region accessible for carbon to grow by breaking down (removal of hydrogen) of ethylene, the speed of development of graphene layers will vary [26, 38].

Generation of empty regions between the graphene grains can be attributed to lower speed of growth, which requires greater time to be occupied. LEEM analysis illustrates these disparities. Diameter of average grain of graphene is revealed to be at an order of ~40 µm. The improvement of temperature greater than 600 °C leads to further deviations such as (i) AES showing fewer carbide formation and graphene provides a leading indication of substantial carbon, (ii) ethylene interaction enhanced by 4 times required by graphene nucleation, (iii) discarded region developed near the graphene boundary is 3-4 times broader, which is about 10-15 µm, (iv) 1/7 times rate of development of graphene compared to that at 550 °C ~4.8 nm/s. Thus, at a temperature of ~550 °C, the development of graphene on Ni surface is one of the quickest methods and comparatively slower at enhanced or decreased temperatures. The upper limit in the evolution speed can be described by some common factors. The contest amongst the mechanisms of dispersion of carbon on the exterior surface towards the head for graphene development and the decrease in carbon on surface by spreading into the volume of material provides the reasoning for reducing rate of development at elevated temperature [26, 38, 39]. The expression relating the energy for stimulating the surface and bulk dispersion of carbon atoms under thermally initiated environment is exponentially related and given by exp (E_s-E_b/kT). The parameter for this relationship is presumed to be identical. Furthermore, a reduced disintegration and attaching of ethylene include some of the variables which provides a reducing speed for development of graphene films. For similar surfaces, the solid reliance of variation in sticking coefficient to temperature values is implausible. However, the development of carbide on surface can occur at reduced temperatures of around 500 °C, where this relationship dependence is observed to be deviating [42, 43, 46].

In contrast to pure Ni, carbides are anticipated to have a lower acuteness towards ethylene. The growth of stimulated carbon may diminish with swift evolution of complete monolayer. The existence of surface carbide [47] can be attributed as one of the reasons for modification in evolution method leading to a reduction of speed of development at ~500 °C. The growth approach involving connection of carbon or group of carbon atoms to the open ends of regions [49, 50] of graphene is the governing mechanism for evolution of graphene on Ni surface around ~500 and 600 °C. If the temperature of evolution can be altered to lower than graphene phase-durability temperature of ~650 °C, a self-regulating

development of graphene can be received on Ni substrates, as per in-situ microscopy measurements of graphene CVD evolution on Ni (111) [26].

As inferred from the experimental results, 550 °C is an ideal temperature for graphene development, which can be based on the interaction between growth of surface carbide, resulting in a diminishing growth of graphene thin film with good quality at temperatures lower than the 500 °C (low), and suspension of carbon into the bulk, which confines the evolution of graphene at temperatures above 600 °C (high) [26, 38, 39], [42, 43, 46, 47].

1.4 Cu-Ni alloy catalyst

As discussed, graphene has found widespread applications due to it's intriguing properties [50, 67-69] resulting from single layer of carbon atoms connected together as per sp2 hybridization resulting in arrangement of carbon atoms with "honeycomb" symmetry. As per the Mermin Wagner theorem, before discovery of removal of single-layer of atoms from graphite [54], there is no known material of single-atomic thickness to survive thermodynamically stable state [55].

The finding of graphene has led to interests in exploring other 2-D materials [54]. Bottom-up growth method (CVD) helps in growing long graphene films [57], whereas mono- and multi-layer graphene sheets can be developed by top-down approach [58] in large quantities. Broad-range of properties of graphene make it useful in varying fields of aerospace, biotechnology, energy, thermal management, etc. [59-61].

Robust flexibility [62, 63], optically clear/visible which allows for electromagnetic radiation (from visible spectrum) to transmit/pass through material [64] and structural resilience [65] make it very beneficial in electronics and photonics applications.

The benefits of cheap, high production and less complexity [66] make the CVD method an ideal process for producing high-domain graphene films with less defects. The breakdown of hydrocarbons during the CVD method helps in evolution of the graphene film at high temperatures by use of catalysts, for example, Cu [67], Ni, Pt, Ga, $NiAl_2O_4$ and others.

The growth of graphene on polycrystalline Ni or Cu foils is well reported in literature, however, the issues relating to absence of manipulation in the amount of graphene layers has led to extra obstacles in its usage for electronics. After thermal annealing step in CVD furnace, the reduction of temperature leads to precipitation of carbon atoms from bulk Ni film on catalyst surface, which regulates thickness of graphene film.

The kinetically self-constraining buildup is the underlying mechanism for growth of mono-layer graphene on top of Cu substrate. The regulation of total amount of layers, coherency and shape of graphene films can be performed by employing a Cu_xNi_{1-x} alloy catalyst [69, 70]. Recently, the synthesis of graphene with appropriate thickness at varying range of temperature on substrate of Ni/Cu alloy on Cu foil was termed as “smart Janus”.

By supplying CH_4 on a base substrate with $Cu_{85}Ni_{15}$ alloy catalyst, a single-crystal monolayer of graphene ~1.5 inch large was obtained. Although graphene films were obtained, the function of response-time and ratio of Cu_xNi_{1-x} alloy during the CVD process, and their regulation of the graphene film thickness is not well understood.

A study of change in composition of Cu_xNi_{1-x} alloy on the number of layers of graphene by thermal CVD process has been recently demonstrated [50]. Additionally, layers of varying thickness ratios of CuNi ratio were grown on substrate for synthesis of graphene in place of a film with a constant CuNi ratio. The inter-dispersion of Cu/Ni layers (heterostructure of Cu/Ni/SiO_2/Si) and the loss of Cu at elevated temperature would lead to substantial transformation in the composition of catalyst over the substrate in course of CVD growth.

Analysis of the surface morphology and number of graphene layers on CuNi bilayer catalyst as a variable of the period for response is discussed. A small sputtering system (ion) was used for growth of Ni film on Si/SiO_2 chip followed by Cu film encompassing on Ni layer by thermal evaporation process to finally obtain and develop alloy catalyst films. A continuous depth of CuNi catalyst layer of 450 nm was maintained by measuring the growth rate of Ni and Cu layers. CuNi films with varying thickness ratios of 3:1, 1:1 and 1:3 were grown. For example, a 3:1 ratio implies film comprises of Cu ~337.5 nm and Ni ~112.5 nm in dimensions.

Graphene film was developed using thermal CVD system (Fig. 1.11) [50]. Cylindrically shaped furnace was employed and chip with Cu/Ni/SiO_2/Si films were input as sample into system, then heated for about 25 minutes at 750 °C with flow of H_2/Ar gas (215/400 sccm, pressure: 250 Torr) into the system, which was followed by heating of the system to 900 °C with combination of CH_4/H_2 (75/15 sccm, pressure: 1.5 Torr) for graphene synthesis. Temperature of furnace system was lowered to room temperature after 5-15 minutes at rate of 20 °C/min.

Raman spectroscopy with electromagnetic (EM) radiation at wavelength of 532 nm and scanning electron microscopy (SEM) in the field emission mode was performed on the samples. Energy dispersive spectrometry (EDS) was used for measurement of the composition of CuNi bilayer after CVD growth. The development of graphene layers on CuNi bilayer catalyst by thermal CVD system is demonstrated [50].

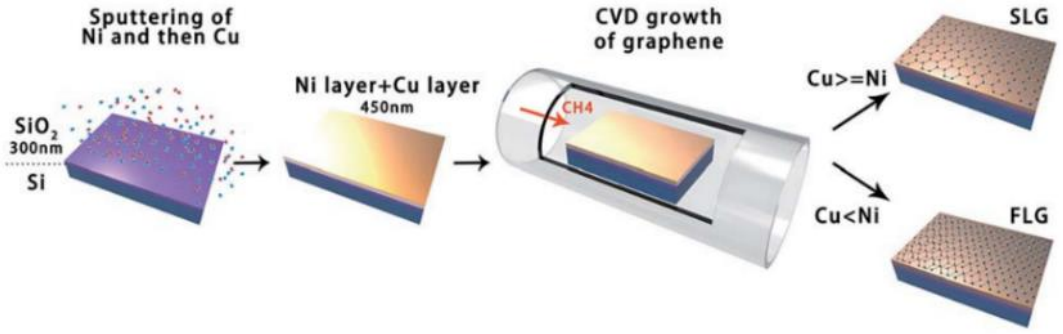

Fig. 1.11 CVD (heat-based) process for development of graphene by using CuNi catalyst (two films), [50]

Multi-layered thin films of Cu/Ni/SiO_2/Si with a constant overall depth of 450 nm of CuNi bilayer was obtained by deposition of Ni layer on SiO_2 (300 nm)/Si chip and thermal evaporation of Cu film on top of the Ni layer. The native oxide was reduced over the surface of metal catalyst film by annealing samples at 750 °C, which was subsequently followed by heating the system to 900 °C for development of graphene with various reaction time. Since the drive for disintegration of CH_4 is greater due to support of Cu catalyst resulting from the very minimal solubility between Cu and carbon, graphene reacts with Cu at a temperature varying from 950-1000 °C, and that for Ni at a comparatively lower values (>850 °C) during a CVD process. An equilibrium between smaller temperature for synthesis (~900 °C) and quality of graphene is achieved by introduction of Ni with Cu as a dual catalyst. In CVD graphene growth, the Cu film can evaporate due to weak wettability of Cu film on SiO2/Si substrate. Consequently, an intermediate Ni film at the intersection of Cu and the base chip can be advantageous to the thermal strength of the catalyst films [50].

Deposition of Ni, CuNi bilayer and synthesis of graphene is demonstrated (Fig. 1.12). Post CVD, a shift in the shade of samples from gray (Ni) to bronze (CuNi) to light gray (CuNi alloy) is detected. Analysis of Raman spectroscopy of graphene films grown on varying CuNi alloy compositions are discussed along with the reaction time (Fig. 1.12). The measurement of peak height and FWHM is done by applying a Gaussian fit to the spectra. A demonstration of the original and Gaussian fitted plots is reported [50]. Cu of 337.5 nm and Ni of 112.5 nm thickness is implied from Cu/Ni ratio of 3:1. Thickness ratio of CuNi alloy can be assumed to be identical to the weight percent (eg. 3:1=75 wt.% Cu) because Cu and Ni have nearly matching density values of 8.92 and 8.90 gcm^{-3}.

The characteristic Raman peaks for graphene: stretching-vibration mode of sp^2 sites at 1579-1588 cm^{-1} (G-band), for example the C=C bonds in fragrant mixtures, and double resonance processes relating to the 2D-peak formed at 2688-2699 cm^{-1} are demonstrated (Fig. 1.12) [50, 67-69]. The thickness calculation of CVD grown graphene thin film is approximated from the I_{2D}/I_G fractional value from Raman spectra relating to the amount of C-C atom (“sp2 hybridization”) cluster formation in graphene and information from the FWHM of 2D-band. For a sample with 5 minutes of growth of graphene, the D-band small peaks are observed at 1350 cm^{-1}. The extent of deviation from crystalline structure of graphene is shown by the D-band which is ascribed to the bond-angle deficiency from the development of sp^3 hybridized network. Growth of graphene with good-quality on Cu-Ni bilayer catalyst system is demonstrated by the lack of D-band in Raman spectra plot. The calculated values of FWHM and I_{2D}/I_G ratios of 2D-band from Raman spectra are discussed [50, 67-69].

A normal change in the values of I_{2D}/I_G ratios and 2D-band FWHM for varying samples developed with distinct Cu-Ni compositions and various time for synthesis was observed. As the period of development was enhanced from 5 to

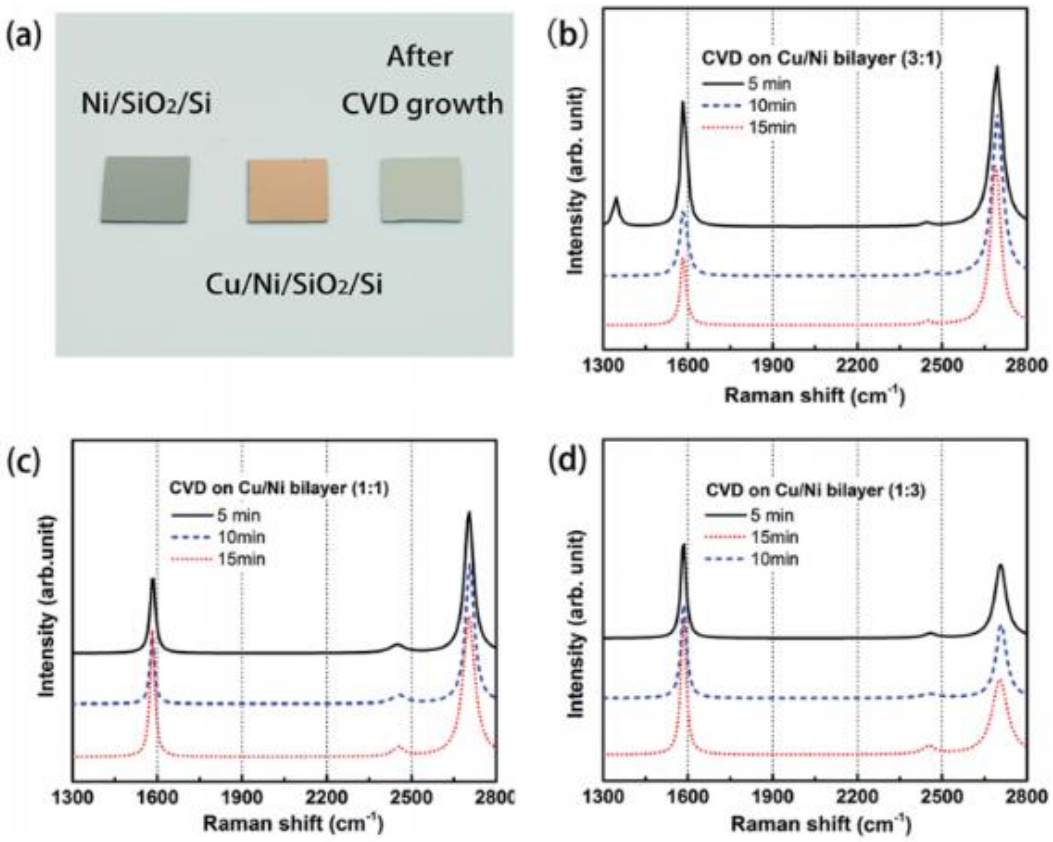

Fig. 1.12 (a) Developed catalyst and CVD synthesis on chips illustrated; Cu-Ni dual films (at.%) in ratio of (b) 3:1, (c) 1:1 and (d) 1:3 at varying periods of synthesis analyzed by Raman spectroscopy [50]

15 minutes, the I_{2D}/I_G fractional magnitude of graphene films improved from 1.18 to 1.97 for higher Cu at.% catalyst (Cu/Ni=3:1). Furthermore, a constant mono-layer graphene was progressively developed from nanocrystalline areas is shown by vanishing D-band in the Raman spectra. Mono-layer graphene formation can be attributed to the thin 2-D band for FWHM varying in 43.4 to 27.9 (Fig. 1.13d). Furthermore, for Cu-Ni catalyst system with 1:1 composition, it was observed that the I_{2D}/I_G ratio reduced from 1.96 to 1.13, and the FWHM improved from 35.1 to 52, when the time is enhanced [50, 67-69]. The number of graphene layers yielded with Cu/Ni=1:1 is considerably dependent on the time of response. During the initial stage of 5 mins., monolayer graphene can be formed and for greater periods of time (15 mins.), bilayer graphene growth takes place. The synthesis of graphene layers typically initiates as two layers for a catalyst thin-film dominant in Ni at.% (Cu/Ni=1:3), and then as the chemical reaction progresses further, graphene thin film develops into few layers [50, 67-69].

As per Raman measurements (symmetrical 2-D band), the depth of sample after a growth period of 15 mins does not go beyond to that of 5 layers of graphene. Additionally, by manipulating the at.% of Cu and Ni in binary alloy system, and varying the time for development of layers, one can grow monolayer-, two layer and multi-layer graphene thin films [50, 67-69]. EDS was employed for determination of the Cu-Ni compositions during CVD process for understanding the principle of development for varying amounts of graphene layers with bilayer catalysts (Fig. 1.14). Ni crystalline lattice (grown as film initially) intermixes with Cu crystalline lattice (also grown as film initially) to develop a new mixture, where both the phases (crystalline solids) co-exist together as a new solid solution around temperature of 750-900°C. Post reaction for 5 and 15 mins around 900 °C, the composition of surface catalyst of thin films was estimated to be around 71.9 and 75.4 wt.% Cu respectively at the Cu-rich side. Self-regulating method is the underlying phenomenon for evolution of graphene monolayer when the system consists of Cu majorly, however, when Ni is present predominantly in the system (Cu: 20.5-24.3 wt.%), phase segregation method controls the synthesis of few-layer graphene [50, 67-69].

The change in phase of Cu from solid to liquid starts at 1085 °C and that of Ni begins around 1455°C. At greater temperatures around 900 °C and lower pressure of 1.5 Torr, the drying-up of Cu leads to a reduction in Cu wt.% over a period. Additionally, the SEM analysis show that the loss of Cu from surface during CVD growth affects the structure of CuNi bilayer and its properties. The surface of catalyst films under similar CVD conditions devoid of CH_4 is demonstrated a contrast study [71].

The Cu loss can be reduced after deposition of graphene layer by CVD process and this provides a better visibility of the graphene regions. The graphene film becomes imperfect on enhancing the reaction time due to creation of voids as observed in Cu-rich catalyst layer [50, 67-69]. The decline in properties of

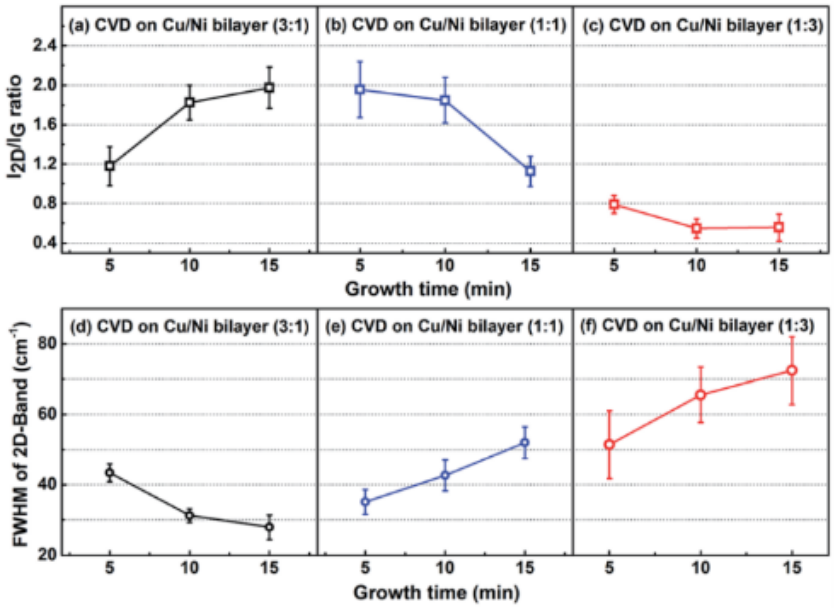

Fig. 1.13 Comparison of $I_{2D/G}$ vs growth time for CVD on CuNi bilayer (a-c) 3:1, 1:1 and 1:3; and FWHM of 2D-band vs growth time (d-f) 3:1, 1:1 and 1:3 [50]

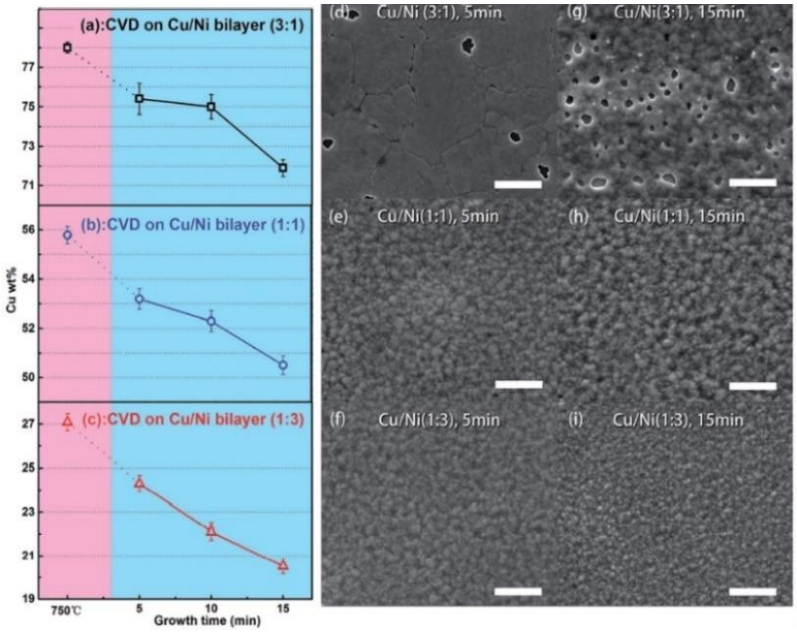

Fig. 1.14 Change in composition of Cu wt.% for varying bilayer catalysts throughout CVD process (a-d-c) Cu:Ni=3:1, (b-e-h) Cu:Ni=1:1, (c-f-i) Cu:Ni=1:3. Topological features of graphene films grown at 900 °C for 5 mins (d-e-f); 15 mins for varying Cu/Ni at.% (scale bar-10μm), [50]

graphene film occurs due to greater vaporization (drying up) and rupturing of Cu film to droplets on SiO_2/Si under the deposition of Cu only as catalyst material. The analysis of method of development from one- to graphene film with dual layers on CuNi alloy with 1:1 at.% is of greater significance. During a reaction time of 5-15 mins., the composition of Cu doesn't change significantly (50.5-53.2wt%), and as a result, the increase in thickness of graphene thin films is dependent upon period for development from nucleation to HGF domains [50, 67-69]. Additionally, the C content at the catalyst surface can be regulated by a proper blend of carbon denying (Cu) and carbon diffusing (Ni) factors. The development of bilayer graphene can be ascribed to the precipitation of C in clusters which are dissipated on catalyst surface from the dilute Ni solution after CVD annealing when the temperature is reduced from high bath temperature to RT. Also, the extent of C atoms soluble in dilute Ni would be in limiting amounts as shown by TEM analysis report [50, 67-69].

1.5 Platinum (Pt) catalyst

The graphene layers produced by different synthesis methods are typically of polycrystalline type as per results reported in several literature. Graphene with grain size in tens of micrometers can be produced by thermal breakdown of SiC. Grains shorter than 10 μm can help in the synthesis of graphene thin films on single crystalline Cu (111) by CVD process. As reported recently [70, 72, 74], reduced sized HGFs of dimensions up to 20 μm can be synthesized on thin Cu sheets by ambient pressure CVD (AP-CVD) process.

Grains with a greater degree of edge roughness with a size of hundreds of micrometers were produced on thin Cu sheets by employing a low-pressure CVD (LP-CVD) process, where the structure were found to be like dendritic growth. Bigger grains of graphene with a size up to millimeter in ultra-high vacuum (UHV) were produced on single crystals of Ru [71] and Ni is reported. However, the shifting of graphene layers from metals with single-crystalline structure to other chips has proven to be a difficult process [70, 72, 74].

The method of entirely etching the metal chip surface by selection of appropriate "etchant" has proven to be faulty with difficulties such as destruction of the layers, creation of metal deposits, severe pollution to the surroundings and greater cost of manufacturing. As methods for etching of metals is complex and usually involves greater costs, the aforesaid techniques are not straightforward for the shifting of graphene from thermodynamically inert to highly "noble metal" chips.

Surface methods were primarily utilized in the analysis/study of graphene grown on such substrates devoid of their transfer to other substrates [74] and as a result, this research and the purposes were restrictive to certain extent. The transfer of graphene developed on Cu to other substrates by technique of electrochemical delamination has been lately described [70]. Etching of Cu

substrate incompletely to approximately 40 nm of Cu in depth during each transfer process and their application to several development and shifting process has been observed in this technique. Report on boiling (“bubbling”) mechanism for shifting graphene domains synthesized in hexagonal geometry (with dimensions of millimeter and single crystal type behavior) on Pt substrates by AP-CVD (AP-atmospheric pressure) to other random chips is demonstrated. Recurring development of graphene thin films on Pt is achieved by this bubbling mechanism, which is not harmful to the destruction of graphene layers and also to the base Pt substrate [72]. One of the benefits of using Pt substrates is that they can be used very frequently, and the graphene layers obtained on these constantly used Pt substrates demonstrate similar properties to the pristine graphene layers without any degradation [70, 72, 74].

Carrier mobility higher than 7100 $cm^2V^{-1}s^{-1}$ and wrinkle depths of very low amounts along with high-level crystalline structure are some of the excellent properties attributed to the graphene layers obtained from this method [70, 72, 74]. The deposition of single-crystal graphene grains of uniform films is discussed. AP-CVD methods were used for development of big-sized single-crystalline graphene domains shaped in hexagonal geometry and thin films of graphene by amalgamation of these islands were received on Pt chips (for both crystal structure orders-uniform across varying orientations of lattice or structural domains with edges across different crystallographic directions). To produce constant films, a greater time for development of the graphene grains was required. The graphene films grown on single-crystalline and poly-crystalline Pt substrates are appearing to be of similar structure types. In this study, polycrystalline Pt foils were employed for growth of graphene layers [74].

The synthesis method is convenient, and the utilization of specific reaction systems is prevented by employing an AP-CVD processing technique. Consequently, this helps in manufacturing of single-crystal graphene layers in greater quantities and at a convenient price. Single-layer graphene films can be conveniently developed on Pt foils even though the dissolution capacity of carbon in Pt is of greater concentrations (~0.9 at.%; 1000°C) (Fig. 1.15) [17, 74]. Comparatively, a higher growth rate and larger space for growth can be possible by using Cu foils. When using CH_4 as the supplier for carbon, the temperature for development of graphene layers can be obtained to be as low as 750°C, and with a greater concentration of CH_4 at 950 °C, the graphene layers can entirely cover the Pt surface in numerous seconds. The development of graphene grains by CVD process is halted before the adjoining domains combine to develop larger self-arranged crystalline order of atoms with similar orientations along all directions in order to regulate their dimensions and concentration of atoms precipitated from bulk catalyst as source of new domain growth. The nucleation concentration of graphene can be increased, and their grain size can be decreased by lowering the temperature for development of graphene layers. At

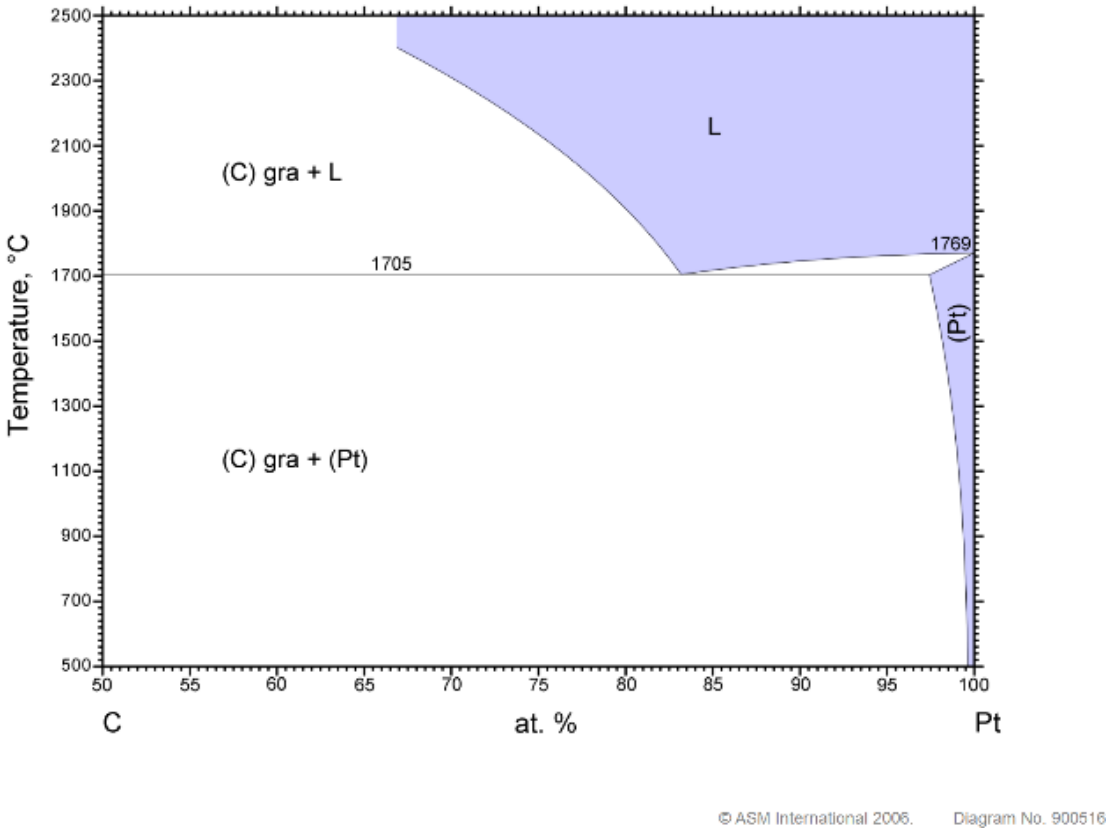

Fig. 1.15 Pt-C phase diagram [17]

temperature of development of graphene thin films below 800 °C, miniature-sized domains of graphene with dimensions lower than 1 μm can be obtained. In this study, temperatures up to 1040 °C were used for growth of bigger-sized crystalline domains of graphene with atomic arrangement similar across varying orientations and thin films by combining them were produced [70, 72, 74].

Nucleation concentration and dimensions of domains of graphene atoms separated by edge boundaries with varying crystallographic orientation of each domain is strongly dependent upon the CH_4 concentration in supplement to the temperature for development of graphene layers. Graphene with greater grain sizes were produced by using lower concentration of CH_4. Accordingly, it was demonstrated that the dimensions of graphene domains increased from 50 to 100 to 500 μm by employing a reducing flow-rate ratio of CH_4/H_2 from 20/400 to 10/700 and 5/700 (specific numbers refer to flow rate in standard cubic centimeter per minute (scc)). Graphene grains tend to develop with straighter edges and a greater regularity with their arrangement is obtained. Leading graphene domains arranged ideally in hexagon type shape with very easy boundaries and horizontal dimensions of up to 1.3 mm on thin Pt sheet with several grains oriented in varying crystallographic orientations are developed when the flow rate of CH_4/H_2 is changed to 4/700 [70, 72, 74].

Comparatively, these grains are greater than the graphene domains obtained on Cu by AP-CVD method are 20-μm in size with crystallographic orientation of atoms without any boundaries, whereas those synthesized on Cu foils by LP-CVD process are 400-μm in size with dendrite type shapes and crystal arrangement of atoms with no edges [70, 72, 74]. Disintegration of hydrocarbons by employing metals for stimulating synthesis (CVD) chemical reaction on surface and precipitation from bulk is one of the primary methods for development of graphene films. Shaky carbon-carbon bonds are etched away by atomic H, which are formed by the disintegration of hydrogen (H_2) compound on the surface of metal in a CVD chamber for development of graphene layers occurs. Subsequently, the process parameters such as precipitation of carbon atoms on surface layer, development of domains and shape governing the growth of graphene are solidly dependent upon a suitable balance between the aforesaid processes. The development of dynamic carbon species slows down and consequently, restrains the nucleation of graphene on reduction of the flow rate of CH_4. The synthesis of sizeable graphene grains is due to decreased nucleation concentration of graphene at low CH_4/H_2 flowrate. Furthermore, in few situations, one domain with uniform arrangement of atoms along all crystallographic directions for 2.5x2.5 mm is observed [70, 72, 74].

Graphene with varying strengths and the edge structures of armchair and zigzag types are obtained. When the CH_4/H_2 flow ratio is reduced, the edges with lower strength are uniquely etched out by the active atomic H, and consequently, the boundaries of graphene layers develop into straighter and regular shaped types.

The larger graphene grains had some shorter bilayer and few-layer region (domains) types as demonstrated. When the quantity of dynamic carbon groups generated have surpassed the threshold limit for growth of single-layer graphene, the development of the aforesaid structures takes place, for example, during the initiation of development of graphene or the varying catalytic events of Pt in distinctive areas [70, 72, 74]. For the CVD synthesis of graphene thin films on Cu catalyst, temperature greater than 1000 °C is necessary, and source for carbon is CH_4.

CH_4 dissolution is higher for a Pt substrate as compared to Cu metal because of it's higher catalytic ability for this disassociation is based on the assumption or experimental observation that the graphene layers can develop at comparatively reduced temperature (750 °C). Furthermore, this is reported to be coherent with theoretical calculations [76]. Pt substrate has sharper catalytic capacity as compared to Cu for H_2 dissolution to develop energetic atomic H^{30} [77].

CHAPTER TWO

EXPERIMENTAL SETUP

2.1 Thin film sputtering deposition of metal catalyst layers

The growth of copper-nickel (Cu_xNi_{1-x}) alloy thin film (<1μm) gradients of transition metal catalyst layers on Silicon dioxide (SiO_2)/ Silicon (Si) substrate is performed by physical vapor deposition (PVD) process at the thin film sputtering facility (Fig. 2.1) at the Joint Institute of Advanced Materials (JIAM), University of Tennessee, Knoxville (UTK). The radio frequency (RF) magnetron/magnetic sputtering process involved first loading of target materials (eg. Cu, Ni metal) onto the magnetron and magnetic target guns, respectively. Next, the pressure inside the main chamber is pumped to pressure of ~$3x10^{-7}$ Torr with a turbomolecular vacuum pump attached to the main chamber, which is connected to mechanical rotary vane pump. The load-lock system is connected to the main chamber via the main gate valve. Another turbo and mechanical roughing pumps are connected to the load lock system for quick sample entry. The SiO_2/Si wafer is loaded onto the load lock sample holder by isolating load lock from main chamber by closing the intermediate gate valve. The wafer is then transferred to the sample holder inside the main chamber by opening the gate valve.

The wafer is placed at appropriate height above the four metal target guns at the base of main chamber, and then, inert process gas, for example, argon (Ar) is introduced into the main chamber at ~25 mTorr via a mass flow controller. The selection of process gas is based on the type of thin film materials to be deposited. After the desired gas pressure is reached inside the chamber, the RF power source supply to Ni and Cu targets is turned on and maintained at 200 W and 230 W, respectively. The Cu target is assembled in the diagonally opposite direction to Ni target for obtaining a composition gradient of Cu_xNi_{1-x} film to find the optimum composition of Cu_xNi_{1-x} alloy for bilayer graphene production initially, which is then followed by sputtering of uniform Cu_xNi_{1-x} alloy film on the entire SiO_2/Si wafer 100mm in diameter.

During sputtering process (Fig. 2.2), the power source creates a negative potential on the magnetron, which behaves as cathode (-) and the ground reference (chamber) acts as anode (+). Thus, the electrons are accelerated away from the magnetron due to this potential gradient. Consequently, the fast-moving electrons collide with the process gas (Ar) atoms and eject outer shell electrons from the gas atoms and generate positively charged process gas ions, which are then accelerated towards negatively charged metal target surface. In this process, the positively charged ions knock-off the metal atoms from metal target surface in a direction so that they are collected on the wafer centrally located inside the chamber. Additionally, the positive ions from process gas atoms recombine with the free moving electrons and generate a plasma glow (light with

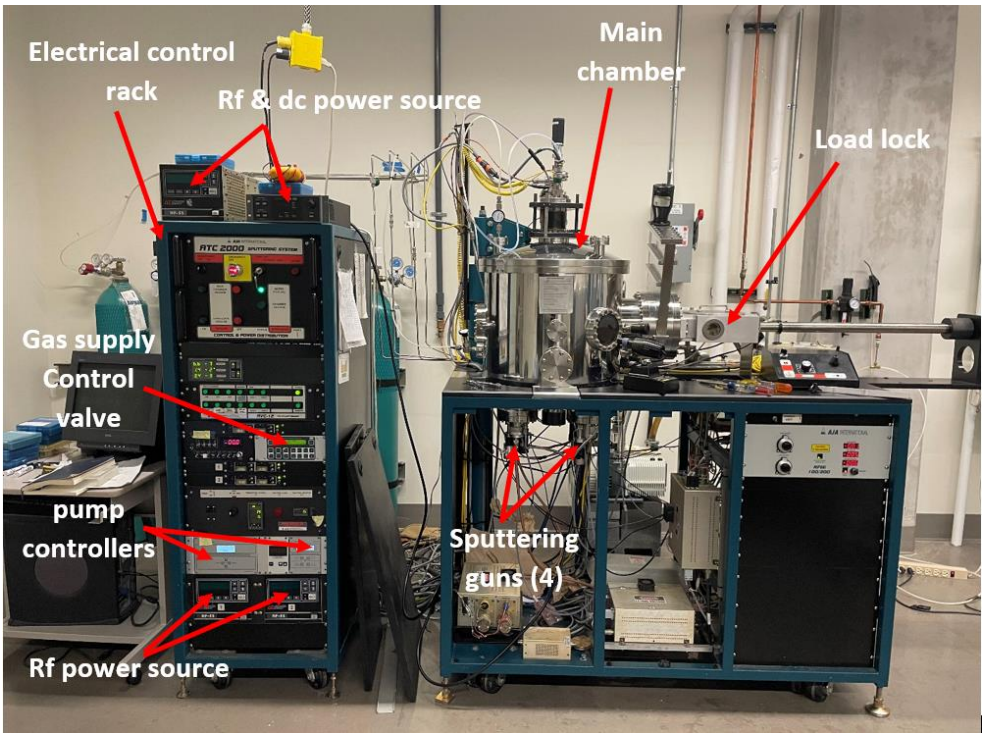

Fig. 2.1 RF magnetron sputtering system (JIAM, UTK)

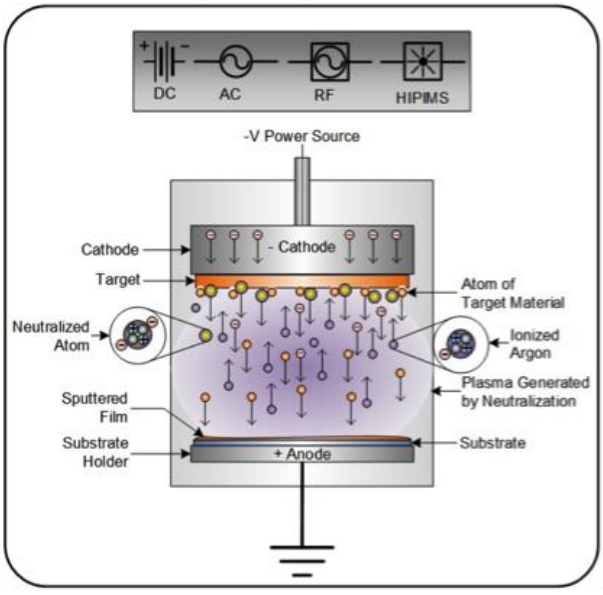

Fig. 2.2 RF magnetron sputtering process [78]

color) due to the electron falling from higher energy state to lower energy state inside the atoms [78].

The aforesaid process is continued for approximately 1 hour and 20 minutes to achieve a coherent film of uniform thickness (< 1µm) onto the SiO_2/Si wafer. After the film of desired thickness is achieved, the RF power source and Ar gas supply is turned off and lastly, the SiO_2/Si wafer with thin film deposition of Cu_xNi_{1-x} (Fig. 2.3) is taken out from the load lock system.

2.2 Chemical vapor deposition of graphene, etching and transfer process

Chemical vapor deposition (CVD) is a chemical process involving thermal decomposition of precursors onto a substrate surface leading to deposition of chemical vapors under high temperature conditions. The process temperature may be reduced by the breakdown and response from plasma due to the high temperature. The benefits of thermal CVD process include thin films with good quality and integrity. Additionally, one can manipulate the morphology, crystallinity, shape and dimensions of the thin film layer by properly adjusting the factors governing the process. In this study, high quality graphene layers were deposited on polycrystalline Cu_XNi_{1-x} alloy thin film deposited on SiO_2/Si wafer at our collaborator, General Graphene's facility in Knoxville, TN.

Graphene layers are deposited on polycrystalline Cu_xNi_{1-x} alloy thin film. The solubility of C in Cu at around 1000°C is very low (~ 75 +/- 0.5 ppm) and that of C in Ni is 1.3 at.%. The growth of bilayer or multi-layered graphene can be manipulated by changing the composition of Cu_xNi_{1-x} alloy film. One of the important parameters for controlling growth of graphene is the processing temperature maintained during the CVD process (Fig. 2.4) [79]. Temperatures close to 1000°C are selected for graphene bi-layer growth during this process. Additionally, the nucleation density and grain size of graphene are regulated by the concentration of CH_4.

The recipe (Fig. 2.5) for CVD bilayer graphene growth on Cu_xNi_{1-x} gradient alloy thin film on SiO_2/Si substrate includes firstly flushing off the surface of sample with CH_4+H_2 gas mixture to strip off any oxide formation by reduction reaction (from C source-CH_4) and H_2 gas for stripping of more complex compounds on the surface, if any present. This gas supply is typically continually running into the quartz tube furnace and never stopped even when there is no growth process going on inside the furnace. Thermal CVD setup at General Graphene (Fig. 2.6) includes a long tube furnace with inlet and outlet ends for gases to flow in and out respectively. The gas supply/flow (standard cubic centimeter per minute-sccm) can be manipulated through electrical control valve run by the software application on computer. A copper foil is placed at the end of tube for maintaining temperature inside the furnace. A small pipe is attached to the stainless-steel flange at the outlet for the gas outflow into the atmosphere. At the inlet side,

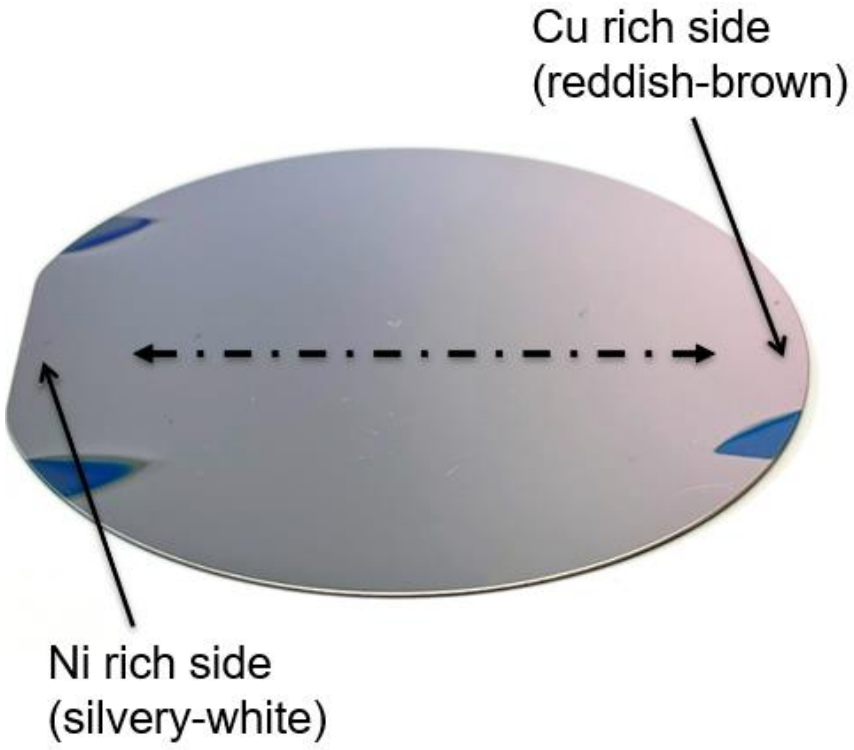

Fig. 2.3 Cu_xNi_{1-x} gradient thin film sputter deposited on Si/SiO_2 wafer

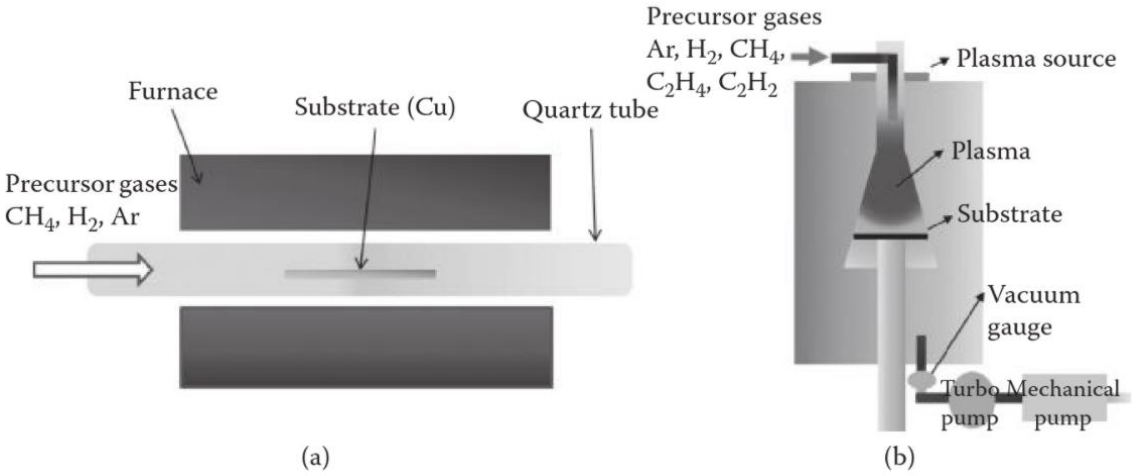

Fig. 2.4 Schematic of (a) thermal CVD and (b) plasma-enhanced CVD (PECVD) process [77]

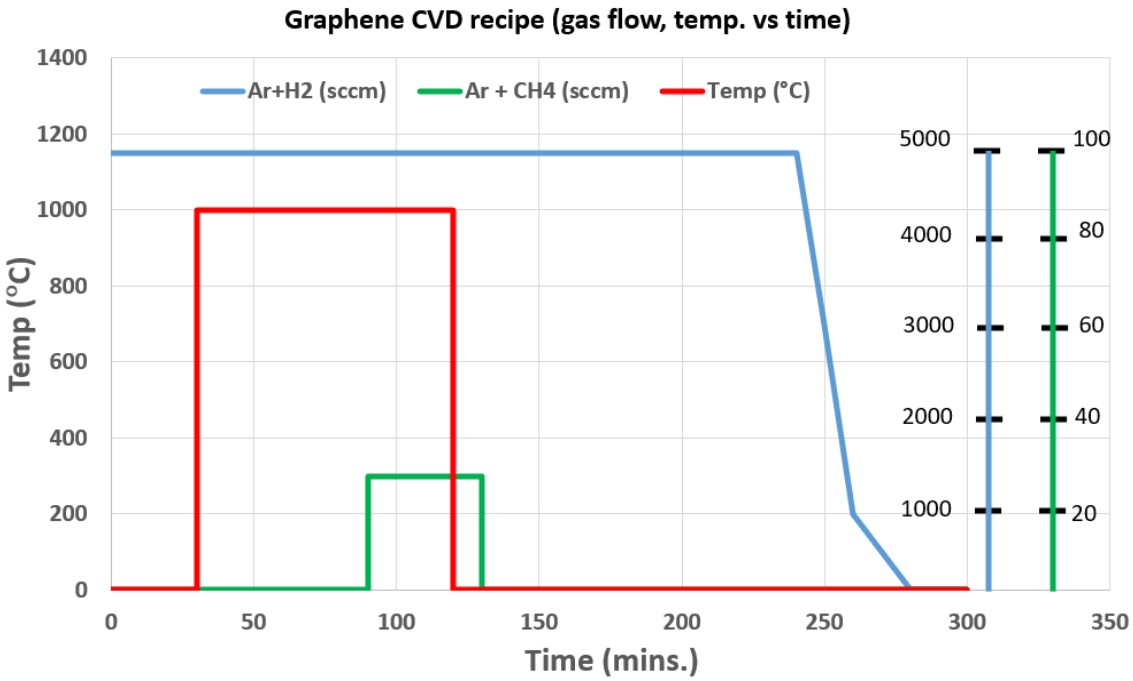

Fig. 2.5 Recipe for CVD graphene bilayer growth on Cu_xNi_{1-x} gradient alloy thin film deposited on Si/SiO_2 substrate developed by General Graphene

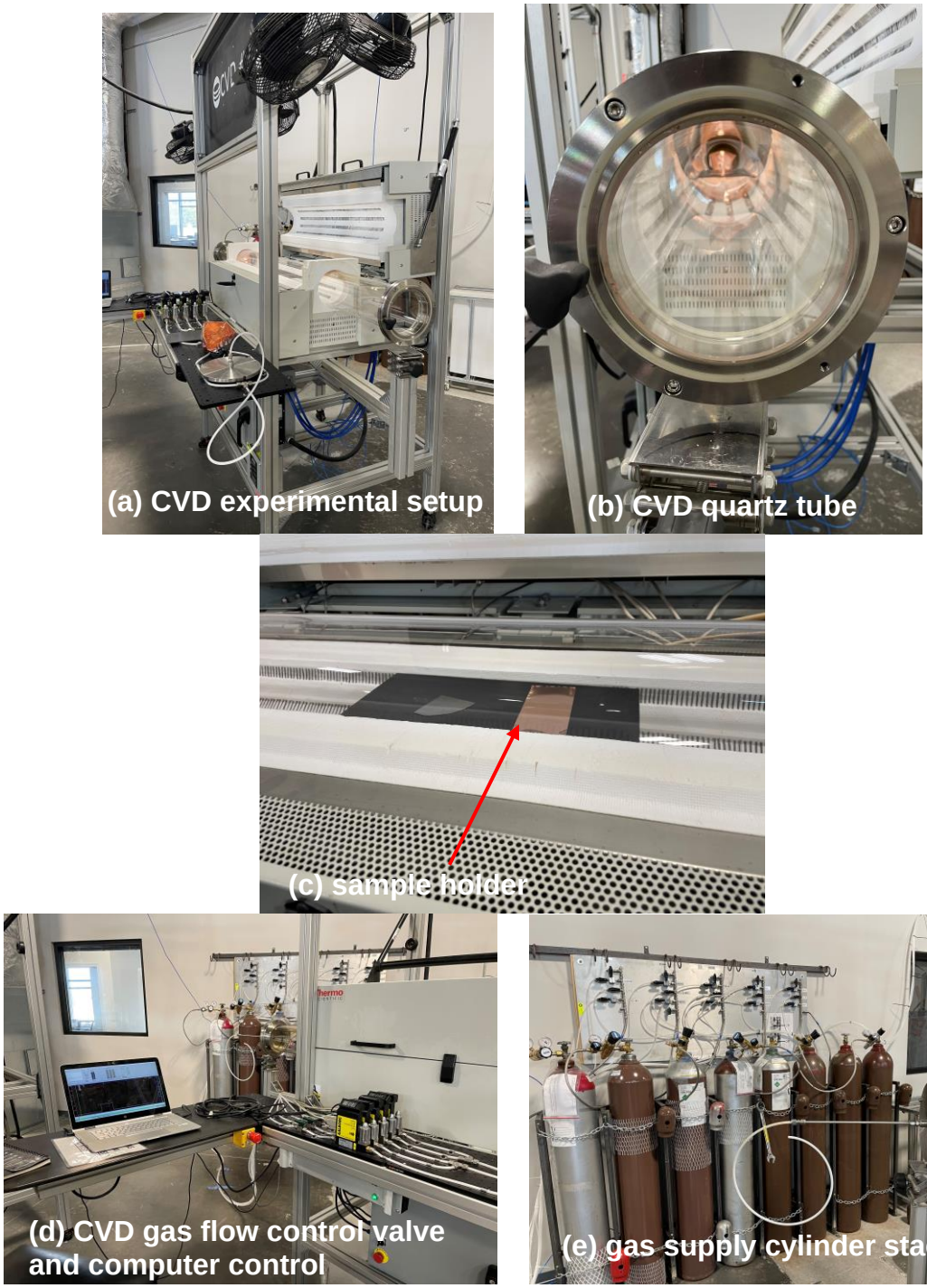

Fig. 2.6 Thermal CVD experimental setup at General Graphene (a) CVD experimental setup, (b) CVD quartz tube, (c) sample holder, (d) CVD gas flow control valve and computer control unit, (e) gas supply cylinder stack

there is a flange with pipe inlet for gas flow into the tube furnace. As mentioned, this inlet tube is connected to flow control valve outside for regulating gas flow from the gas cylinder into the tube furnace. A stainless-steel plate (rectangular shaped) is used as sample holder for the wafer or Cu foil, which can be slowly pushed in or pulled outward from the tube inlet side into the furnace by use of long rods with a hook at the end. There are cooling fans on top of the furnace to keep it cool. The temperature inside the furnace can be monitored/controlled by two thermocouples placed on the door of furnace (Fig. 2.6).

The temperature of the tube furnace is made sure to be at RT before beginning the CVD graphene growth process. After this, the ends of knobs on the inlet flange are slowly opened and the CuNi/SiO_2/Si wafer is slowly pushed inside and to the middle of furnace. Then the Cu foil is placed at the inlet side as heat shelf for the furnace and the inlet flange is slowly tightened. As shown in the recipe (Fig. 2.5), at the start of the CVD growth process, inert Ar (95.7%) + H_2 (2.5%) gas (mixture) is flushed into the furnace for 5 l/min at 5000 sccm to flush out any O_2/H_2O for maintaining inert gas atmosphere inside the furnace. As mentioned, it also helps to reduce any Cu oxide on the surface (also helps to smooth and anneal it) of sample. After 30 minutes, the heat is ramped up to a temperature of T=1000°C from RT and held at this temperature for 1 hour and 30 minutes. After 1 hour from beginning of heat ramp-up, a mixture of 95.5% Ar + 4.5% CH_4 is started to flow into the tube at ~25 sccm (constant flowrate) for about 45 minutes and then stopped. During this period, the CH_4 dissociates into C molecules and seeds onto the surface of Cu_xNi_{1-x} alloy and starts forming grains, which coalesce together to form C molecules on the surface inform of graphene layers. As reported in literature [3], larger grain size of graphene can be achieved by lower concentration of CH_4 because nucleation density of graphene is lower at a decreased CH_4/H_2 flow-rate ratio as there will be less carbon species. Also, the graphene grains become more and more structured with straight edges. Thus, the catalytic breakdown of hydrocarbons on metals is an essential step in introducing carbon species. Also, the development of dynamic atomic H on metals from molecular H_2 in CVD leads to etching away of weak carbon-carbon bonds. Thus, these two competing processes strongly govern the nucleation, growth and grain size of graphene. After 2 hours from start of synthesis process, the temperature inside the furnace drops down to T<100°C, and the door of the furnace is then opened. The tube furnace slowly cools down to RT in about half hour and then, the sample is taken out from the furnace by opening the knobs on the flange at the inlet side of furnace. The substrate plate is slowly pulled out from the tube (Fig. 2.6).

After CVD deposition of graphene on Cu_xNi_{1-x} alloy thin film on SiO_2/Si substrate, graphene is spin-coated with polymethyl methacrylate (PMMA) followed by curing. The purpose of PMMA layer is to provide protection and structural support to the graphene layer during the etching process. The cured sample is then placed in the aqueous bath of ammonium per sulphate (APS) solution for

etching (Fig. 2.7) away the Cu_xNi_{1-x} layer from the sandwich of PMMA/graphene/Cu_xNi_{1-x}/SiO_2/Si. After placing the CVD sample in the APS bath for overnight, the graphene layer floats on the surface of APS solution and the SiO_2/Si wafer drops down to the bottom of tub due to its gravity.

The graphene sample is ready for transfer to a fresh SiO_2/Si wafer. A wet transfer process (Fig. 2.8) is applied at General Graphene for this purpose, which involves gentle removal of graphene layer floating in APS bath onto a thin plastic foil assisted with a pipette for removal of any water bubbles and then placing the graphene layer into a bucket of deionized (DI) water. After cleaning the graphene layers for few minutes, it is then transferred to SiO_2/Si wafer. During this transfer, care should be taken to avoid any bubble formation by use of pipette, if required. The sample is left in vacuum for drying overnight.

After the CVD graphene sample has dried out, next step involves cleaning the surface by placing it in a bath of acetone for rinsing off any impurities/oxide on surface of graphene. After cleaning with acetone for a few minutes, the graphene sample is then rinsed in isopropyl alcohol (IPA) bath, which is followed by finally blow off the droplets of solution with help of an air dryer. The CVD graphene sample is now ready for optical imaging and Raman spectroscopy measurements.

2.3 Energy dispersive spectroscopy

After deposition of Cu_xNi_{1-x} alloy thin film, one of the next steps involved analysis of the atomic% of Cu and Ni in the film, which governed the growth of graphene layers by the CVD process. Consequently, we performed energy dispersive spectroscopy (EDS) to obtain the composition of Cu_xNi_{1-x} alloy, to correlate the graphene growth to associated Cu_xNi_{1-x} alloy composition.

The scanning electron microscope (SEM) has an electron source gun, which emits electrons and are subsequently accelerated to the surface of the specimen, which after interaction with the surface atoms are then scattered in varying directions. Typically, secondary electron and backscattered electron detectors collect the secondary and backscattered electrons, respectively to generate images (Fig. 2.9). The detection of individual elements (at.%) is based on the analysis of characteristic x-rays emitted by each element based on the elements unique atomic structure, which are observed as a distinguished set of peaks in the electromagnetic emission spectrum. The EDS analysis is performed at the microscopy facility at JIAM, UTK on the Zeiss EVO SEM (Fig. 2.10). Additionally, we performed high-resolution surface analysis of graphene layers on the Zeiss Auriga SEM (Fig. 2.11).

For the EVO-EDS analysis, settings included secondary electron detector (SE1), magnification of 10kX, electron gun source (EHT) at voltage of 10kV & 20kV and

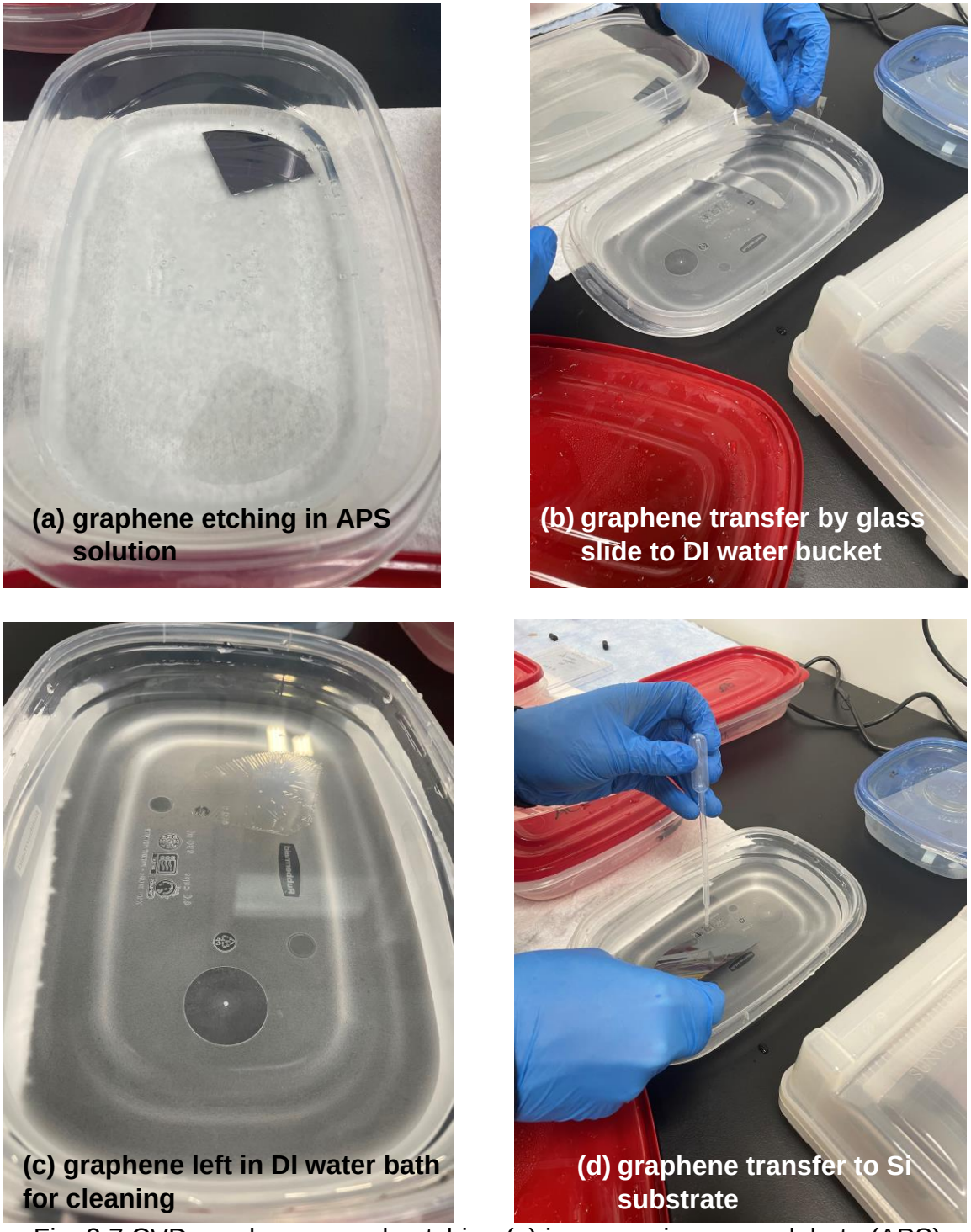

Fig. 2.7 CVD graphene sample etching (a) in ammonium per sulphate (APS) solution and wet transfer process (b-d) onto new SiO_2/Si wafer

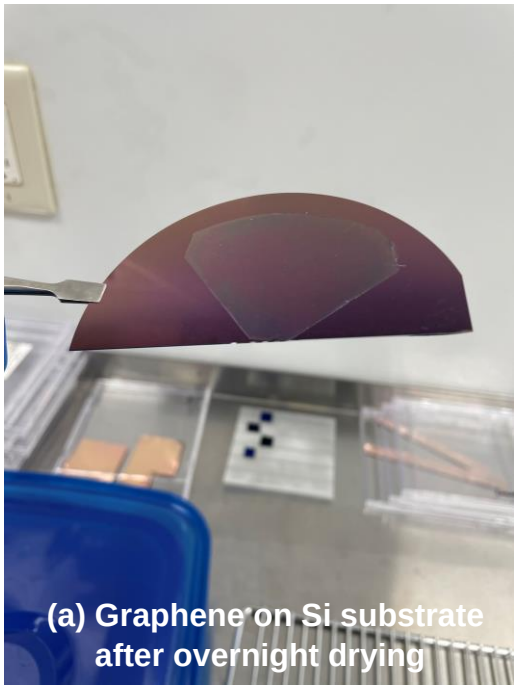

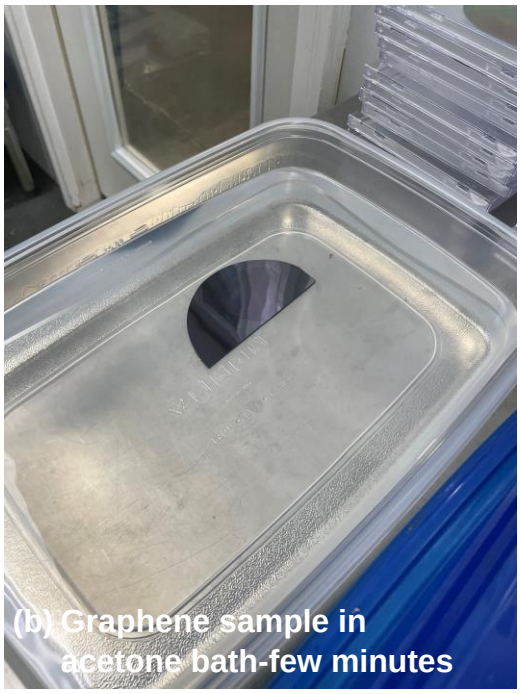

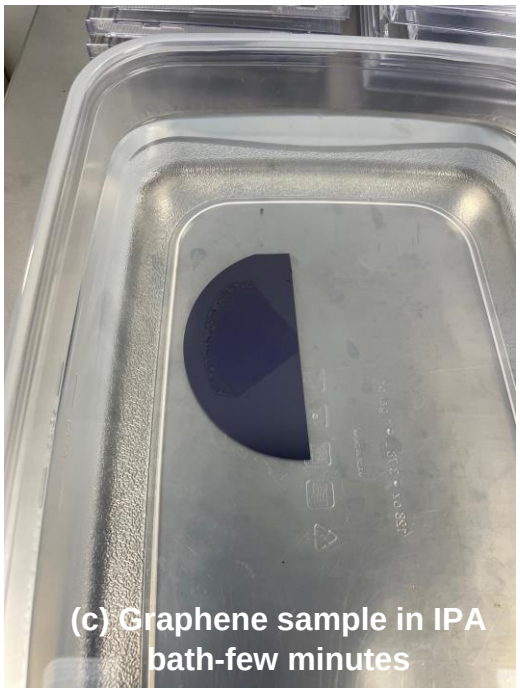

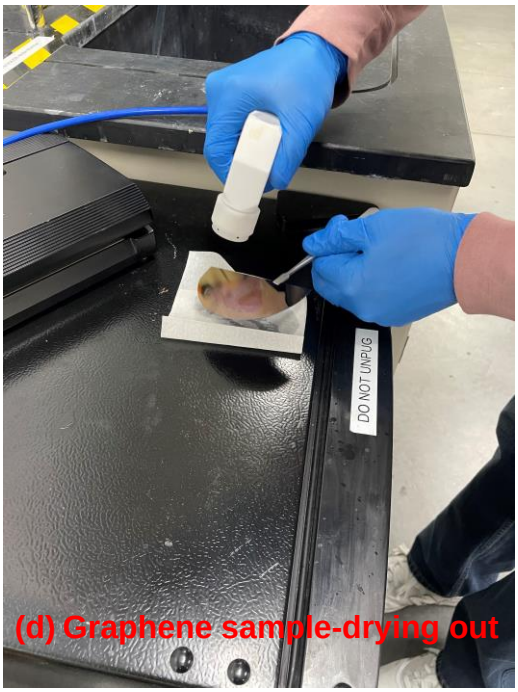

Fig. 2.8 Surface cleaning/rinsing of the CVD-graphene sample (a) Graphene on Si substrate after overnight drying, (b) Graphene sample in acetone bath (5-10 minutes, (c) Graphene sample in Iso-propyl alcohol (IPA) bath (5-10 minutes), (d) Graphene sample (drying out)

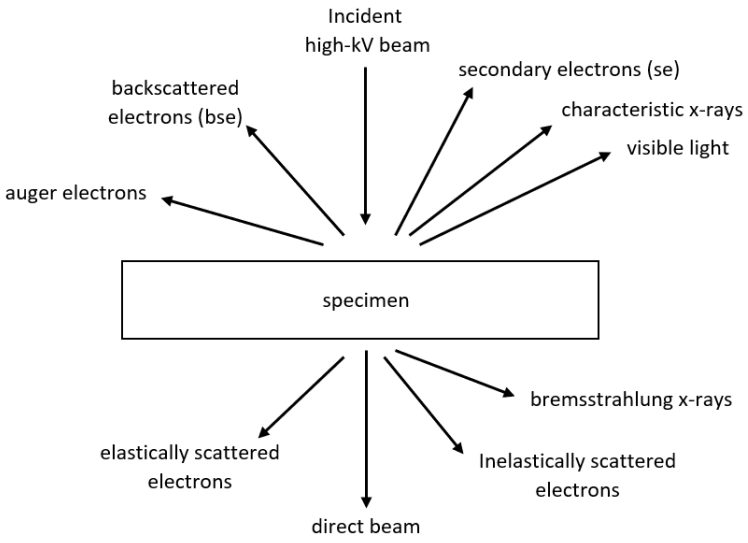

Fig. 2.9 Underlying principle of SEM-scattering of electrons

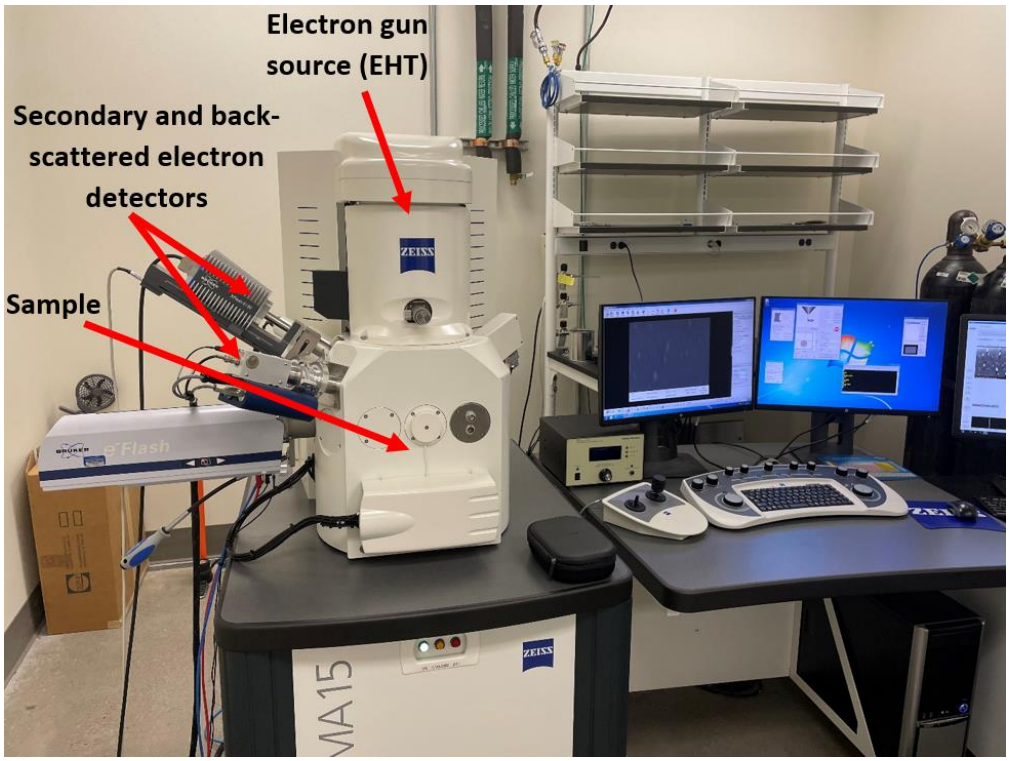

Fig. 2.10 Zeiss EVO scanning electron microscope (SEM)

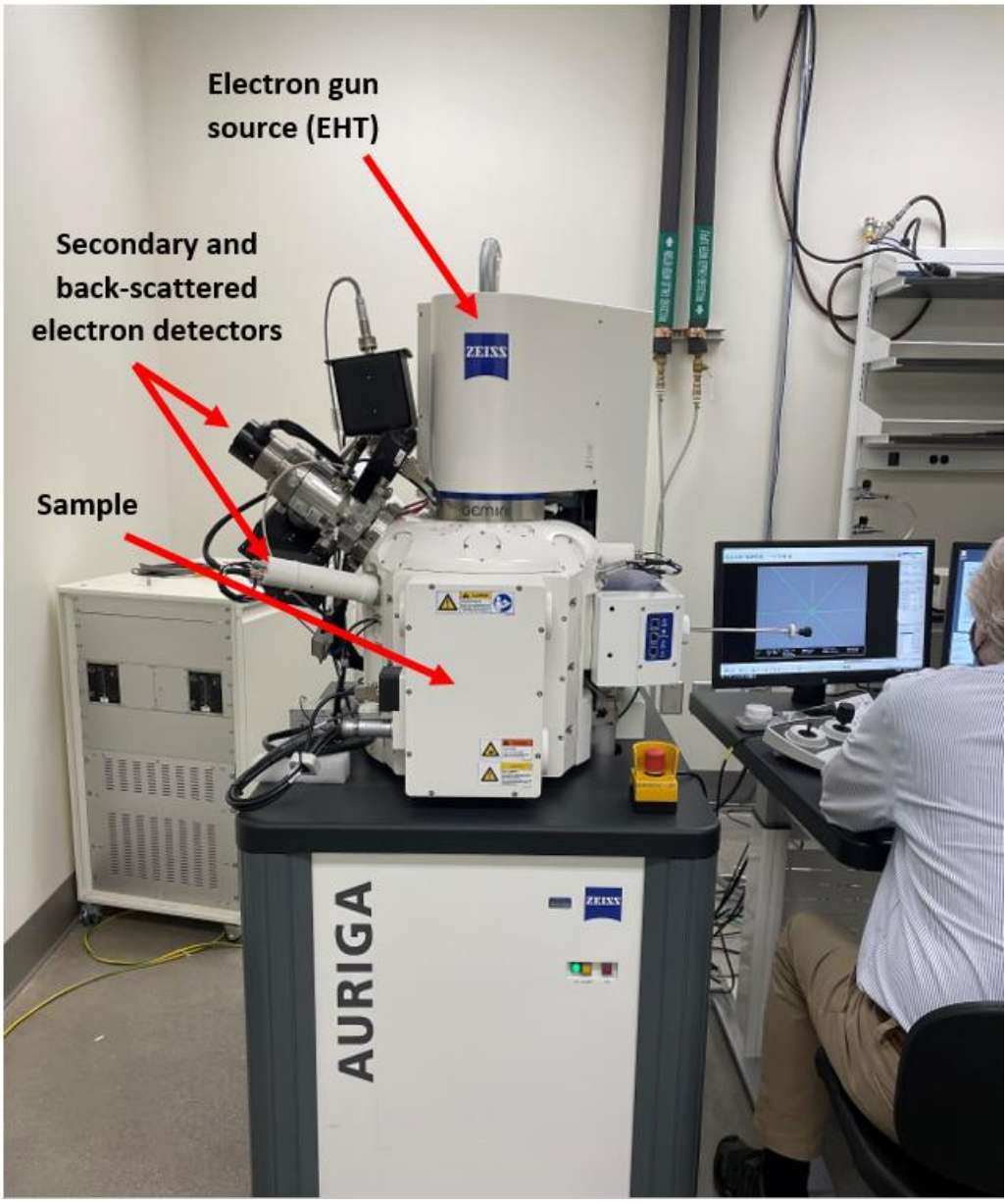

Fig. 2.11 Zeiss Auriga high-resolution scanning electron microscope (SEM)

selection of the working distance in between 8-10 mm from the pole piece. Similar settings are maintained for Zeiss Auriga, however, the magnification was increased to 40kX-80kX for obtaining high-resolution images of the Cu_xNi_{1-x} alloy catalyst and the graphene layers.

2.4 Raman spectroscopy measurements

The growth quality of graphene layers is confirmed by performing Raman spectroscopy measurements at the facility at General Graphene, Knoxville, TN. Basically, this involved capturing the Raman spectra (intensity vs Raman shift (cm^{-1})) and evaluating the peaks (G-1600 cm^{-1}, 2D-2690 cm^{-1}) relating to the structural disorder in graphene. The intensity ratio of 2D band to G band (I_{2D}/I_G) and full-width half maximum (FWHM) is also measured. Typically, Raman measurement involves focusing a laser (electromagnetic) beam (532 nm) onto a spot through a monochromator. Elastically scattered radiation at the wavelength corresponding to the laser line (Rayleigh scattering) is filtered out by a notch filter, edge pass filter or band pass filter and the rest of light is collected and dispersed onto a detector (Figs. 2.12 and 2.13) [80].

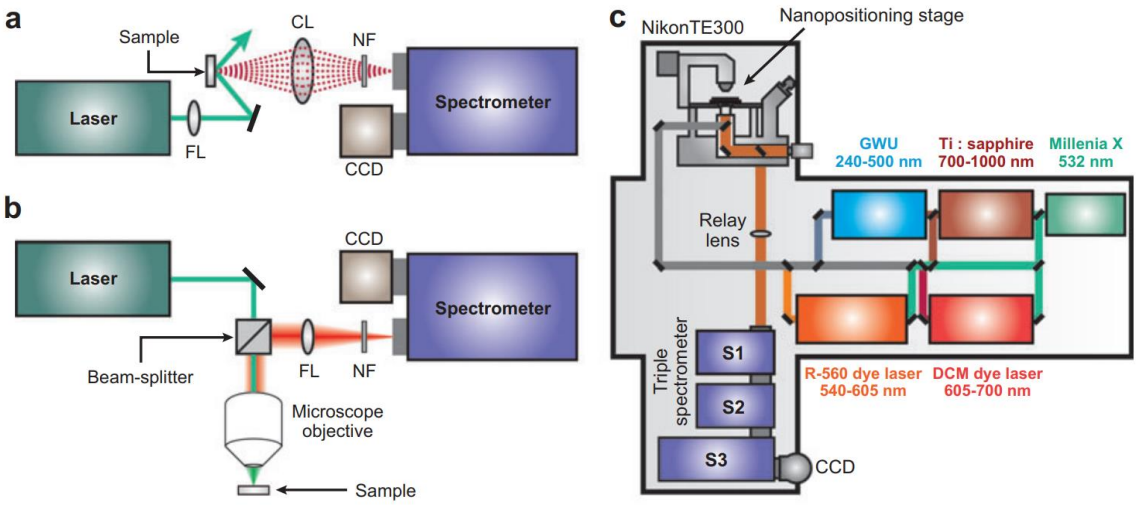

Fig. 2.12 Raman spectroscopy line diagram [80]

Fig. 2.13 Raman spectroscopy experimental setup at General Graphene

CHAPTER THREE

EXPERIMENTAL RESULTS

3.1 Combinatorial sputtering of Cu_xNi_{1-x} alloy

The number of graphene layers grown on Cu_xNi_{1-x} alloy combinatorial sputtered on Si/SiO_2 substrate can be controlled by the composition of Cu_xNi_{1-x} alloy. As a result, one of the initial tasks of this work involved sputtering Cu_xNi_{1-x} alloy thin film gradients on Si/SiO_2 substrates. The focus is on determining appropriate compositions of this alloy that provide uniform and coherent bilayer graphene growth. The rationale is to adjust the alloy carbon solubility such that bilayer graphene is formed at ~1000°C growth, where the solubility limit of carbon (C) in Cu is approximately 75 +/- 0.5 ppm and C in Ni is 1.3 at.% as per their respective phase diagrams. To achieve a large composition gradient, initially the corresponding powers for Ni and Cu target in the sputtering system was set to 200W (target bias ~560-570 V) and 115W (target bias ~280V), respectively (sputtering parameters maintained, Table 3.1). During this film growth, the substrate is not rotated to obtain a gradient of Cu_xNi_{1-x} alloy thin film with varying composition across the diameter of Si/SiO_2 wafer. A Cu_xNi_{1-x} alloy thin film with approximately uniform thickness of ~1 µm (Fig. 3.1) is obtained after sputtering for a period of ~ 1 hour and 6 minutes.

3.2 Characterization of sputtered Cu_xNi_{1-x} alloy thin film on Si/SiO_2 wafer

The composition of Ni and Cu across the combinatorically sputtered Cu_xNi_{1-x} alloy thin film on the Si/SiO_2 substrate is determined at five equi-spaced (16.6mm) positions (Fig. 3.2). The energy dispersive x-ray spectroscopy (EDS) analysis is performed on Carl Zeiss EVO scanning electron microscope (SEM) (Table 3.2). The EDS spectra of the 5 measurements across the gradient Cu_xNi_{1-x} thin film (Fig. 3.3) demonstrates the peak ratio of Cu and Ni varying as expected with Ni rich peak is observed at ~ 0.849 eV and Cu peak is obtained at ~ 0.928 eV, which is corresponding to the L_α values for both metals. The operating parameters were a working distance (WD) of 8-10 mm, 10 kX magnification, and an electron source voltage (EHT) for electron gun at 10kV.

Additionally, the HR-SEM images of all five positions across Cu_xNi_{1-x} alloy gradient (surface) is captured by Carl Zeiss Auriga SEM with operating conditions as EHT=5kV, WD=8-10mm and magnification: 40kX, 80kX (Fig. 3.4). The HR-SEM images show the Cu_xNi_{1-x} alloy grains very clearly as one moves from position#1 (Ni rich side) towards position#5 (Cu rich side). The grain size appears to be decreasing as one moves from Ni to Cu rich domains. Also, grain shape appears to be changing from disordered spheres to uniform spherical shaped structures along gradient of Ni to Cu rich regions. Glancing angle x-ray diffraction (GI-XRD) scans were taken at positions 1-5; the data shows a clear

Table 3.1 Combinatorial sputtering parameters

Time (mins.)	Gun#1 (Ni)			Gun#3 (Cu)		
	F	Volt (V)	R	F	Volt (V)	R
0	200 W	570	1	115 W	288	1
10	200 W	566	1	115 W	287	1
20	200 W	568	1	115 W	286	1
30	200 W	567	2	115 W	286	2
40	200 W	570	1	115 W	285	2
50	200 W	571	1	115 W	284	2
60	200 W	562	1	115 W	284	2
66	200 W	564	1	115 W	284	2

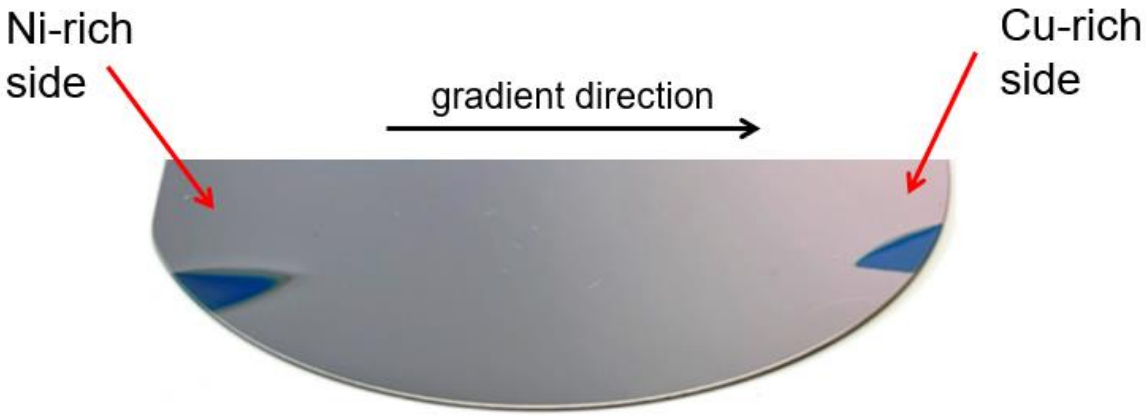

Fig. 3.1 Cu_xNi_{1-x} alloy thin film gradient combinatorial sputtering on Si/SiO_2 wafer

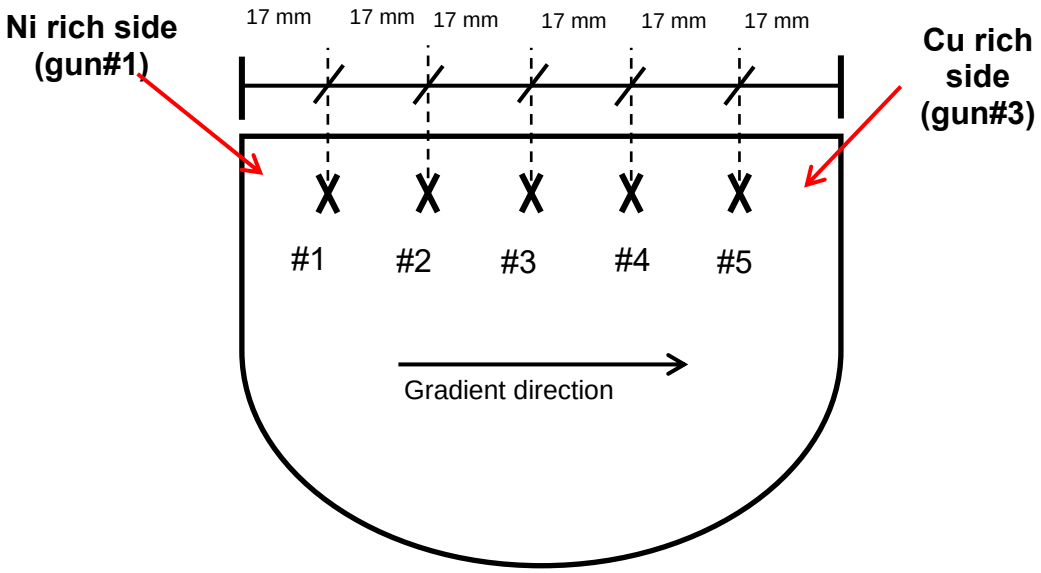

Fig. 3.2 EDS analysis of Cu_xNi_{1-x} alloy sputtered on Si/SiO_2 wafer with layout of positions for measuring at. % of Ni and Cu in the Cu_xNi_{1-x} alloy across gradient

Table 3.2 EDS analysis of Cu_xNi_{1-x} alloy film (Ni at.% and Cu at.%)

Position	**Cu (at. %)**	**Ni (at. %)**
#1	25	75
#2	35	65
#3	51	49
#4	68	32
#5	83	17

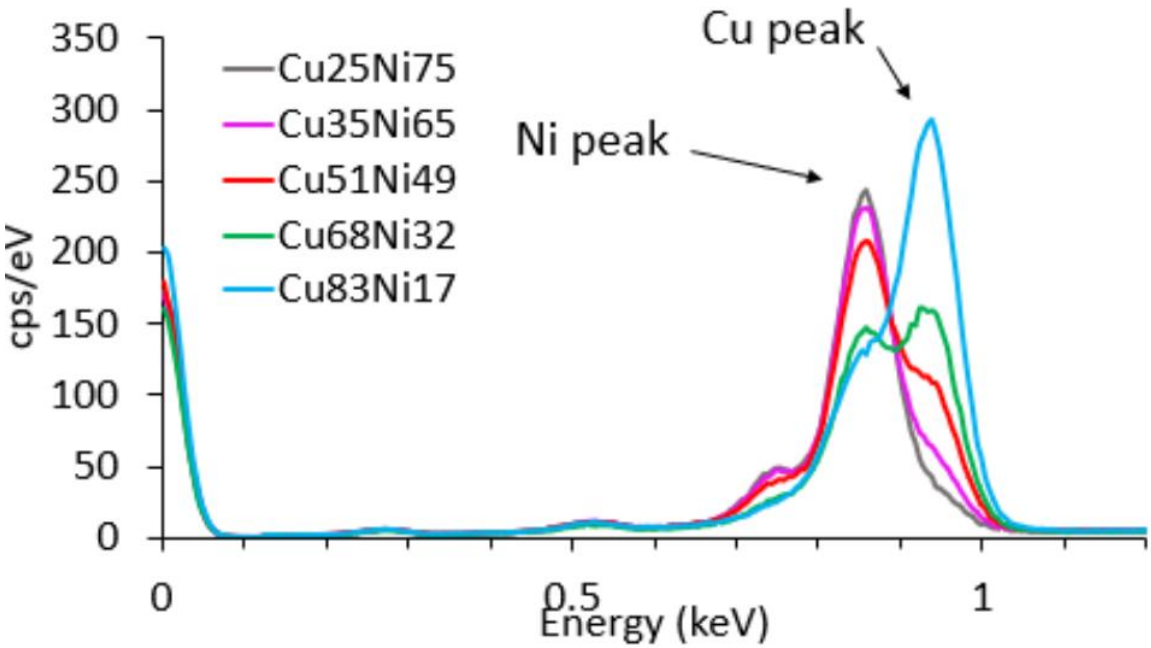

Fig. 3.3 EDS spectrum showing Ni and Cu peaks for all five positions across Cu_xNi_{1-x} alloy gradient

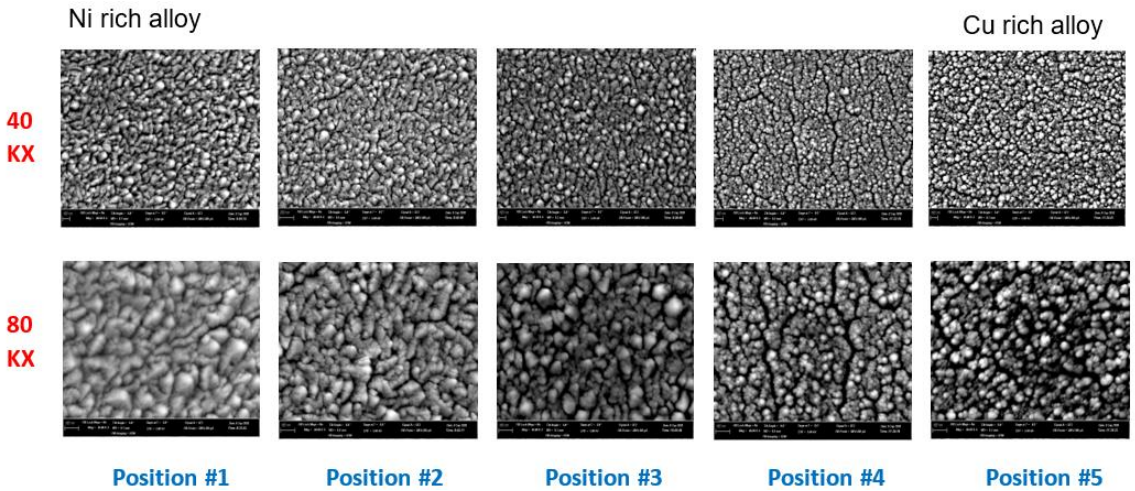

Fig. 3.4 HR-SEM imaging-position#1-5, magnification: 40kX, 80kX, EHT~5kV, WD~9mm

FCC structure with a solid solution where the peaks shift towards large 2θ values with increasing nickel concentration and the change in lattice parameter calculated by the software as ~3.53, 3.54, 3.55, 3.57 to 3.58 Å (Fig. 3.5). Consistent with the Vegard's law relationship, the composition calculation of this Cu_xNi_{1-x} alloy shows close match with experimental results for at. % from EDS analysis (Fig. 3.6) (Table 3.3).

The optical images of CVD graphene growth (Figs. 3.7 & 3.8) for this sputtered Cu_xNi_{1-x} alloy thin film gradient on Si/SiO_2 substrate show the graphene growth transition from high Cu at.% region (left side, Figs. 3.7 & 3.8) towards high Ni at. % region (right side, Figs. 3.7 & 3.8). Accordingly, we observed that at very high Cu at. %, the SiO_2 film didn't dewet properly shown by the light purple domains (Fig. 3.7). As we slowly move towards the higher at. % Ni side (right), we see some small graphene islands but still the area which did not dewet is higher. As we keep moving towards the elevated Ni at. % side (right) further, we realize an enhancement in the coverage of graphene island growth regions and reduction in areas which didn't dewet efficiently until the point where we see no further areas from improper dewetting but can detect complete coverage of area by uniform graphene domains. Beyond this point, as we keep moving towards higher Ni at. % regions (right side), we see an improvement (coherent) in the CVD graphene growth areas and can now perceive the multilayered regions in light brown color demonstrating the overlap of graphene layers. Thus, we concluded that the region showing the transition from monolayer to bilayer to multilayer graphene growth regions (high Cu at. %) is an interesting region for us. Accordingly, next we wanted to analyze the appropriate composition range for Cu_xNi_{1-x} alloy catalyst providing this fine regulation of the growth domains for varying the number of graphene layers.

Furthermore, the results from Raman spectroscopy (Fig. 3.9) of CVD grown graphene layers on Cu_xNi_{1-x} alloy gradient film confirm our hypothesis for the transition observed in CVD growth of graphene from monolayer to bilayer to multilayer graphene layers. For the regions which didn't dewet properly (extreme left, Fig. 3.7 & 3.8), we notice no peaks in the Raman spectra. As we move down (Fig. 3.9), we observe a sharp G peak (~1500 cm^{-1}) and 2D peak (~2700 cm^{-1}) intensity indicating the monolayer graphene domains. As we shift further down (Fig. 3.9), we observe an increase in the G peak intensity and decrease in 2D peak intensity reflecting the multilayered graphene islands formation on Cu_xNi_{1-x} alloy substrate. Thus, a decrease in intensity ratio of 2D/G peaks and an increase in full-width half maximum (FWHM) of 2D peaks is detected as one moves from monolayer (top) to multi-layer graphene regions (bottom).

3.3 Combinatorial sputtering of Cu_xNi_{1-x} alloy on Si with increased Cu power

As the bilayer graphene growth occurred at relatively higher copper concentration, we sputtered a second gradient sample with higher average copper

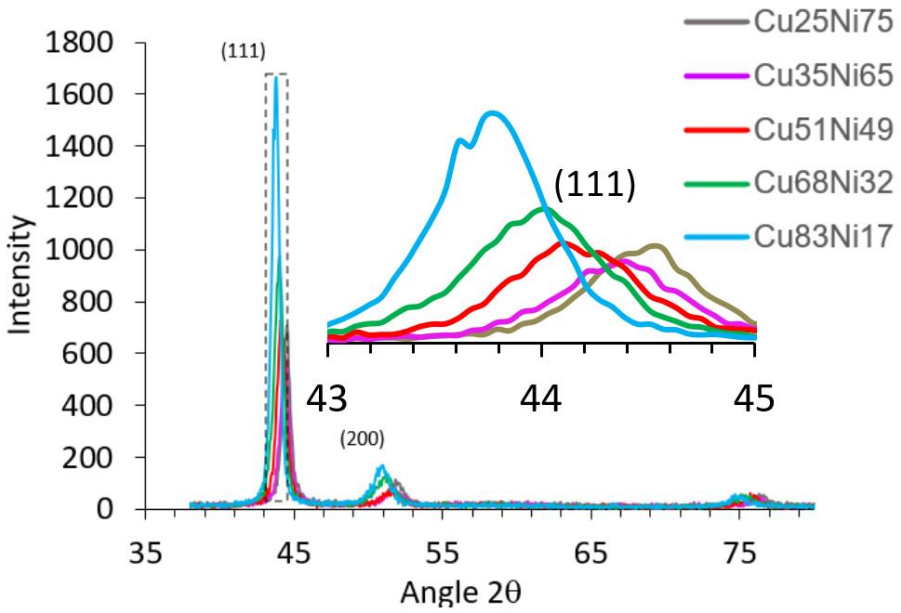

Fig. 3.5 GI-XRD plot showing shift in the position (2θ) of curves towards left for 5 positions across gradient as Ni at.% (concentration) decreases for Cu_xNi_{1-x} alloy

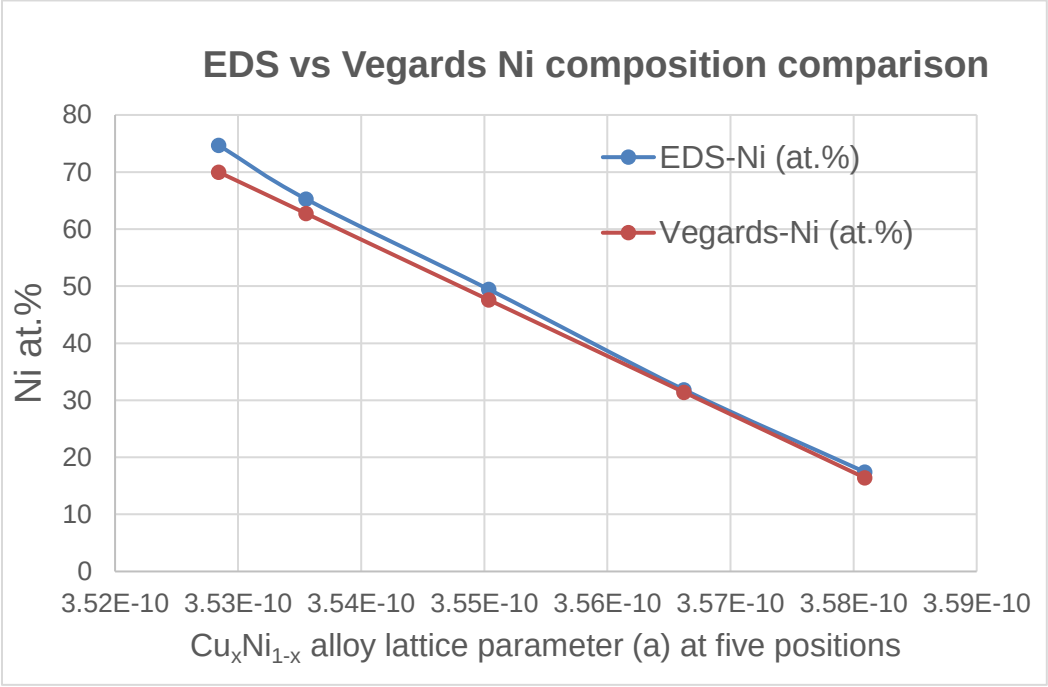

Fig. 3.6 EDS vs Vegards Ni at. % plot comparison for Cu_xNi_{1-x} alloy experimental lattice parameters at five positions across the gradient

Table 3.3 EDS vs Vegards Ni at. % comparison for Cu_xNi_{1-x} alloy experimental lattice parameters at five positions across the gradient

Position	**Lattice parameter** (GI-XRD)	**EDS Ni at. %**	**Vegards Ni at. %**
#1	3.5284E-10	75	70
#2	3.5355E-10	65	63
#3	3.5504E-10	49	48
#4	3.5662E-10	32	31
#5	3.5809E-10	17	16

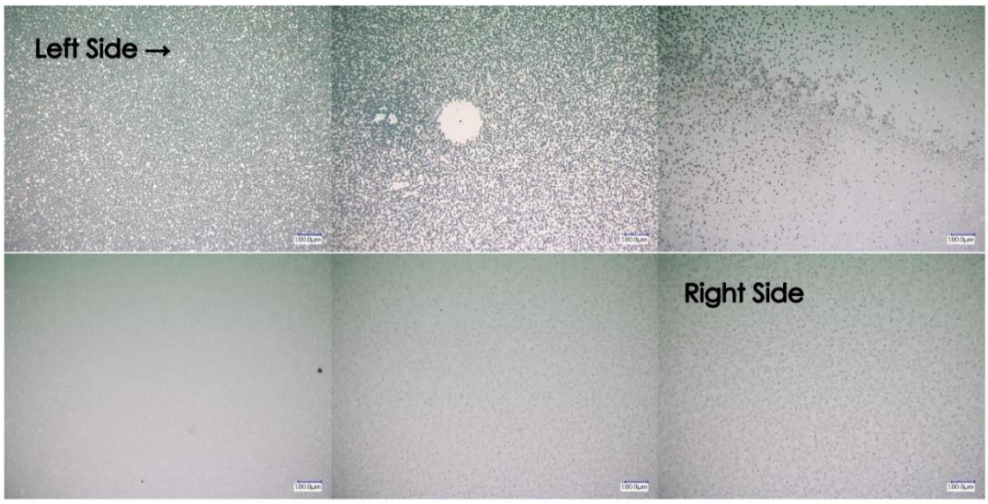

Fig. 3.7 Optical images of CVD graphene growth on Cu_xNi_{1-x} alloy at magnification scale of 100 µm from high Cu at. % rich region (left) towards high Ni at. % rich region (right)

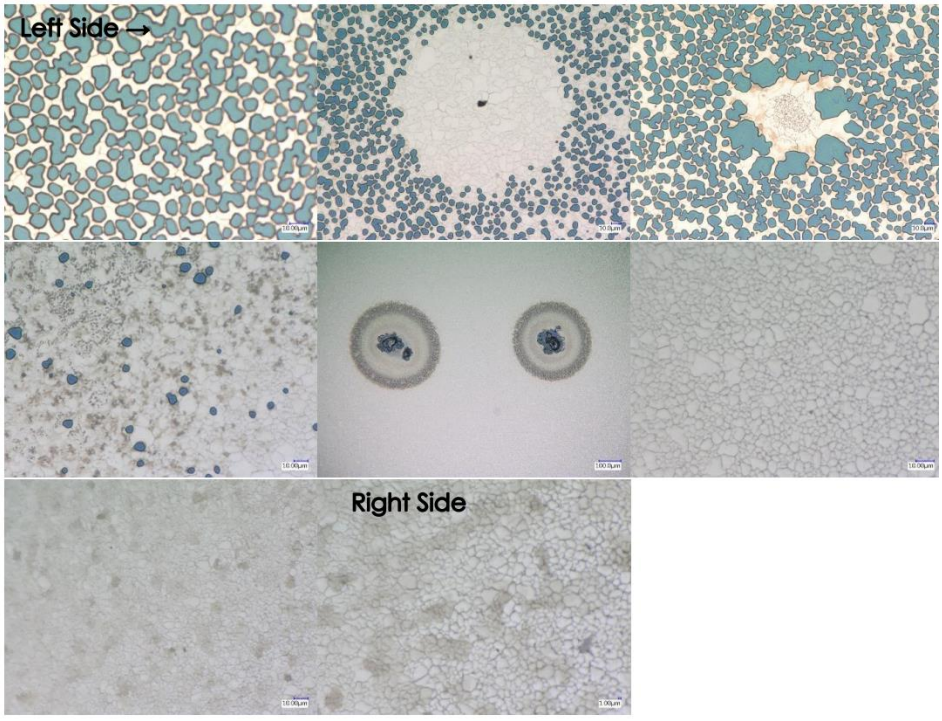

Fig. 3.8 Optical images of CVD graphene growth on Cu_xNi_{1-x} alloy at the magnification scale of 1 µm from high Cu at. % rich region (left) towards high Ni at. % rich region (right).

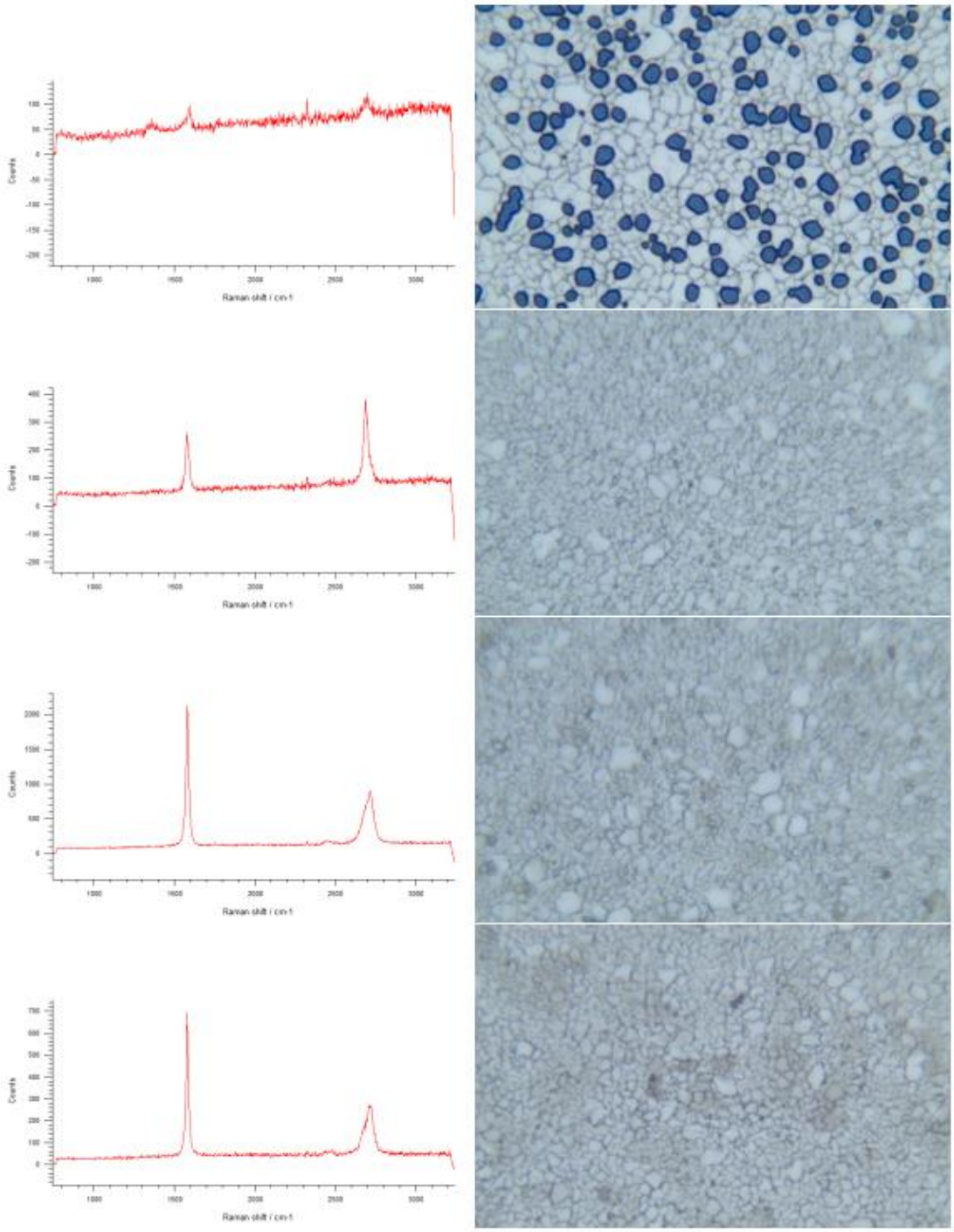

Fig. 3.9 Raman spectroscopy of CVD grown graphene layers on Cu_xNi_{1-x} alloy gradient film showing monolayer to bi-layer to multi-layer graphene transition. Increase in the G peak (~1500 cm^{-1}) intensity, decrease in 2D peak (~2700 cm^{-1}) intensity and increase of FWHM of 2D peaks as one moves from higher Cu at. % (top) to higher Ni at. % (bottom). Decrease in intensity ratio of 2D/G peaks is observed as one moves from mono-layered (top) to multi-layer region (bottom)

concentration to better elucidate the range for Cu_xNi_{1-x} alloy catalyst composition governing the monolayer to bilayer graphene transition (Fig. 3.10).

To do this we doubled the copper RF magnetron sputtering power (Tables 3.4 and 3.5). After increasing the sputtering power, EDS analysis at five positions across the Cu_xNi_{1-x} alloy film is performed with conditions for the SEM as magnification-10kX, EHT-20kV, working distance: ~8-10mm. The Cu_xNi_{1-x} alloy composition (at. % Cu, at. % Ni) for the five positions across the substrate from EDS analysis is found to be position #1 (~42%, 58%), position #2 (~51, 49%), position #3 (~69%, 31%), position #4 (~85%,15%) and position #5 (~94%, 6%) (Fig. 3.11 & Table 3.6) respectively. The L_α and K_α lines (Fig. 3.11) show the expected Cu/Ni peak ratio change with position along the gradient in composition (at. %) of the Cu_xNi_{1-x} alloy. A blow-up of L_α lines (Fig. 3.12) show the Cu and Ni peaks at ~0.85 and ~0.93 kV and that for K_α (Fig. 3.13) shows Cu and Ni peaks at ~7.47 and ~8.04 kV, respectively.

3.4 EDS analysis of initial CVD grown graphene layers on Si/SiO_2 substrate (test sample)

As per the optical images of initial CVD graphene growth (Figs. 3.7 & 3.8) on Cu_xNi_{1-x} alloy gradient on Si/SiO_2 substrate, we're able to conclude three different domains of interest based on the no. of layers of graphene received which is dependent on the change in Cu_xNi_{1-x} alloy composition as one moves from left (high Cu at. %) to right (high Ni at.%) of the Cu_xNi_{1-x} alloy sputter deposited substrate. Accordingly, we wanted to analyze appropriate composition range for Cu_xNi_{1-x} alloy catalyst providing this controlling of different growth domains for graphene layers especially for monolayer, bilayer and multilayer graphene growth modes.

Subsequently, a test sample (Fig. 3.14) from the high Cu at. % rich region (right) of first CVD graphene growth on the Cu_xNi_{1-x} alloy film sputter deposited on Si/SiO_2 initial wafer is cut out and analyzed under the EVO SEM (Fig. 3.12) at the operating conditions (magnification-10kX, EHT-20kV, working distance-8 to 10mm). As per EDS analysis, the at. % (Cu, Ni) of this transferred graphene layers from the high Cu at.% regions are analyzed at four locations from relatively higher Cu at.% (left) to lower Cu at.% (right) of test sample (Fig. 3.14). For the first two positions, the composition is found to be position #1 (~48% Cu, 52% Ni) and position #2 (~37%, 63%) respectively (Table 3. 7). The remaining two positions (#3 & #4) are found to have same composition as position #2. The L_α EDS spectrum show the Ni and Cu peaks at ~0.86, 0.92 kV and K_α spectra show the Ni and Cu peaks at ~7.47, 8.04 kV for the two positions respectively (Figs. 3.15-3.17).

The next step in this study involved exploring synthesis of graphene at higher Cu at.% and finding the appropriate composition governing the monolayer to bilayer

Table 3.4 Sputtering parameters maintained during run#1

Time (mins.)	Gun#1 (Ni)			Gun#3 (Cu)		
	F	Volt (V)	R	F	Volt (V)	R
0	200 W	504	1	230 W	429	3
15	200 W	503	1	230 W	424	3
30	200 W	510	2	230 W	422	3
45	200 W	505	2	230 W	421	3
60	200 W	502	2	230 W	418	3
75	200 W	497	2	230 W	416	3
90	200 W	505	2	230 W	414	3

Table 3.5 Sputtering parameters maintained during run#2

Time (mins.)	Gun#1 (Ni)			Gun#3 (Cu)		
	F	Volt (V)	R	F	Volt (V)	R
0	200 W	509	0	230 W	414	3
15	200 W	495	0	230 W	414	3
30	200 W	494	1	230 W	414	3
45	200 W	490	1	230 W	411	3
60	200 W	487	2	230 W	410	3
75	200 W	477	2	230 W	407	3
90	200 W	475	2	230 W	405	3

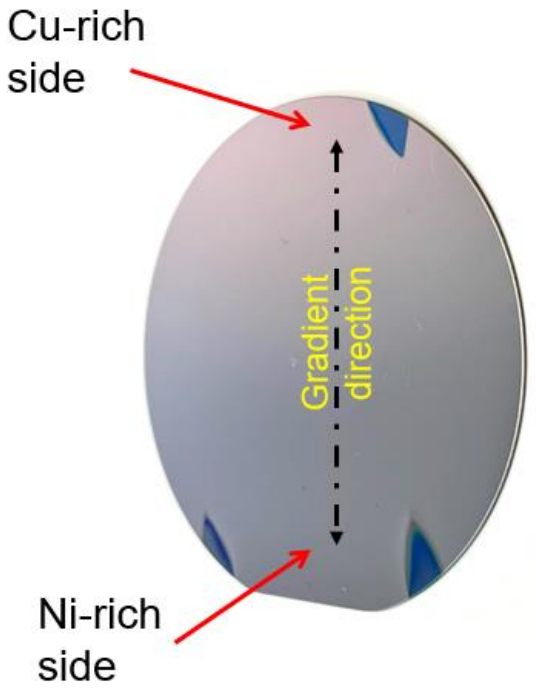

Fig. 3.10 Cu_xNi_{1-x} alloy combinatorial sputtering on Si/SiO_2 substrate (≅2 µm)

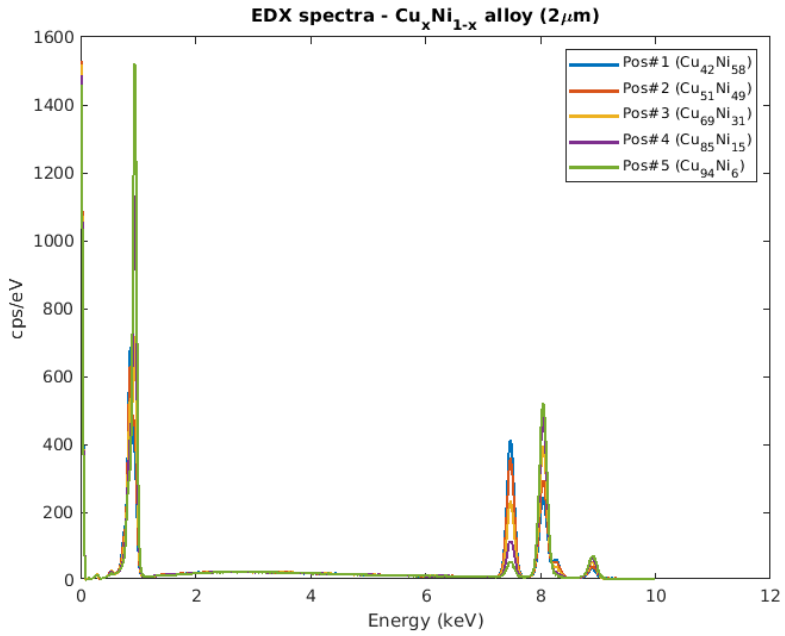

Fig. 3.11 EDS analysis of Cu_xNi_{1-x} alloy (K_α & L_α lines) showing Ni & Cu rich side

Table 3.6 Cu and Ni at.% from EDS analysis

Position	Cu (at. wt.%)	Ni (at. wt.%)
#1	42	58
#2	51	49
#3	69	31
#4	85	15
#5	94	6

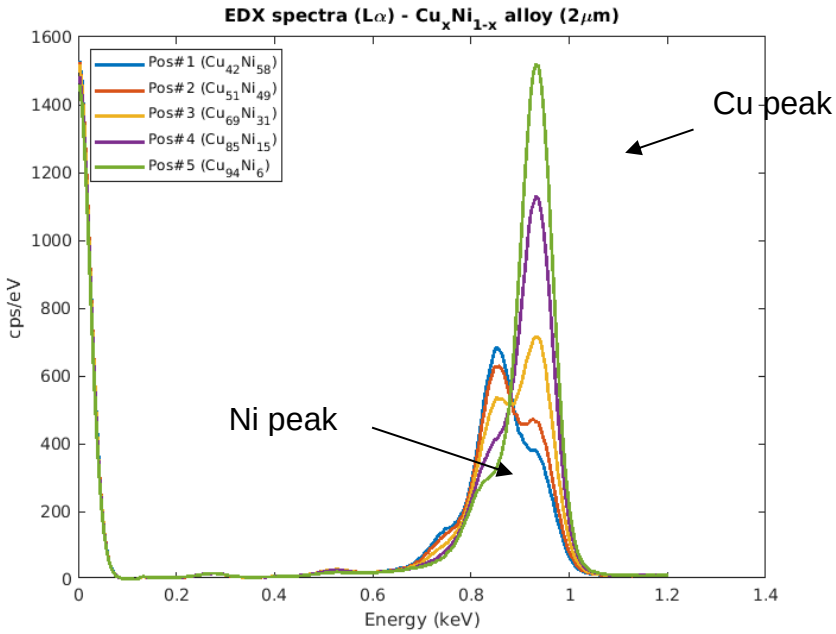

Fig. 3.12 Eds analysis (L_α) spectrum for five positions across Cu_xNi_{1-x} alloy gradient

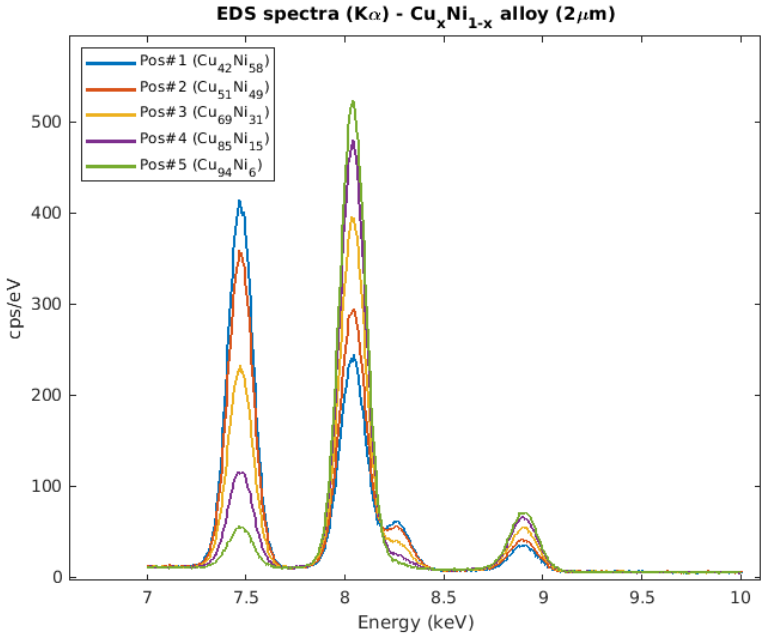

Fig. 3.13 EDS spectrum (K_α) for five positions across Cu_xNi_{1-x} alloy gradient

Table 3.7 EDS analysis with at. % Cu & Ni for the five positions across Cu & Ni gradient for CVD graphene growth on Cu_xNi_{1-x} alloy on 285 nm thick SiO_2 layer on Si wafer

at. %	Cu	Ni
Pos#1	89	11
Pos#2	85	15
Pos#3	69	31
Pos#4	49	51
Pos#5	35	65

EVO SEM parameters
EHT: 20 kV
WD: ~8-9 mm
Magnification: 10 kX
SE1 detector

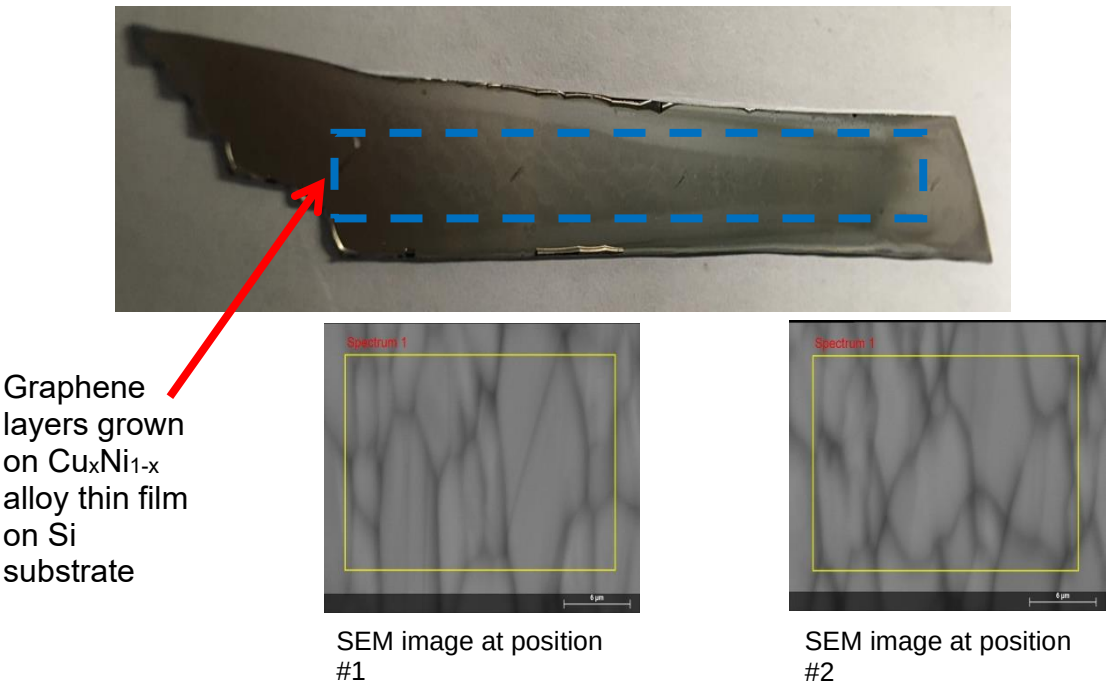

Fig. 3.14 Initial graphene growth (CVD) on combinatorial sputtered Cu_xNi_{1-x} alloy thin film (≅2 μm) on Si/SiO_2 substrate SEM-EDS analysis (test sample)

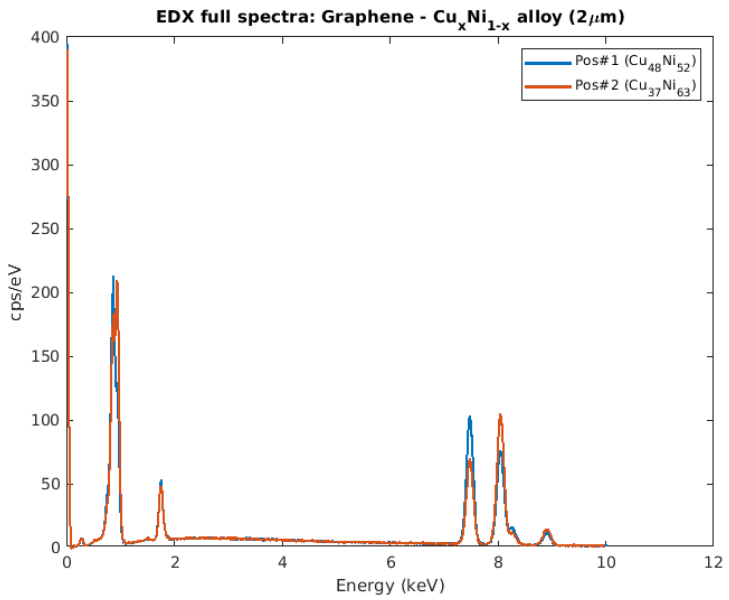

Fig. 3.15 EDS analysis (spectrum) of CVD grown graphene layers on Cu_xNi_{1-x} alloy (initial test sample)

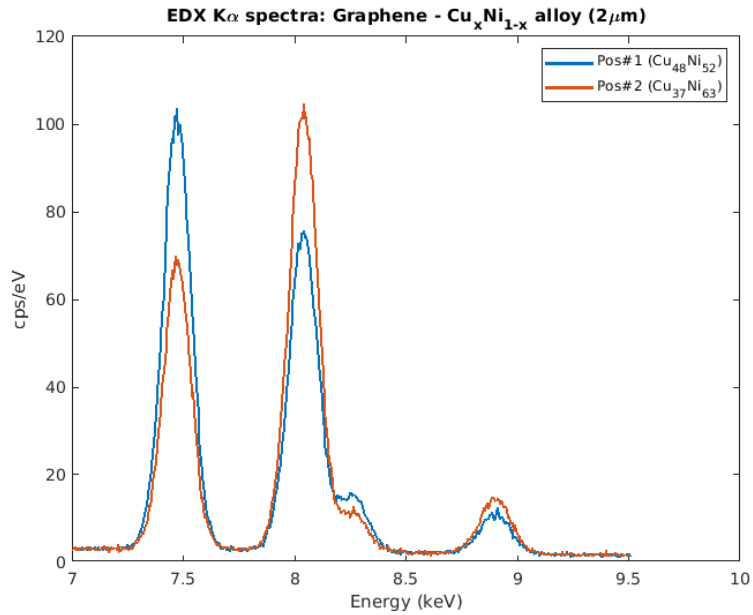

Fig. 3.16 EDS analysis (K_α) spectrum for graphene growth on Cu_xNi_{1-x} alloy gradient

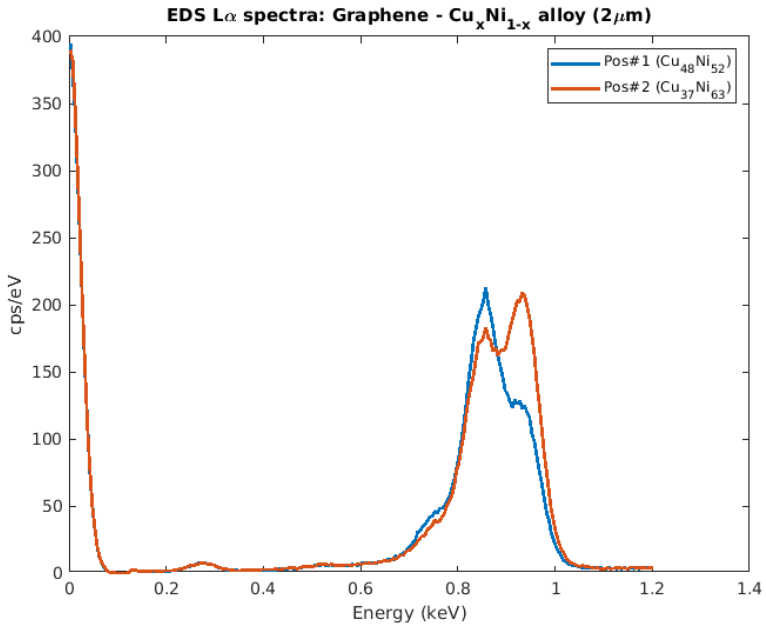

Fig. 3.17 EDS spectra (L_α) for graphene growth on Cu_xNi_{1-x} alloy on Si/SiO_2 substrate

graphene growth. As per our initial hypothesis, as the Cu at.% increases, the low solubility of C in Cu provides less amount of C atoms available for forming the graphene layers upon cooling in the thermal CVD furnace from 1000 °C to RT. Furthermore, this study would provide better understanding for finely manipulating (regulating) the growth of number of graphene layers based on the composition of Cu_xNi_{1-x} alloy catalyst sputter deposited on Si/SiO_2 substrate.

3.5 CVD graphene growth at higher Cu at. % of Cu_xNi_{1-x} alloy

As discussed earlier, the number of graphene layers formed during CVD process depends upon the temperature set inside the furnace and the composition of Cu_xNi_{1-x} alloy deposited on Si/SiO_2 substrate. To realize the composition of Cu_xNi_{1-x} alloy associated with the corresponding locations of monolayer, monolayer to bilayer transition and bilayer to multilayer graphene growth transition in the high Cu at. % rich region (~42 - 94% Cu), Raman spectroscopy was performed on graphene growth by CVD process for a set of Cu_xNi_{1-x} alloy sputter deposited on Si/SiO_2 samples at different growth temperatures of 1000 °C, 1020 °C and 1050 °C.

At 1000 °C, we observe the G peak (~1600 cm^{-1}) and 2D peak (~2700 cm^{-1}) for regions 1-4 and small intensity G peak for region 5 (Fig. 3.18). Regions 3-5 represent monolayer graphene regions with intensity ratio $I_{2D/G} > 1$ ($\cong 2$) which is Cu at. % > ~69%. Regions 1 and 2 represent multilayer graphene domains which refers to Cu at. % < ~51%. Regions with intensity ratio of $I_{2D/G}$ ~1 demonstrating domains of AB stacked bilayer zones fall between the regions of 2 and 3 which is Cu at. % in range 51-69%. As per Raman spectra, the multilayer to monolayer transition occurs from regions 3-2 for Cu at. % decreasing from 69-51%. The Raman spectra reflects 2D peak with more width (FWHM) as the no. of layers transition from monolayer to bilayer and tri-layer region (Fig. 3.18) which is shift from regions 5-1. Typically, the D-mode is caused by the disordered structure of graphene (sp^2 hybridized carbon systems). However, the absence of D peaks (1350 cm^{-1}) and presence of both narrow G and 2D peaks in Raman spectra demonstrate high quality monolayer graphene films (Fig. 3.18) at temperature of 1000 °C.

At 1020 °C, the G and 2D peaks are missing for regions 3-5, which show thin film with no monolayer and multilayer graphene domains formation (Fig. 3.19). Monolayer graphene domains are observed for regions 1 and 2 (Fig. 3.19). At 1050 °C, the Raman spectra is showing wider and shorter G and 2D peaks with an additional small D peak at 1600 cm^{-1} demonstrating that the layers are rotated and of poor quality (fig. 3.20) indicating disorderly layers. A more intricate synthesis process is observed for growth at higher temperatures.

Additionally, particle (dot) formation (aggregates) is observed (please refer to the appendix section at end of thesis for details) in the regions of high Cu at. %,

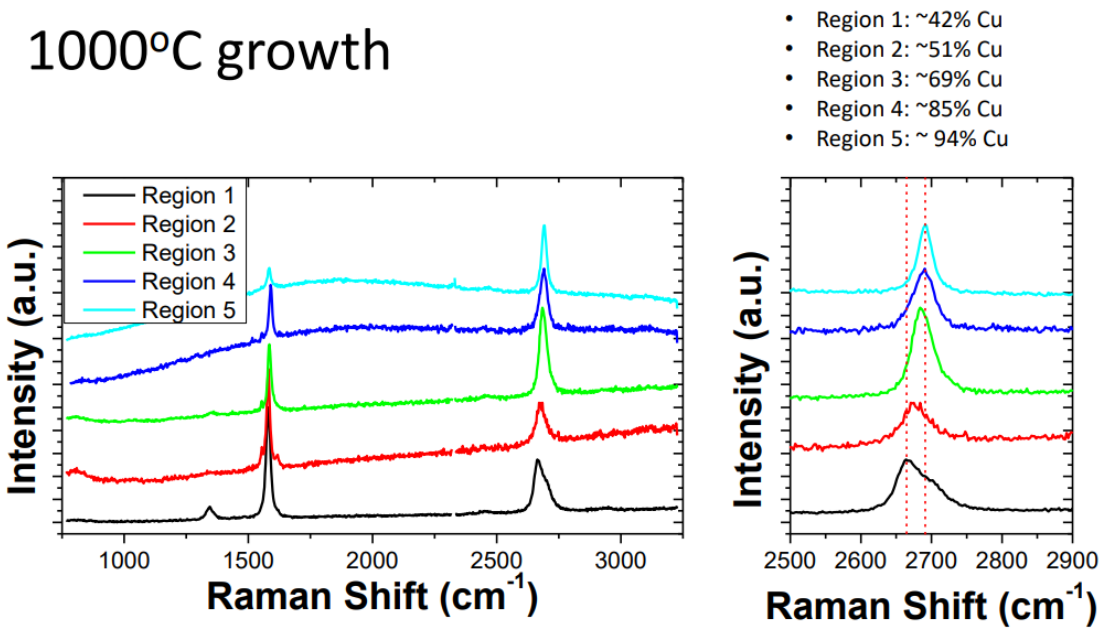

Fig. 3.18 Raman spectra for graphene CVD growth at 1000 °C with 5 regions of varying Cu at.% and 2D peak blow-up

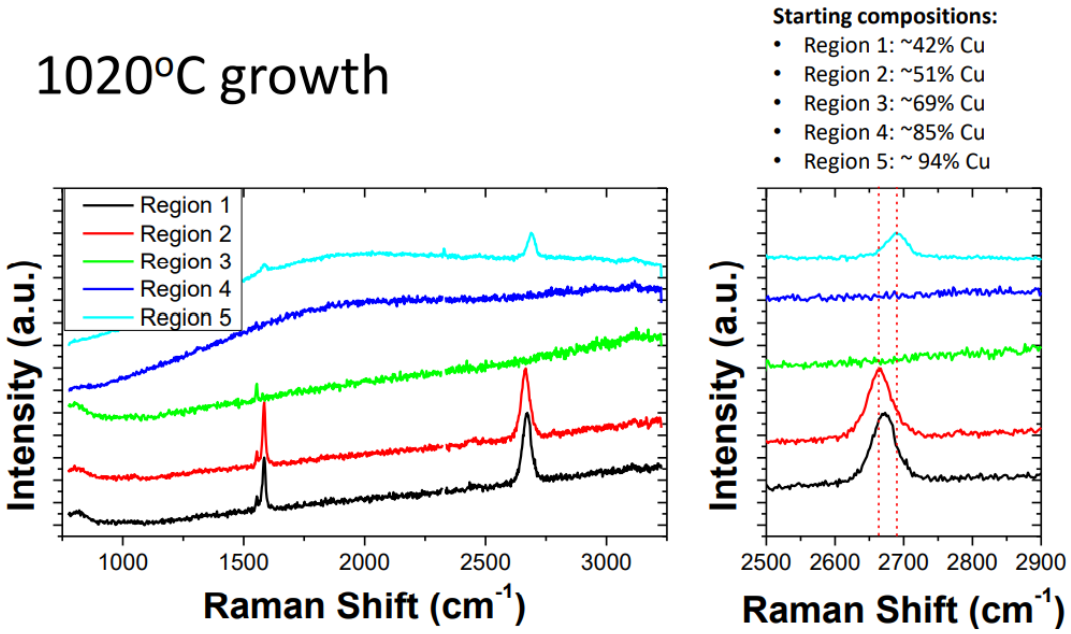

Fig. 3.19 Raman spectra for graphene CVD growth at 1020 °C with 5 regions of varying Cu at.% and 2D peak blow-up

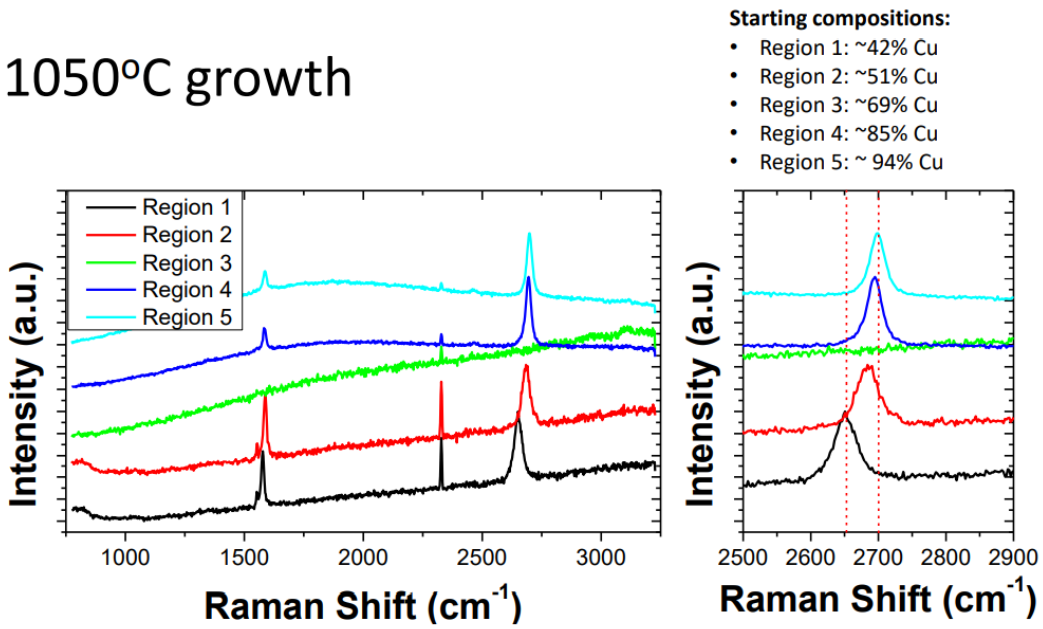

Fig. 3.20 Raman spectra of graphene CVD growth at 1050 °C with 5 regions of varying Cu at.% and 2D peak blow-up

which is assumed to be metal (copper) silicide ($SiCu_x$). The optical images of graphene grains at two locations, one at the center of wafer (Appendix I, Fig. 1) and other near the high Cu at.% region (Appendix I, Fig. 2) shows that the silicide formation in latter can be related to the discoloration and small grains. To confirm our hypothesis if the silicide particle (dot) formation (Appendix I, Fig. 3) is either copper silicide or silicide oxide (SiO_x), EDS analysis of graphene growth on Cu_xNi_{1-x} alloy deposited under same conditions on Si/SiO2 wafer is performed at 5 kV EHT.

The EDS analysis for CVD graphene growth with dots by area selection covering all dots (Appendix I, Figs. 3 and 4) show at. % Ni-3.47% and Cu-96.25%. For the region on graphene layer growth without any dot formation (Appendix I, Figs. 5 and 6), EDS analysis show at. % Ni-51.20% and Cu-48.79%. Additionally, EDS analysis of silicide particles by drawing small circular areas (selection) covering only dots (Appendix I, Figs. 7 and 8) show at. % Cu-94.07%, Ni-3.83%, Si-0.40% and O-1.7%. The EDS mapping (Appendix I, Figs. 9 and 10) of the dots clearly shows presence of oxygen and thus, SiO_x (SiO_2) particle formation is concluded (Appendix II).

As a first step in reducing formation of metal silicide particle formation, thickness of oxide layer (SiO_2) on top of Si wafer is increased to ~285nm from lower quality ~100 nm SiO_2 layer thickness. Accordingly, a thin film of Cu_xNi_{1-x} alloy is sputtered on thicker (~285 nm) SiO_2 oxide layer on Si wafer under similar operating conditions as last time. After CVD graphene growth at 1000 °C, Raman spectroscopy measurements (Appendix III, Figs. 11 and 12) are taken at 5 spots including the center of wafer (each point 2 cm apart) showing nice 2D and G peaks for first 3 regions with respective intensity ratios of bands (range) $I_{2D/G} \cong$ 0.34-1.02, 0.3-2.02, 0.71-2.06 with majority of area showing $\cong$1, which complies a consistency with AB-stacked bilayer graphene. The Raman measurements for CVD graphene growth at 1050 °C show some wide 2D peaks for regions with Cu at. % in-between 51%-85% (Appendix III, Figs. 13 and 14). However, the G peaks are missing for all regions. This implies incoherent CVD growth of graphene at 1050°C.

The EDS analysis of CVD grown graphene sample at 1000°C is performed at 20 kV EHT at 5 locations with 2 positions along each side off the center (including center as position) near the diameter edge (~1 cm below edge) of Si/SiO_2 wafer along horizontal Cu_xNi_{1-x} alloy gradient direction with 2 cm gap in-between these positions (Fig. 3.21). As per EDS analysis, at. % (Cu, Ni) for all five positions (Table 3.7) is analyzed to be #1 (~89% Cu, 11% Ni), #2 (85% Cu, 15% Ni), #3 (69% Cu, 31% Ni), #4 (49% Cu, 51% Ni), #5 (35% Cu, 65% Ni). As matching with the previous results, there are three positions on the wafer, one at the center and remaining two positions from the center towards the Ni rich region showing no silicide particle formation (Fig. 3.21(c)-(e)). The EDS spectra (Fig. 3.22) for five positions show gradient with peaks for Ni and Cu rich regions. A blow-up of the

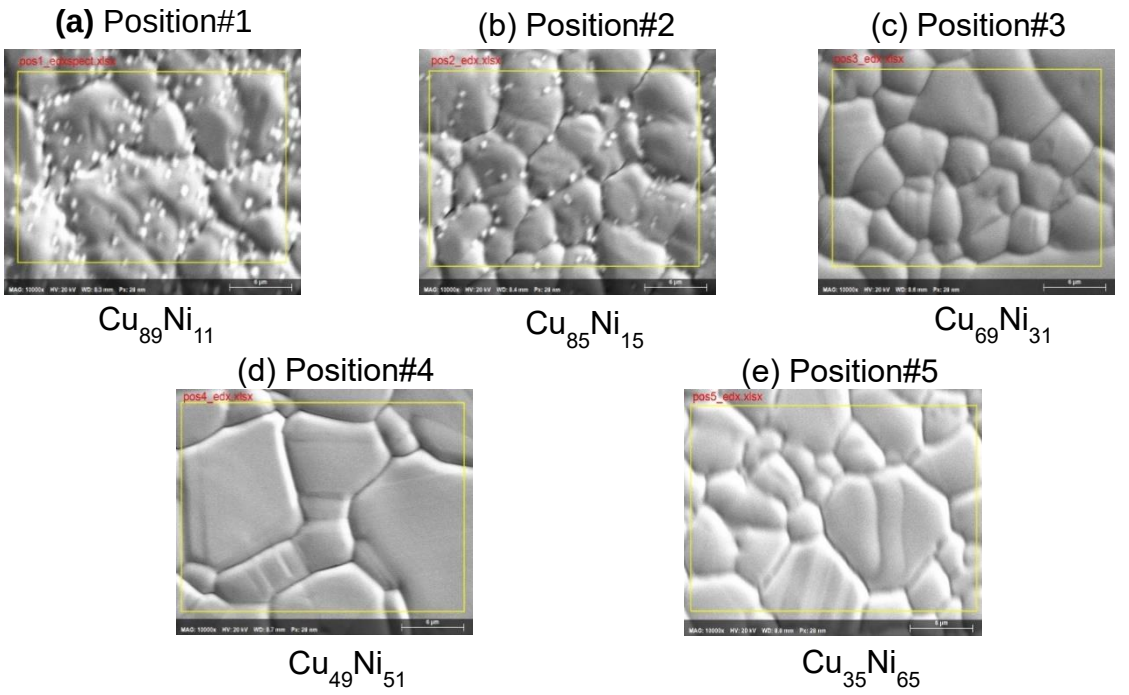

Fig. 3.21 SEM images taken at 20kV EHT source from EDS analysis for varying Ni and Cu at.% in Cu_xNi_{1-x} alloy (a) position#1-$Cu_{89}Ni_{11}$, (b) position#2-$Cu_{85}Ni_{15}$, (c) position#3-$Cu_{69}Ni_{31}$, (d) position #4- $Cu_{49}Ni_{51}$, (e) position #5-$Cu_{35}Ni_{65}$

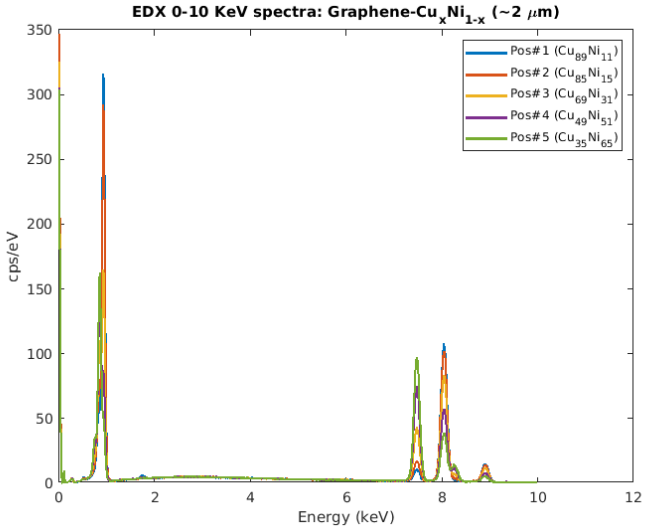

Fig. 3.22 EDS spectra (0-20 kV) of CVD graphene growth on Cu_xNi_{1-x} alloy on 285 nm SiO_2 layer on Si substrate

EDS spectra from 0-10 kV (Fig. 3.22) and from 7-10 kV (Fig. 3.23) show nice gradient in the at.% of Cu and Ni peaks.

3.6 Confirmation of variation in graphene thickness with gradient in composition of Cu_xNi_{1-x} alloy catalyst thin film

As one can infer, the 2D/G ratio decreases when moving from the Cu-rich side of catalyst to the Ni-rich side, which is observed to be consistent with number of layers increasing (Fig. 3.24(a)). Luminescent background decreases going from Cu-rich to Ni-rich side. Luminescence of the base catalyst is mostly quenched by alloying the Cu with ~30% Ni (Fig. 3.24(a)). Ni-rich 2D peak is composed for multiple peaks and not a single Lorentzian peak (Fig. 3.24(b)). Cu-rich side is composed of a single peak. It provides further confirmation of a transition from single to multilayer graphene across the catalyst. Thus, gradient catalyst of Cu_xNi_{1-x} alloy is indeed effective in growing a gradient in varying thickness and therefore can serve as a method to rapid prototype recipe/catalyst combinations to grow graphene of controllable thickness.

A coarse gradient confirming transition from multilayer and monolayer graphene is demonstrated (Fig. 3.25). Optical images of graphene transferred from the gradient catalyst onto Si wafer show the variation in areal coverage by change of color. Low Cu at.% (or high Ni at.%) results in non-uniform multilayer coverage (2D/G<1) as one can interpret from the optical images and 2D/G Raman maps. Low Cu at.% (high Ni at.%) results in large variation in graphene thickness. Graphene thickness is often larger at grain boundaries because these regions have high carbon mobility (nucleation) and results in more graphene precipitation during cooling. Both bilayer and monolayer coverage are observed at 69 at.% Cu. Uniform monolayer graphene (2D/G>1) corresponds to 94 at.% Cu. Transition from bilayer to monolayer graphene regions is observed for compositions ~69 at.% Cu.

A smooth gradient from monolayer to bilayer graphene is observed for graphene grown on Cu_xNi_{1-x} alloy catalyst from 61-85 at.% Cu (Fig. 3.25). 85 at.% Cu results in monolayer graphene (2D/G>1). The 69 at.% Cu corresponds to a mixture of monolayer and bilayer graphene. 61 at.% Cu matches large area coverage of bilayer graphene (for bilayer 2D/G ~1). Consequently, catalyst gradient provided us to rapidly recognize a recipe/composition that helps in regulating bilayer graphene growth.

Finally, we conclude that for Cu_xNi_{1-x} alloy catalyst, single layer graphene growth occurs with $x>68.9\%$, bilayer growth dominates in the range of $47.6\%<x<68.95\%$ and multilayer (>=3) growth occurs for $x<47.6\%$.

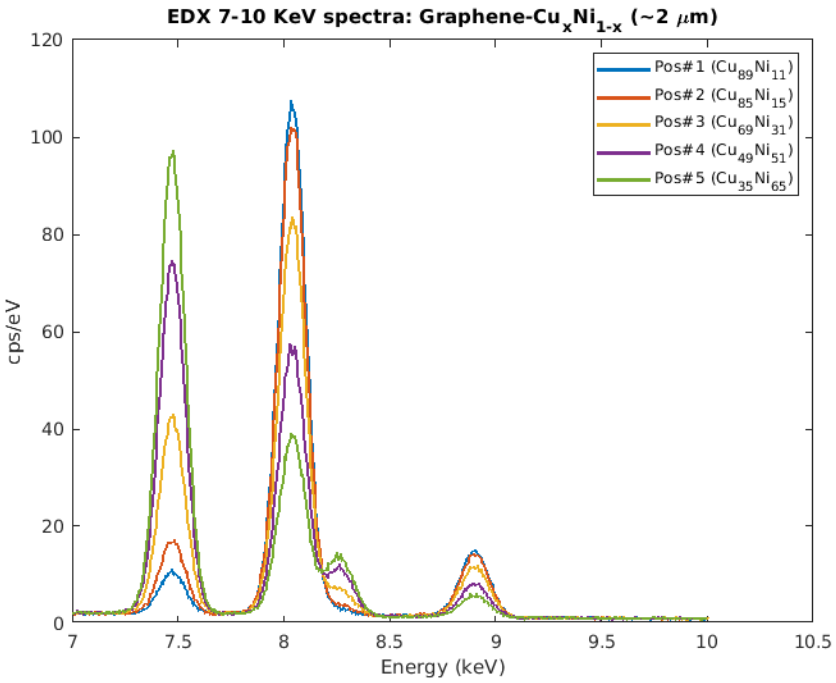

Fig. 3.23 EDS spectra blow-up (7-10 kV) of CVD graphene growth on Cu_xNi_{1-x} alloy on 285 nm thick SiO_2 layer on Si wafer

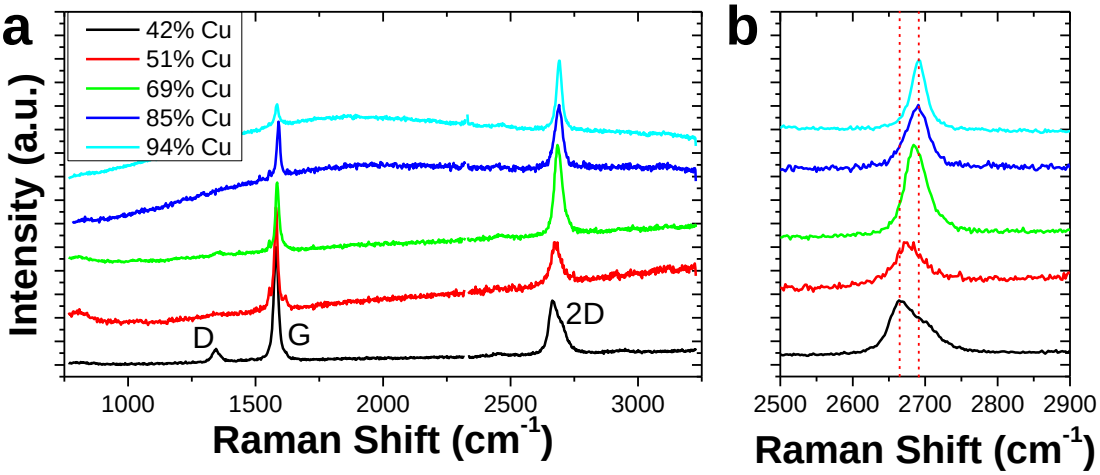

Fig. 3.24 (a) Raman spectra of graphene grown on composition gradient Cu_xNi_{1-x} catalyst and (b) Raman spectra showing magnified 2D peak spectra for graphene grown on the composition gradient Cu_xNi_{1-x} catalyst

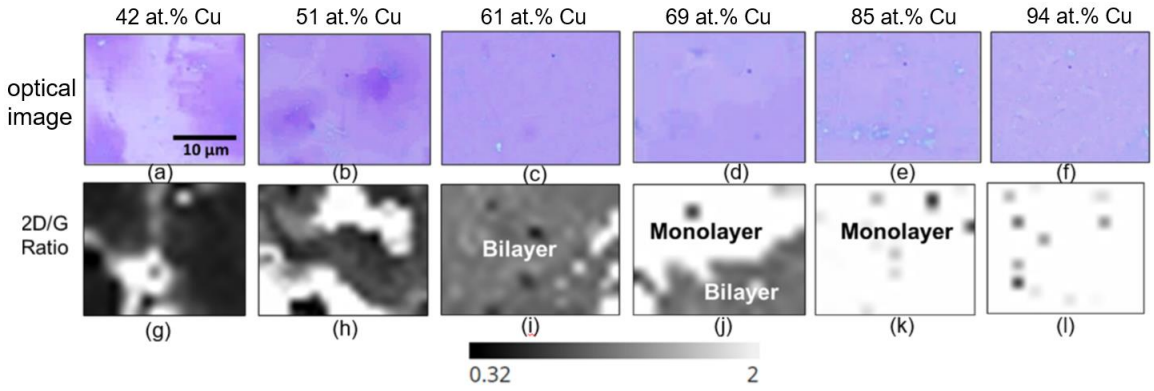

Fig. 3.25 Optical images of graphene grown on the Cu_xNi_{1-x} alloy gradient catalyst (42-94 at.% Cu) after transfer to Si wafer. Raman maps report the 2D/G ratio of the transferred graphene showing graphene layer thickness

3.7 Discovering optimum Cu at.% for bilayer CVD graphene growth on magnetron sputtered Cu_xNi_{1-x} alloy on Si/SiO_2 substrate

The steps for identifying novel Cu at. % (composition) favoring bi-layer graphene CVD growth involved measurements of Raman (spectra and mapping) for region on the bilayer growth showing both sharp G peak at 1600 cm^{-1} and 2D peak at 2700 cm^{-1} with intensity ratio $I_{2D/G} \cong 1$. Accordingly, bi-layer coverage is estimated to be around 63 mm from the Cu rich side of wafer, which is showing approximately around ~60-61 at.% Cu. For confirming this composition, EDS analysis is performed at this position and at points every 2 mm in the range covering +/- 10 mm off this 63 mm spot (Table 3.8) which is 53-73 mm region off the Cu rich side (Fig. 3.26).

The composition at 63 mm spot is found to be Ni-41.4 at. % and Cu-58.6 at. % (Table 3.8). SEM images show coherent bilayer islands in this region (Figs. 3.27) and the spectrum from EDS analysis show peaks of Ni and Cu almost overlapping and thus demonstrating small change in composition of Ni and Cu from 31.05 at.% (63 -10 mm) to 52.44 at.% (63 +10 mm) and 68.95 at. % (63 -10 mm) to 47.56 at. % (63 +10 mm) respectively (Figs. 3.28-3.31). The next step involved wet transfer of bi-layer graphene layer onto fresh Si/SiO_2 substrate after etching out the Cu_xNi_{1-x} alloy layer below graphene layer. The optical image (Fig. 3.32) confirms CVD growth of uniform bilayer islands on the wafer, which is confirmed by the Raman spectroscopy measurements (Fig. 3.33) demonstrating a narrow G peak (1600 cm^{-1}) and comparatively wider 2D peak (2700 cm^{-1}) indicating an intensity ratio $I_{2D/G} \cong 1$.

3.8 Large area bi-layer CVD graphene growth (~Cu 63 at.%)

After obtaining the composition of ideal Cu at.% as 63 at.% (~37 at.% Ni) in the best possible bi-layer domain of uniform and coherent growth, the next step involved sputtering a uniform Cu_xNi_{1-x} alloy thin-film (without any gradient) on a test Si/SiO_2 wafer (100 nm SiO_2). To do so, we had set the Ni and Cu target bias to 120 W and 115 W respectively and sputtered for 3 hours with rotation of the sample for obtaining uniform and thick films of >3 μm across the wafer (Fig. 3.34). The sputtering parameters including the bias voltage and reflected power (Table 3.9) is found to be stable during the process. EDS analysis is performed to confirm the composition of Cu is ~63 at.% in a radius region of 3 cm at four points along the X and Y axes (Fig. 3.35). The composition of Cu at these 4 locations starting from the center of wafer is analyzed to be 62.27, 63.08, 63.58, 63.63, 63.84 which is nearly matching our estimate of Ni at.% ~63 at.% for bi-layer growth of graphene film (Table 3.10). The EDS spectra (Figs. 3.36, 3.37) shows a curve with distinctive Cu and Ni gradient peaks at K_α=7.48 eV and K_α=8.046 eV respectively for SEM-EDS parameters of EHT-20 kV, working distance ~8-10 mm and magnification of 10 kX.

Table 3.8 EDS analysis of graphene bilayer on Cu_xNi_{1-x} alloy sputtered on Si/SiO_2

Location	Ni atomic%	Cu atomic%	x co-ordinate (mm)	y co-ordinate (mm)
63 mm	41	59	75	81
63+2mm	44	56	75	83
63+4mm	46	54	75	85
63+6mm	48	52	75	87
63+8mm	50	50	75	89
63+10mm	52	48	75	91
63-2 mm	39	61	75	79
63-4 mm	37	63	75	77
63-6 mm	35	65	75	75
63-8 mm	33	67	75	73
63-10 mm	31	69	75	71

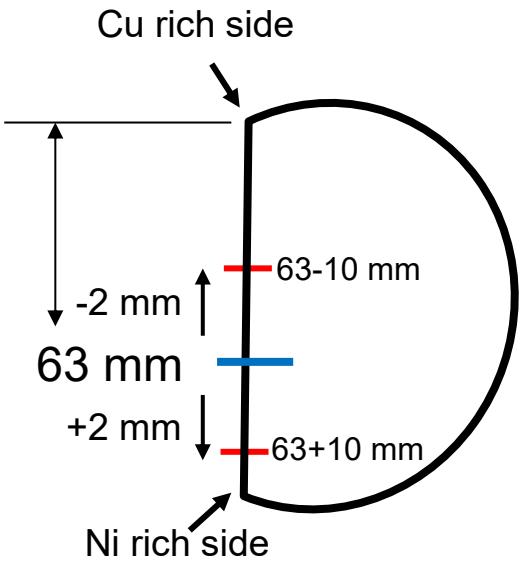

Fig. 3.26 Location of region showing bi-layer growth is ~63mm from Cu rich side

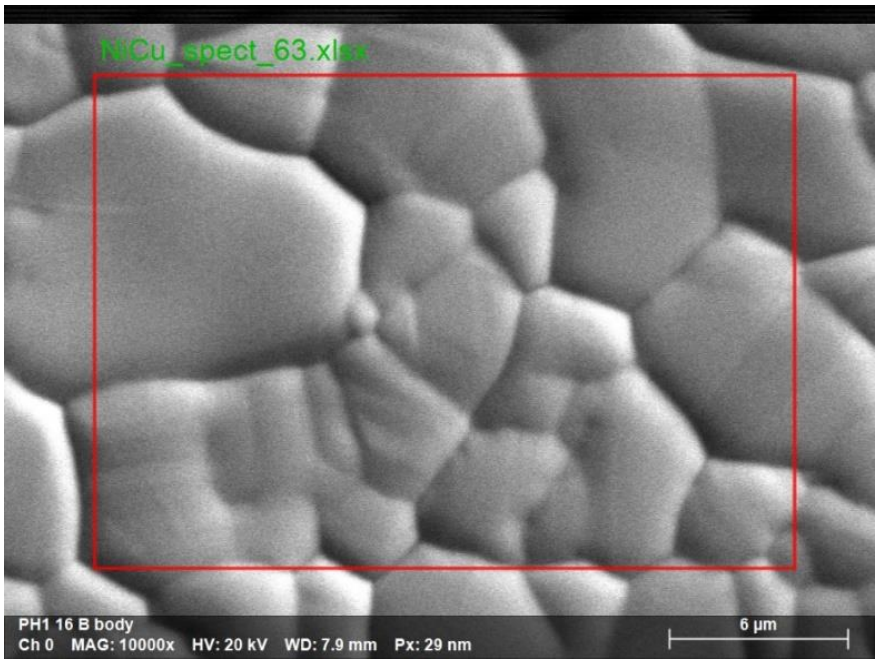

Fig. 3.27 EDS analysis at 63 mm position (Cu-58.6 at.%, Ni-41.4 at.%)

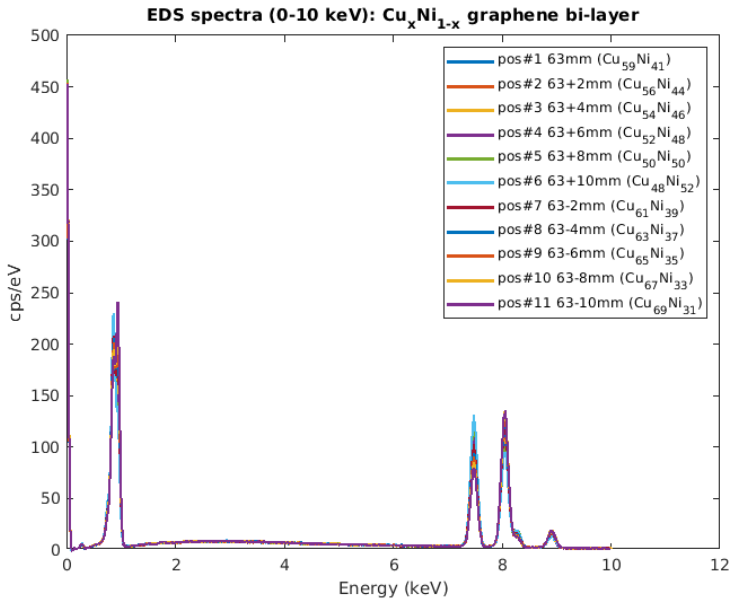

Fig. 3.28 EDS analysis spectra for Cu_xNi_{1-x} alloy composition gradient across the bi-layer region (+/- 10 mm from 63 mm spot) showing Ni and Cu peaks for K_α and L_α lines.

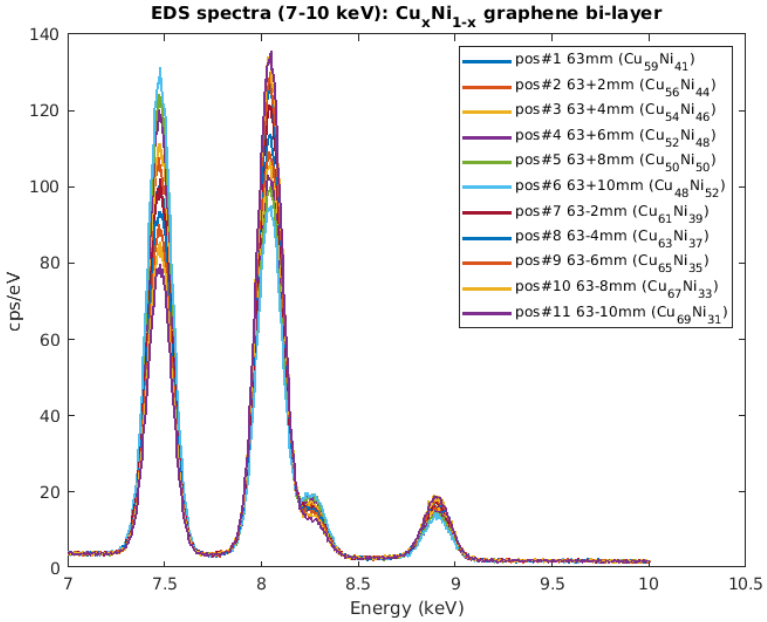

Fig. 3.29 EDS spectra (K_α) for locations from 53 mm to 73 mm with blow-up of Ni and Cu peaks

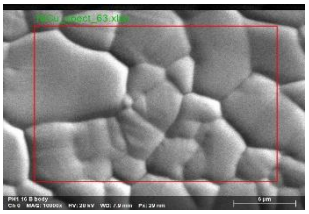

$Cu_{59}Ni_{41}$ (63 mm)

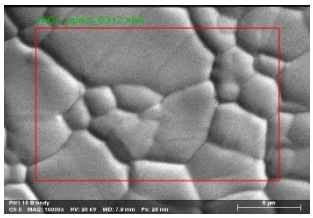

$Cu_{56}Ni_{44}$ (63+2mm)

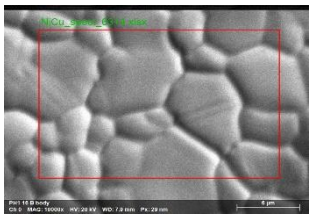

$Cu_{54}Ni_{46}$ (63+4mm)

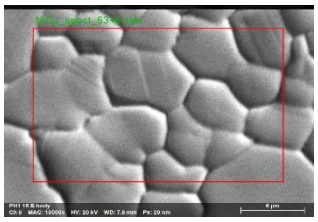

$Cu_{52}Ni_{48}$ (63+6mm)

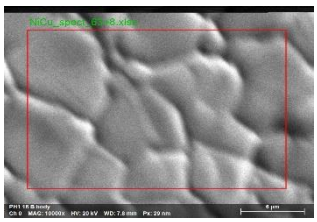

$Cu_{50}Ni_{50}$ (63+8mm)

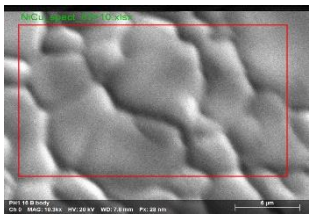

$Cu_{48}Ni_{52}$ (63+10mm)

Fig. 3.30 SEM images for locations every +2 mm from 63 mm

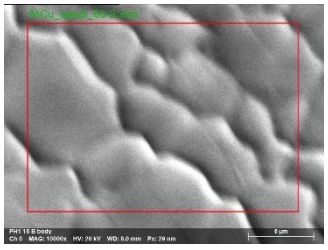

$Cu_{61}Ni_{39}$ (63-2mm)

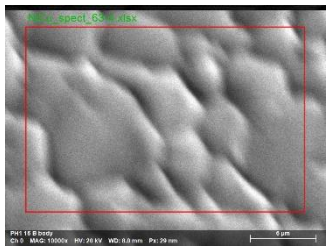

$Cu_{63}Ni_{37}$ (63-4mm)

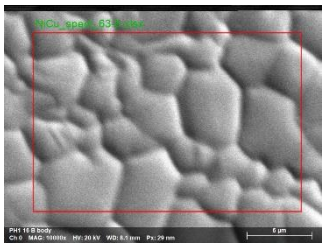

$Cu_{65}Ni_{35}$ (63-6mm)

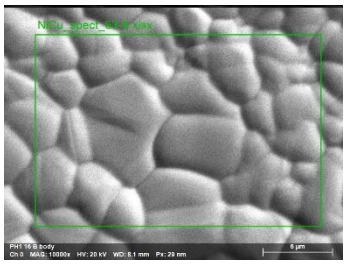

$Cu_{67}Ni_{33}$ (63-8mm)

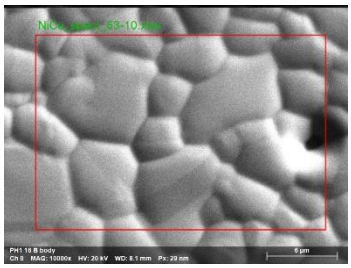

$Cu_{69}Ni_{31}$ (63-10mm)

Fig. 3.31 SEM images for locations every -2mm from 63 mm spot

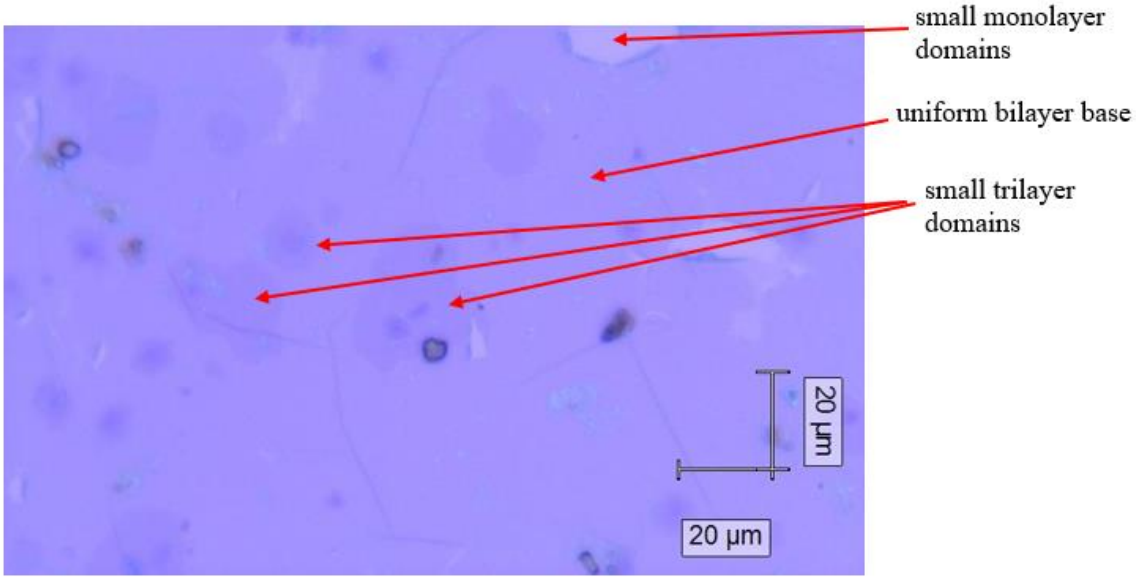

Fig. 3.32 Domains of bi-layer graphene growth at 58.8 mm from Cu rich side

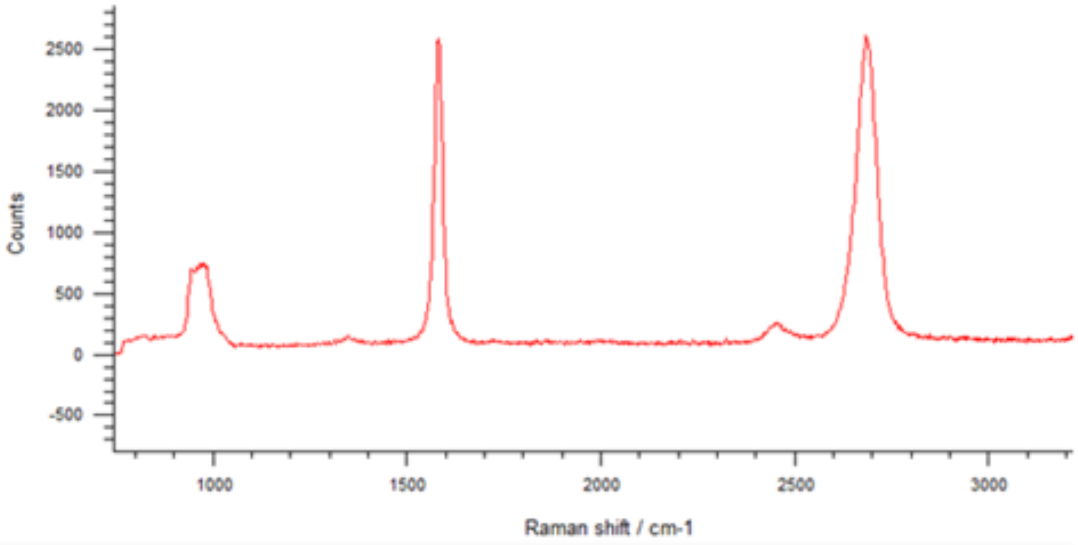

Fig. 3.33 Raman spectra for bi-layer growth at 58.8 mm from the Cu rich side showing G peak (~1600 cm^{-1}) and 2D peak (~2700 cm^{-1})

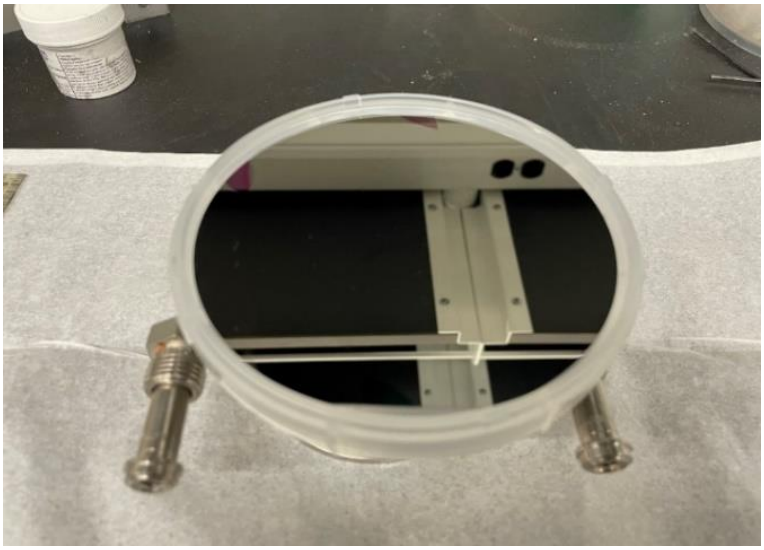

Fig. 3.34 Sputtered Cu_xNi_{1-x} alloy thin-film with ~63 at.% Cu for bi-layer graphene

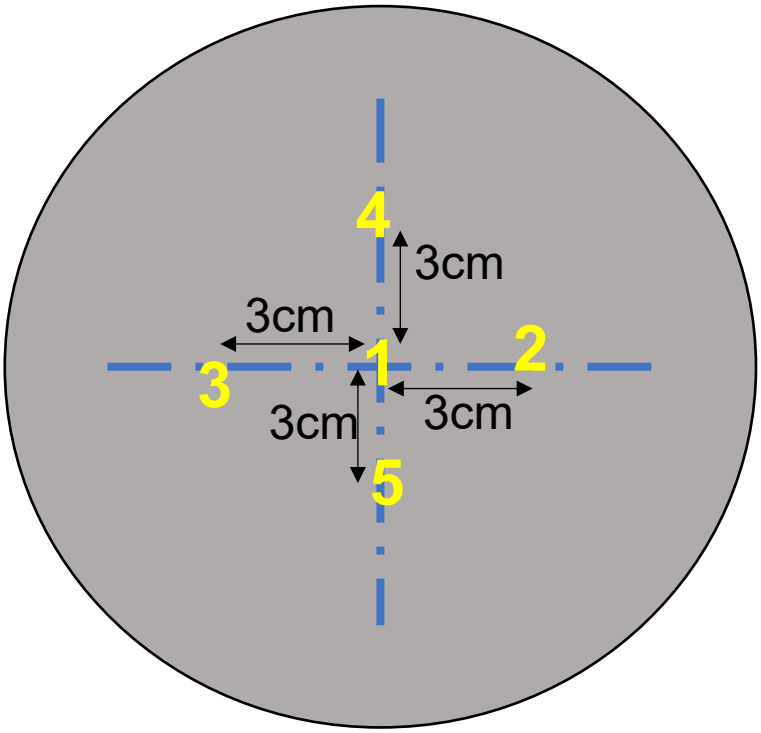

Fig. 3.35 Locations for EDS analysis of uniform Cu_xNi_{1-x} alloy (~63 at.% Cu) sputtered on Si/SiO_2 substrate for graphene bilayer

Table 3.9 Sputtering conditions for Cu_xNi_{1-x} alloy with uniform ~63 at.% Cu for bi-layer growth

Time	**Gun#1 (Ni)**			**Gun#3 (Cu)**		
(mins.)	**F**	**Volt (V)**	**R**	**F**	**Volt (V)**	**R**
0	120 W	372	0	115 W	320	0
30	120 W	366	0	115 W	315	0
60	120 W	365	0	115 W	315	0
90	120 W	365	0	115 W	312	0
120	120 W	363	0	115 W	310	0
150	120 W	360	0	115 W	308	0
180	120 W	358	0	115 W	305	0

Table 3.10 EDS results for Cu_xNi_{1-x} alloy (~63 at.% Cu) sputtered on Si/ SiO_2 substrate for graphene bilayer

Position	**Cu at.%**	**Ni at.%**	**x co-ordinate (mm)**	**y co-ordinate (mm)**
center (#1)	62	38	62	65
+3cm, X (#2)	63	37	92	65
-3cm, X (#3)	64	36	32	65
+3cm, Y (#4)	64	36	62	95
-3cm, Y (#5)	63	37	62	35

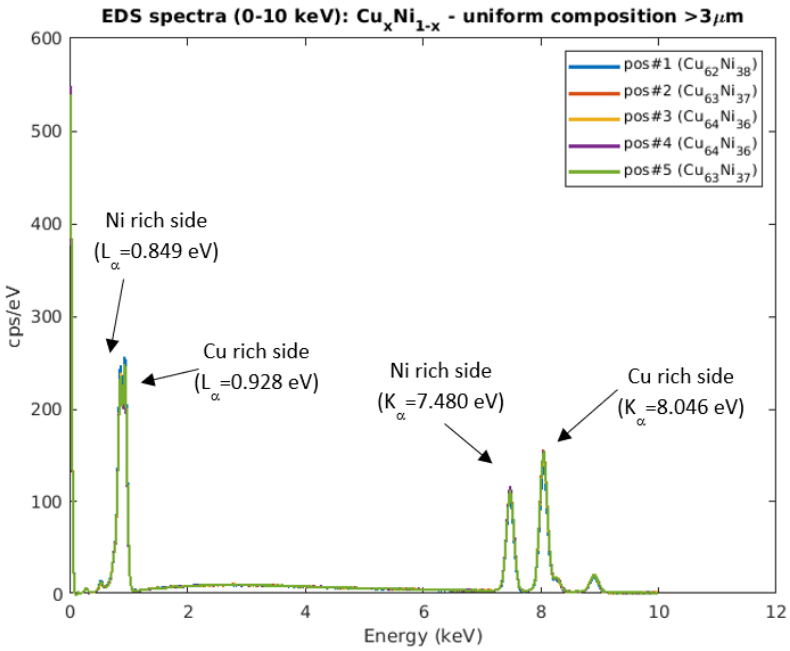

Fig. 3.36 EDS spectra 0-10 kV for Cu_xNi_{1-x} alloy thin film with uniform ~ 63 at.% Cu (37% at.% Ni)

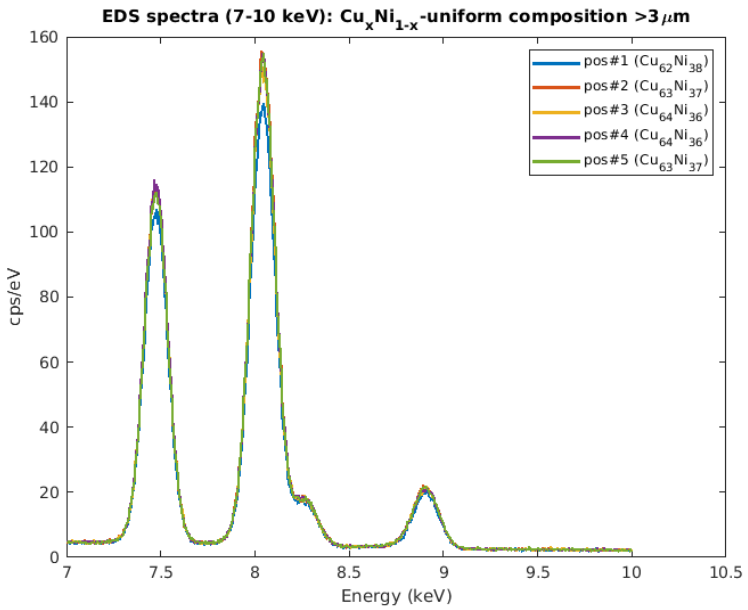

Fig. 3.37 EDS spectra (K_α) for Cu_xNi_{1-x} alloy thin film with uniform ~ 63 at.% Cu (37% at.% Ni)

CHAPTER FOUR

DISCUSSIONS

4.1 Graphene growth processing control parameters

During sputtering and chemical vapor deposition growth experiments, there are several processing variables governing the growth of graphene layers. As mentioned earlier, the deposition of Cu_xNi_{1-x} alloy thin film (catalyst) layer by magnetron sputtering is an essential first step. The composition of Cu_xNi_{1-x} alloy catalyst layer is governed by the sputtering rate of metal targets and the corresponding RF sputtering power set for both the metal targets. The thickness of layer is related to the amount of time the sputtering gun is turned on. For this experiment on regulating the growth of graphene layers, a thicker Cu_xNi_{1-x} alloy catalyst layer of ~2 µm is employed, which enhances the reaction rate for the chemical reaction involving breaking down of methane (CH_4) into C atoms. The quality of Cu_xNi_{1-x} alloy catalyst layer grown on Si/SiO_2 substrate is dominated by the sputtering main chamber vacuum pressure, which is typically maintained at ~$7x10^{-7}$T - $1x10^{-8}$ T and the flow rate of inert sputtering gas (Ar) generally kept at 5 standard cubic centimeter per minute (sccm).

The processing variables such as the flow rate of CH_4 maintained inside the thermal CVD chamber during growth of graphene layer is important variable controlling the domain size and the number of graphene layers. Also, it's critical to introduce the inert gas mixture of Ar/H_2 before starting CH_4 gas flow to remove any other gases present in the chamber which can deposit on the surface film and affect its quality and hinders the growth process. Similarly, the ramping rate for heating, holding time at high temperature (~1000°C), high temperature maintained inside the furnace and cooling rate of furnace are equally important factors for consideration in the CVD graphene growth recipe controlling the size of domains.

A comparative study on processing temperature control on bilayer graphene growth coverage conducted at temperatures of 990°C, 975°C and 960°C (Fig. 4.1) demonstrate mostly 2L coverage (~29-33%) at 975°C by reducing temperature by approximately 15°C from 990°C and overall increment in 2L coverage by ~70% at 960°C with respect to that at 990°C.

4.2 Proof-of-concept for using gradient catalyst to refine recipe for achieving bilayer coverage

A wafer with $Cu_{63}Ni_{37}$ alloy was sputtered to grow large area graphene with predominantly bilayer coverage (Fig. 4.2). The distribution of the number of layers can be identified by optical images (Fig. 4.2(a)). Raman spectra was

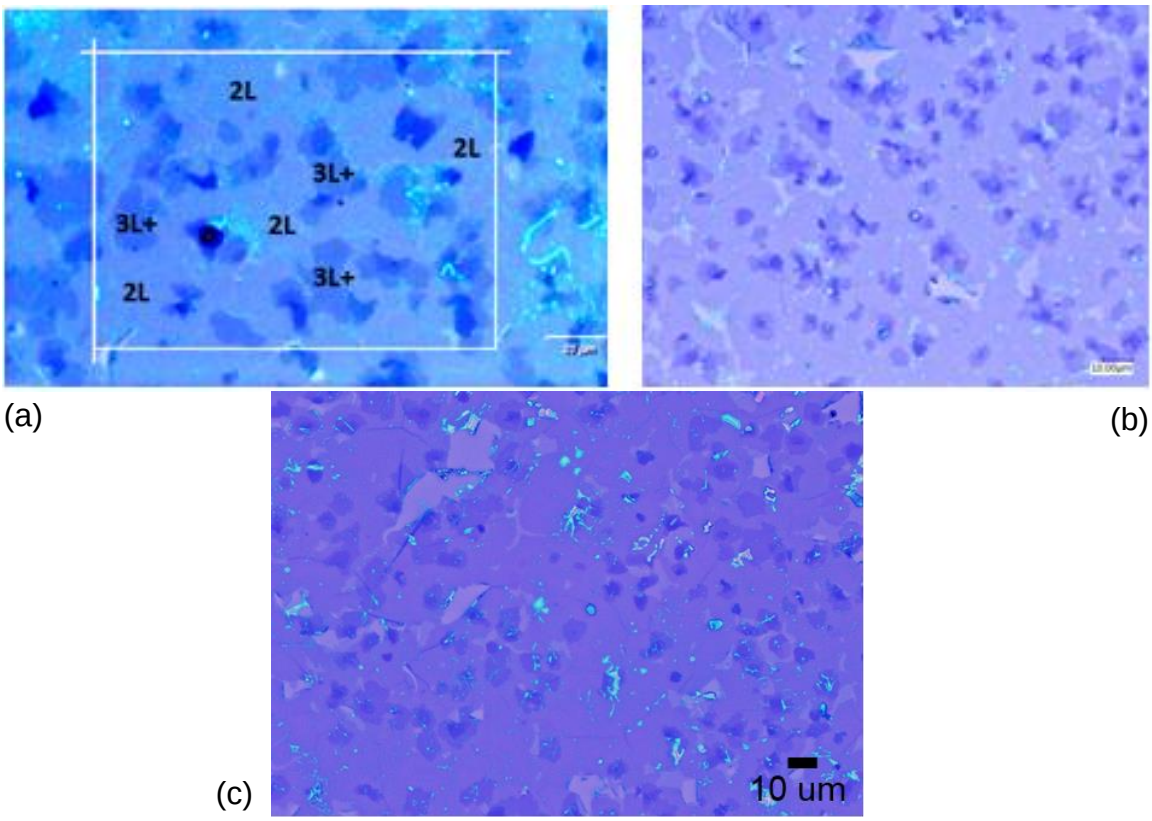

Fig. 4.1 Graphene growth comparison shown by optical images for CVD synthesis at (a) 990°C, (b) 975°C and (c) 960°C; and bar chart showing fractional coverage comparison for growth at 960°C, 975°C and 990°C

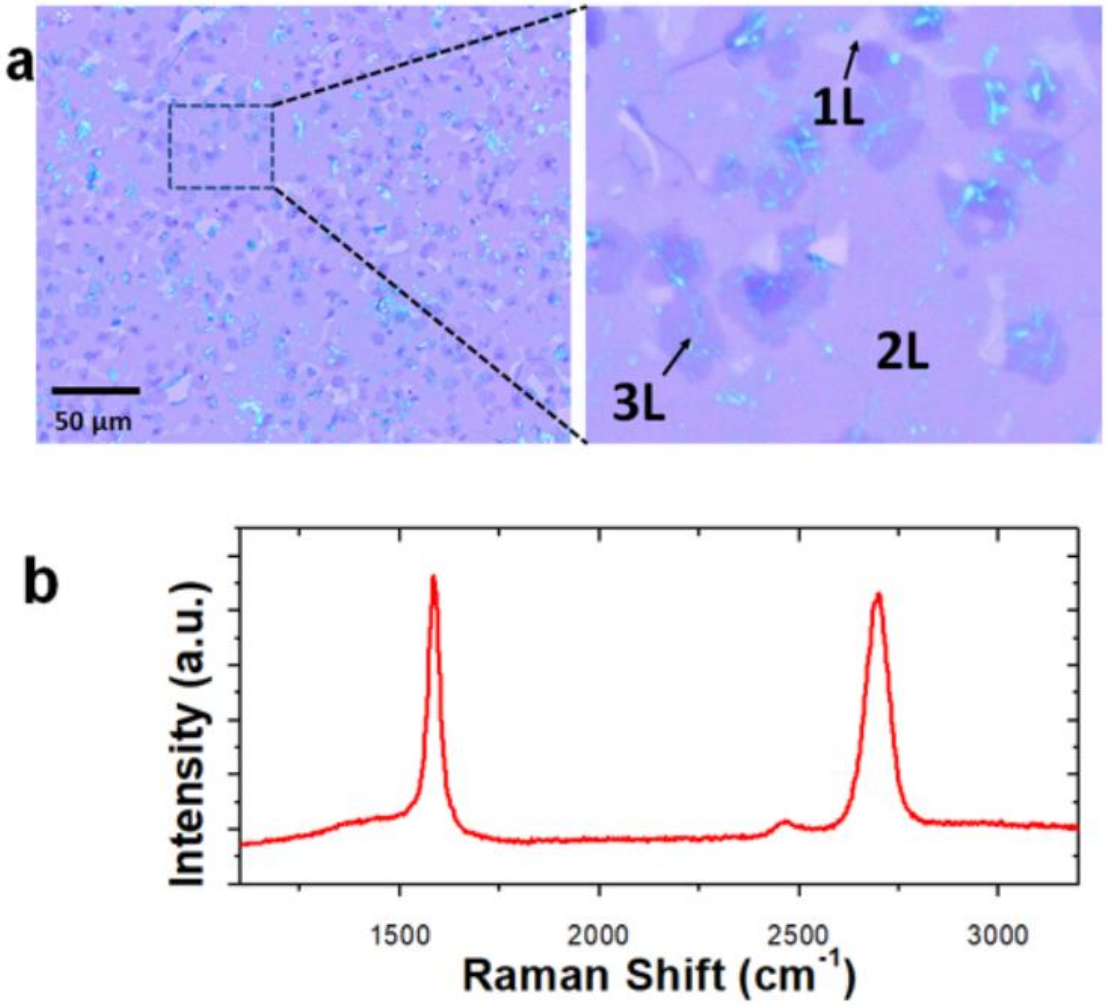

Fig. 4.2 Large area bilayer CVD graphene growth (a) optical image comparison for 1L, 2L and 3L domain coverages, (b) Raman spectra showing 2L coverage

collected for confirming that the layer thickness with majority coverage is 2L (Fig. 4.2(b)), which is indicated by 2D/G ratio of 1. Large area images were analyzed for determination of the distribution of layers (Fig. 4.2(c)). Images were converted to greyscale and the histogram was used for analysis. >70% of the coverage was bilayer graphene. This is the final proof-of-concept that the combinatorial sputtering can be used to rapidly identify recipes for graphene layer control.

CHAPTER FIVE

CONCLUSIONS AND RECOMMENDATIONS

5.1 Ending remarks

A combinatorial library of Cu_xNi_{1-x} (copper-nickel) alloy thin films were successfully co-sputtered on Si/SiO_2 substrate for providing a catalyst thin film for CVD growth of graphene layers. Large area bi-layer growth of graphene was effectively achieved. In this study, critical processing parameters for CVD graphene growth were identified. We conclude that temperature of CVD bath furnace, rate of cooling, precursor gas ratio especially CH_4:H_2 (methane: hydrogen) are important for regulating the behavior of H_2 for either CVD growth of graphene or etching of graphene layers. The SiO_2 (silicon di-oxide) layer thickness is important for controlling the diffusion of Cu (copper) and Si (silicon) atoms into CVD grown graphene layer. At lower thickness (~70-100 nm), we observed the formation of copper silicide nanoparticles in the graphene layer. After increasing the thickness of SiO2 oxide layer to 185 nm, copper-silicide particle formation reduced. The cooling rate of furnace is important in obtaining large area domains (or islands) of graphene. A slow and gradual cooling rate of furnace provided with good CVD growth of graphene layers. Also, by reducing CVD bath temperature from 990 °C to 975 (-15 °C), we obtained larger-area CVD growth of graphene domains (increment in bilayer coverage by ~27%-30%), and from 990 °C to 960 (-30 °C), further increment in bilayer coverage by ~70% was achieved. Characterization methods of EDS, XRD, optical microscopy and Raman analysis were useful in obtaining composition (at.%) of Cu_xNi_{1-x} alloy, identification of phases, imaging of graphene domains and identifying number of graphene layers grown respectively. We show that graphene layers single layer growth occurs with $x>68.95\%$, bilayer growth dominates from $47.56\%<x<68.95\%$, and multilayer ($>=3$) growth occurs for $x<47.56\%$.

LIST OF REFERENCES

[1] Paolo Bandavalli, "**Graphene and related nanomaterials: properties and applications**," Micro & Nano Technologies series, Elsevier, 2017. ISBN: 978-0-323-48101-4.

[2] Wonbong Choi, and Jo-won Lee, "**Graphene: synthesis and applications**", Taylor & Francis group, 2011-10-11. ISBN: 978-1-4398-6188-2.

[3] Cabrero-Vilatela, A., Weatherup, R.S., Braeuninger-Weimer, P., Caneva, S., Hofmann, S., "***Towards a general growth model for graphene CVD on transition metal catalysts***," J. Nanosc. Roy. Soc. of Chem., v. 8, 2016, pp. 2149. https://doi.org/10.1039/c5nr0873h

[4] Yang, X., Zhang, G., Prakash, J., Chen, Z., Gauthier, M., Sun, S., "***Chemical vapour deposition of graphene: layer control, the transfer process, characterization, and related applications***," J. Intl. Rev. Phys. Chem., v. 38 (2), 2019, pp. 149-199. https://doi.org/10.1080/0144235X.2019.1634319

[5] Geng, D., Wu, B., Guo, Y., Huang, L., Xue, Y., Chen, J., Yu, G., Jiang, L., Hu, W., Liu, Y., "***Uniform hexagonal graphene flakes and films grown on liquid copper surface***," J. PNAS, v. 109 (21), 2012, pp. 7992-7996. https://doi.org/10.1073/pnas.1200339109/-/DCSupplemental

[6] Novoselov, K.S., Geim, A.K., Morozov, S.V., Jiang, D., Zhang, Y., Dubonos, S.V., Grigorieva, I.V., Firsov, A.A., "***Electric field effect in atomically thin carbon films***," J. Science Reports, v. 306 (5696), 2004, pp. 666-670. https://doi.org/10.1126/science.1102896

[7] Geim, A.K., Novoselov, K.S., "***The rise of graphene***," J. Nat. Mat., v. 6, 2007, pp. 183-191. https://doi.org/10.1038/nmat1849

[8] Novoselov, K.S., Geim, A.K., Morozov, S.V., Jiang, D., Katsnelson, M.I., Grigorieva, I.V., Dubonos, S.V., Firsov, A.A., "***Two-dimensional gas of massless Dirac fermions in graphene***," J. Nature, v. 438, 2005, pp. 197-200. https://doi.org/10.1038/nature04233

[9] Neto, A.H.C., Guinea, F., Peres, N.M.R., Novoselov, K.S., Geim, A.K., "***The electronic properties of graphene***," J. Rev. Modern Phys., v. 81, 2009, pp. 109-162. https://doi.org/10.1103/RevModPhys.81.109

[10] Li, X., Zhu, Y., Cai, W., Borysiak, M., Han, B., Chen, D., Piner, R.D., Colombo, L., Ruoff, R.S., "***Transfer of large-area graphene films for high-performance transparent conductive electrodes***," J. ACS Nano Lett., v. 9, 2009, pp. 4359-4363. https://doi.org/10.1021/nl902623y

[11] Huang, M., Ruoff, R.S., "***Growth of single-layer and multilayer graphene on Cu/Ni alloy substrates***," J. ACS Acc. Chem. Res., v. 53, 2020, pp. 800-811. https://doi.org/10.1021/acs.accounts.9b00643

[12] Lin, L., Deng, B., Sun, J., Peng, H., Liu, Z. "***Bridging the gap between reality and ideal in chemical vapor deposition growth of graphene***," J. Chem. Rev., v. 118, 2018, pp. 9281-9343. https://doi.org/10.1021/acs.chemrev.8b00325

[13] Geim, A.K., "***Graphene: Status and prospects***," J. Science, v. 324, 2009, pp. 1530-1535. https://doi.org/10.1126/science.1158877
[14] Yan, Z., Peng, Z., Sun, Z., Yao, J., Zhu, Y., Liu, Z., Ajayan, P.M., Tour, J.M., "***Growth of bilayer graphene on insulating substrates***," J. ACS Nano, v. 5, 2011, pp. 8187-8192. https://doi.org/10.1021/nn202829y
[15] Lee, S., Lee, K., Zhong, Z., "***Wafer scale homogeneous bilayer graphene films by chemical vapor deposition***," J. Nano Letters, v. 10, 2010, pp. 4702-4707. https://doi.org/10.1021/nl1029978
[16] Yan, K., Peng, H., Zhou, Y., Li, H., Liu, Z., "***Formation of bilayer bernal graphene: layer-by-layer epitaxy via chemical vapor deposition***," J. Nano Lett., v. 11, 2011, pp. 1106-1110. https://dx.doi.org/10.1021/nl104000b
[17] Massalski, T.B., Okamoto, H., Subramanian, P.R., Kacprzak, L., "**Binary alloy phase diagrams**," 2nd edition, ASM international, 1990, ISBN:978-0-87170-403-0. https://www.asminternational.org/online-catalog/alloy-phase-diagrams/-/journal_content/56/10192/57718G/PUBLICATION
[18] Li, X., Cai, W., An, J., Kim, S., Nah, J., Yang, D., Piner, R., Velamakanni, A., Jung, I., Tutuc, E., Banerjee, S.K., Colombo, L., Ruoff, R.S., "***Large-area synthesis of high-quality and uniform graphene films on copper foils***," J. Science reports, v. 324, 2009, pp. 1312-1315. https://doi.org/10.1126/science.1172104
[19] Li, X., Cai, W., Colombo, L., Ruoff, R.S., "***Evolution of graphene growth on Ni and Cu by carbon isotope labeling***," J. Nano Lett., Amer. Chem. Soc., v. 9 (2), 2009, pp. 4269-4272. https://doi.org/10.1021/nl902515k
[20] Kim, K.S., Zhao, Y., Jang, H., Lee, S.Y., Kim, J.M., Kim, K.S., Ahn, J.H., Kim, P., Choi, J.Y., Hong, B.H., "***Large-scale pattern growth of graphene films for stretchable transparent electrodes***," J. Nat. Letters, v. 457, 2009, pp. 706-710. https://doi.org/10.1038/nature07719
[21] Reina, A., Jia, X., Ho, J., Nezich, D., Son, H., Bulovic, V., Dresselhaus, M.S., Kong, J., "***Large area, few-layer graphene films on arbitrary substrates by chemical vapor deposition***," J. Nano Letters, v. 9 (1), 2009, pp. 30-35. https://doi.org/10.1021/nl801827v
[22] Sutter, P.W., Flege, J.I., Sutter, E.A., "***Epitaxial graphene on ruthenium***," J. Nat. Materials., v. 7, 2008, pp. 406-411. https://doi.org/10.1038/nmat2166
[23] Gao, L., Guest, J.R., Guisinger, N.P., "***Epitaxial graphene on Cu (111)***," J. Nano Letters, v. 10, 2010, pp. 3512-3516. https://doi.org/10.1021/nl10167606
[24] Sun, Z., Yan, Z., Yao, J., Beitler, E., Zhu, Y., Tour, J.M., "***Growth of graphene from solid carbon source***," J. Nat. Letter, v. 468, 2010, pp. 549-552. https://doi.org/10.1038/nature09579
[25] Amini, S., Garay, J., Liu, G., Balandin, A., Abbaschian, R., "***Growth of large-area graphene films from metal-carbon melts***," J. Appl. Phys., v. 108, 2010, pp. 094321-1-094321-7. https://doi.org/10.1063/1.3498815

[26] Addou, R., Dahal, A., Sutter, P., Batzill, M., "***Monolayer graphene growth on Ni (111) by low temperature chemical vapor deposition***," J. Appl. Phys., v. 100, 2012, pp. 021601. https://doi.org/10.1063/1.3675481
[27] Li, X., Magnuson, C.W., Venugopal, A., Tromp, R.M., Hannon, J.B., Vogel, E.M., Colombo, L., Ruoff, R.S., "***Large-area graphene single crystals grown by low-pressure chemical vapor deposition of methane on copper***," J. Amer. Chem. Soc., v. 133, 2011, pp. 2816-2819. https://dx.doi.org/10.1021/ja109793s
[28] Bae, S., Kim, H., Lee, Y., Xu, X., Park, J.S., Zheng, Y., Balakrishnan, J., Lei, T., Kim, Y.J., Kim, K.S., Ozyilmaz, B., Ahn, J.H., Hong, B.H., Lijima, S., "***Roll-to-roll production of 30-inch graphene films for transparent electrodes***," J. Nat. Nanotech. Letters, v. 5, 2010, pp. 574-578. https://doi.org/10.1038/NNANO.2010.132
[29] Bhaviripudi, S., Jia, X., Dresselhaus, M.S., Kong, J., "***Role of kinetic factors in chemical vapor deposition synthesis of uniform large area graphene using copper catalyst***," J. Amer. Chem. Soc., v. 10, 2010, pp. 4128-4133. https://doi.org/10.1021/nl102355e
[30] Kim, K., Lee, Z., Regan, W., Kisielowski, C., Crommie, M.F., Zettl, A., "***Grain boundary mapping in polycrystalline graphene***," J. ACS Nano, v. 5 (3), 2011, pp. 2142-2146. https://doi.org/10.1021/nn1033423
[31] Huang, P.Y., Ruiz-Vargas, C.S., van der Zande, A.M., Whitney, W.S., Levendorf, M.P., Kevek, J.W., Garg, S., Alden, J.S., Hustedt, C.J., Zhu, Y., Park, J., McEuen, P.L., Muller, D.A., "***Grains and grain boundaries in single-layer graphene atomic patchwork quilts***," J. Nat. Letters., v. 469, 2011, pp. 389-393. https://doi.org/10.1038/nature09718
[32] Yazyev, O.V., Louie, S.G., "***Electronic transport in polycrystalline graphene***," J. Nat. Materials Letters, v. 9, 2010, pp. 806-809. https://doi.org/10.1038/NMAT2830
[33] Wu, B., Geng, D., Guo, Y., Huang, L., Xue, Y., Zheng, J., Chen, J., Yu, G., Liu, Y., Jiang, L., Hu, W., "***Equiangular hexagon-shaped-controlled synthesis of graphene on copper surface***," J. Adv. Mat., v. 23, 2011, pp. 3522-3525. https://doi.org/10.1002/adma.201101746
[34] Robertson, A.W., Warner, J.H., "***Hexagonal single crystal domains of few-layer graphene on copper foils***," J. Nano Letters, v. 11, 2011, pp. 1182-1189. https://dx.doi.org/10.1021/nl104142k
[35] Yu, Q., Jauregui, L.A., Wu, W., Colby, R., Tian, J., Su, Z., Cao, H., Liu, Z., Pandey, D., Wei, D., Chung, T.F., Peng, P., Guisinger, N.P., Stach, E.A., Bao, J., Pei, S.S., Chen, Y.P., "***Control and characterization of individual grains and grain boundaries in graphene grown by chemical vapor deposition***," J. Nat. Mat., v. 10, 2011, pp. 443-449. https://doi.org/10.1038/NMAT3010
[36] Gao, L., Ren, W., Zhao, J., Ma, L., Chen, Z., Cheng, H.M., "***Efficient growth of high-quality graphene films on Cu foils by ambient pressure chemical***

vapor deposition," J. Appl. Phys. Letters, v. 97, 2010, pp. 183109, 97, 1-2. https://doi.org/10.1063/1.3512865

[37] Li, X., Cai, W., Colombo, L., Ruoff, R.S., "***Evolution of graphene growth on Ni and Cu by carbon isotope labeling***," J. Nano Letters, v. 9 (12), 2009, pp. 4268-4272. https://doi.org/10.1021/nl902515k

[38] Shelton, J.C., Patil, H.R., Blakely, J.M., "***Equilibrium segregation of carbon to a Ni (111) surface: A surface phase transition***," J. Surf. Sci., v. 43 (2), 1974, pp. 493-520. https://doi.org/10.1016/0039-6028(74)90272-6

[39] Reina, A., Thiele, S., Jia, X., Bhavirpudi, S., Dresselhaus, M.S., Schaefer, J.A., Kong, J., "***Growth of large-area single- and bi-layer graphene by controlled carbon precipitation on polycrystalline Ni surfaces***," J. Nano. Res., v. 2, 2009, pp. 509-516. https://doi.org/10.1007/s12274-009-9059-y

[40] Wofford, J.M., Nie, S., McCarty, K.F., Bartelt, N.C., Dubon, O.D., "***Graphene islands on Cu foils: The interplay between shape, orientation and defects***," J. ACS Nano Lett., v. 10, 2010, pp. 4890-4896. https://doi.org/10.1021/nl102788f

[41] Gao, L., Guest, J.R., Guisinger, N.P., "***Epitaxial graphene on Cu (111)***," J. ACS Nano Lett., v. 10, 2010, pp. 3512-3516. https://doi.org/10.1021/nl1016706

[42] Lahiri, J., Miller, T.S., Ross, A.J., Adamska, L., Oleynik, I.I., Batzill, M., "***Graphene growth and stability at nickel surfaces***," New J. of Phys., v. 13, 2011, pp. 314204. https://doi.org/10.1088/1367-2630/13/2/025001

[43] Gamo, Y., Nagashima, A., Wakabayashi, M., Terai, M., Oshima, C., "***Atomic structure of monolayer graphite formed on Ni (111)***," J. Surf. Sci., v. 374 (1997), 1997, pp. 61-64. https://doi.org/10.1016/S0039-6028(96)00785-6

[44] Lahiri, J., Lin, Y., Bozkurt, P., Oleynik, I.I., Batzill, M., "***An extended defect in graphene as a metallic wire***," J. Nat. Nanotech., v. 5, 2010, pp. 326-329. https://doi.org/10.1038/NNANO.2010.53

[45] Gruneis, A., Kummer, K., Vyalikh, D.V., "***Dynamics of graphene growth on a metal surface: a time-dependent photoemission study***," New. J. Phys., v. 11, 2009, pp. 073050,1-9. https://doi.org/10.1088/1367-2630/11/7/073050

[46] McCarroll, J.J., Edmonds, T., Pitkethly, R.C., "***Interpretation of a complex low energy electron diffraction pattern: carbonaceous and sulphur-containing structures on Ni (111)***," J. Nat., v. 223, 1969, pp. 1260-2362. https://doi.org/10.1038/2231260a0

[47] Lahiri, J., Miller, T., Adamska, L., Oleynik, I.I., Batzill, M., "***Graphene growth on Ni (111) by transformation of a surface carbide***," J. ACS Nano Lett., v. 11 (2), 2011, pp. 518-522. https://doi.org/10.1021/nl103383b

[48] Loginova, E., Bartelt, N.C., Feibelman, P.J., McCarty, K.F., "***Factors influencing graphene growth on metal surfaces***," New J. Phys., v. 11, 2009, pp. 063046, 1-20. https://doi.org/10.1088/1367-2630/11/6/063046

[49] Laginova, E., Bartelt, N.C., Feibelman, P.J., McCarty, K.F., "***Evidence for graphene growth by C cluster attachment***," New J. Phys., v. 10, 2008, pp. 093026, 1-16. https://doi.org/10.1088/1367-2630/10/9/093026
[50] Wu, T., Liu, Z., Chen, G., Dai, D., Sun, H., Dai, W., Jiang, N., Jiang, Y.H., Lin, C.T., "***A study of the growth-time effect on graphene layer number based on Cu-Ni bilayer catalyst system***," J. Roy. Soc. Chem. Adv., v. 6, 2016, pp. 23956-23960. https://doi.org/10.1039/c5ra27075h
[51] Hesjedal, T., "***Continuous roll-to-roll growth of graphene films by chemical vapor deposition***," J. Appl. Phys., v. 98, 2011, pp. 133106. https://doi.org/10.1063/1.3573866
[52] Bianco, A., Cheng, H.M., Enoki, T., Gogotsi, Y., Hurt, R.H., Koratkar, N., Kyotani, T., Monthioux, M., Park, C.R., Tascon, J.M.D., Zhang, J., "***All in the graphene family - A recommended nomenclature for two-dimensional carbon materials***," J. Carbon, v. 65, 2013, pp. 1-6. https://doi.org/10.1016/j.carbon.2013.08.038
[53] Novoselov, K.S., Geim, A.K., Morozov, S.V., Jiang, D., Zhang, Y., Dubons, S.V., Grigorieva, I.V., Firsov, A.A., "***Electric field effect in atomically thin carbon films***," J. Science, Reports, v. 306 (5696), 2004, pp. 666-669. https://doi.org/10.1126/science.1102896
[54] Mermin, N.D., Wagner, H., "***Absence of ferromagnetism or antiferromagnetism in one- or two-dimensional isotropic heisenberg models***," J. Phy. Rev. Lett., v. 17 (22), 1966, pp. 1133-1136. https://doi.org/10.1103/PhysRevLett.17.1133
[55] Novoselov, K.S., Jiang, D., Schedin, F., Booth, T.J., Khotkevich, V.V., Movrozov, S.V., Geim, A.K., "***Two-dimensional atomic crystals***," J. PNAS, v. 102 (30), 2005, pp. 10451-10453. https://doi.org/10.1073/pnas.050284102
[56] Kobayashi, T., Bando, M., Kimura, N., Shimuzu, K., Kadono, K., Umezu, N., Miyahara, K., Hayazaki, S., Nagai, S., Mizguchi, Y., Murakami, Y., Hobara, D., "***Production of a 100-m-long high-quality graphene transparent conductive film by roll-to-roll chemical vapor deposition and transfer process***," J. Appl. Phys. Lett., v. 102, 2013, pp. 023112, 1-4. https://doi.org/10.1063/1.4776707
[57] Gee, C.-M., Tseng, C.-C., Wu, F.-Y., Chang, H.-P., Li, L.-J., Hsieh, Y.-P., Lin, C.-T., Chen, J.-C., "***Flexible transparent electrodes made of electrochemically exfoliated graphene sheets from low-cost graphite pieces***," J. Displays, Elsevier, v. 34, 2013, pp. 315-319. https://dx.doi.org/10.1016/j.displa.2012.11.002
[58] Chen, C.-H., Lin, C.-T., Hsu, W.-L., Chang, Y.-C., Yeh, S.-R., Li, L.-J., Yao, D.-J., "***A flexible hydrophilic-modified graphene microprobe for neural and cardiac recording***," J. Nanomed.: Nanotech., Biology and Medicine, Elsevier, v. 9, 2013, pp. 600-604. https://dx.doi.org/10.1016/j.nano.2012.12.004
[59] Jung, S.M., Mafra, D.L., Lin, C.-T., Jung, H.Y., Kong, J., "***Controlled porous structures of graphene aerogels and their effect on supercapacitor***

performance," J. Roy. Soc. Chem., v. 7, 2015, pp. 4386-4393. https://doi.org/10.1039/c4nr07564a

[60] Dai, W., Yu, J., Wang, Y., Song, Y., Alam, F.E., Nishimura, K., Lin, C.-T., Jiang, N., "***Enhanced thermal conductivity for polyimide composites with a three-dimensional silicon carbide nanowire@graphene sheets filler***," J. Mat. Chem. A, Roy. Soc. Chem., v. 3, 2015, pp. 4884-4891. https://doi.org/10.1039/c4ta06417h

[61] Hu, Y., Sun, X., "***Flexible rechargeable lithium ion batteries: advances and challenges in materials and process technologies***," J. Mat. Chem. A, v. 2, 2012, pp. 10712-10738. https://doi.org/10.1039/c4ta00716f

[62] Zhou, G., Li, F., Cheng, H.-M., "***Progress in flexible lithium batteries and future prospects***," J. Roy. Soc. Chem., energy & environ. sci., v. 7, 2014, pp. 1307-1338. https://doi.org/10.1039/c3ee43182g

[63] Li, Q., Guo, B., Yu, J., Ran, J., Zhang, B., Yan, H., Gong, J.R., "***Highly efficient visible-light-driven photocatalytic hydrogen production of CdS-cluster-decorated graphene nanosheets***," J. Amer. Chem. Soc., v. 133, 2011, pp. 10878-10884.

[64] Lee, C., Wei, X., Kysar, J.W., Hone, J. "***Measurement of the elastic properties and intrinsic strength of monolayer graphene***," J. Science, v. 321, 2008, pp. 385-388. https://doi.org/10.1126/science.1156211

[65] Jo, G., Choe, M., Cho, C-Y., Kim, J.H., Park, W., Lee, S., Hong, W.K., Kim, T.-W., Park, S.-J., Hong, B.H., Kahng, Y.H., Lee, T., "***Large-scale patterned multi-layer graphene films as transparent conducting electrodes for GaN light-emitting diodes***," J. Nanotech., IOP, 2010, pp. 1-6. https://10.1088/0957-4484/21/17/175201

[66] Gao, L., Ren, W., Zhao, J., Ma, L.-P., Chen, Z., Cheng, H.-M., "***Efficient growth of high-quality graphene films on Cu foils by ambient pressure chemical vapor deposition***," J. Appl. Phys. Lett., v. 97, 2010, pp. 183109, 1-3. https://doi.org/10.1063/1.3512865

[67] Choi, H., Lim, Y., Park, M., Lee, S., Kang, Y., Kim, M.S., Kim, J., Jeon, M., "***Precise control of chemical vapor deposition graphene layer thickness using Ni_xCu_{1-x} alloys***," J. Mat. Chem. C., v. 3, 2015, pp. 1463-1467. https://doi.org/10.1039/c4tc01979b

[68] Wu, T., Zhang, X., Yuan, Q., Xue, J., Lu, G., Liu, Z., Wang, H., Wang, H., Ding, F., Yu, Q., Xie, X., Jiang, M., "***Fast growth of inch-sized single-crystalline graphene from a controlled single nucleus on Cu-Ni alloys***," J. Nat. Mat., v. 15, 2016, pp. 43-48. https://doi.org/10.1038/NMAT4477

[69] Huang, M., Bakharev, P.V., Wang, Z.J., Biswal, M., Yang, Z., Jin, S., Wang, B., Park, H.J., Li, Y., Qu, D., Kwon,Y., Chen, X., Lee, S.H., Willinger, M.G., Yoo, W.J., Lee, Z., Ruoff, R.S., "***Large-area single-crystal AB-bilayer and ABA-trilayer graphene grown on a Cu/Ni (111) foil***," J. Nat. Nanotech., v. 15, 2020, pp. 289-295. https://doi.org/10.1038/s41565-019-0622-8

[70] Gao, L., Ren, W., Xu, H., Jin, L., Wang, Z., Ma, T., Ma, L.P., Zhang, Z., Fu, Q., Peng, L.M., Bao, X., Cheng, H.M., "***Repeated growth and bubbling***

transfer of graphene with millimetre-size single-crystal grains using platinum," J. Nat. Comm., v. 3 (699), 2012, pp. 1-7. https://doi.org/10.1038/ncomms1702

[71] Pan, B.Y., Zhang, H., Shi, D., Sun, J., Du, S., Liu, F., Gao, H.-J., "***Highly ordered, millimeter-scale, continuous, single-crystalline graphene monolayer formed on Ru (0001)***," J. Adv. Matter., v. 21, 2009, pp. 2777-2780. https://doi.org/10.1002/adma.200800761

[72] Sutter, P., Sadowski, J.T., Sutter, E., "***Graphene on Pt (111): Growth and substrate interaction***," J. Phys. Rev. B., v. 80, 2009, 245411, 1-10. https://doi.org/10.1103/PhysRevB.80.245411

[73] Wintterlin, J., Bocquet, M.-L., "***Graphene on metal surfaces***," J. Surf. Sci., Elsevier, v. 603, 2009, pp. 1841-1852. https://doi.org/10.1016/j.susc.2008.08.037

[74] Siller, R.H., Oates, W.A., McLennan, R.B., "***The solubility of carbon in palladium and platinum***," J. Less-Common Met., v. 16, 1968, pp. 71-73. https://doi.org/10.1016/0022-5088(68)90158-6

[75] Au, C.-T., Ng, C.-F., Liao, M.-S., "***Methane dissociation and syngas formation on Ru, Os, Rh, Ir, Pd, Pt, Cu, Ag, and Au: a theoretical study***," J. Catalysts, v. 185, 1999, pp. 12-22. https://doi.org/0021-9517/99

[76] Gomez, T., Florez, E., Rodriguez, J.A., Illas, F., "***Reactivity of transition metals (Pd, Pt, Cu, Ag, Au) toward molecular hydrogen dissociation: extended surfaces versus particles supported on TiC (001) or small is not always better and large is not always bad***," J. Phys. Soc. Chem. C, v. 115, 2011, pp. 11666-11672. https://dx.doi.org/10.1021/jp2024445

[77] Wonbong Choi, and Jo-won Lee, "**Graphene: synthesis and applications**", Taylor & Francis group, 2011-10-11. ISBN: 978-1-4398-6188-2.

[78] Semicore, "**What is Sputtering? Magnetron Sputtering?**," available on web: https://www.semicore.com/what-is-sputtering

[79] Gao, L., Ren, W., Xu, H., Jin, L., Wang, Z., Ma, T., Ma, L.P., Zhang, Z., Fu, Q., Peng, L.M., Bao, X., Cheng, H.M., "***Repeated growth and bubbling transfer of graphene with millimetre-size single-crystal grains using platinum***," J. Nat. Comm., v. 3 (699), 2012, pp. 1-7. https://doi.org/10.1038/ncomms1702

[80] Stiles, P.L., Dieringer, J.A., Shah, N.C., Duyne, R.P.V., "***Surface-enhanced Raman spectroscopy***," J. Annu. Rev. Anal. Chem., vol. 1, 2008, pp. 601-626. https://doi.org/10.1146/annurev.anchem.1.031207.112814

[81] Cho, J.H., Gorman, J., Na, S.R., Cullinan, M., "***Growth of monolayer graphene on nanoscale copper-nickel alloy thin flms***," J. Carbon, Elsevier, vol. 115, 2017, pp. 441-448. https://dx.doi.org/10.1016%2Fj.carbon.2017.01.023

APPENDIX

I. Analysis of copper silicide dot formation (optical images and EDS)

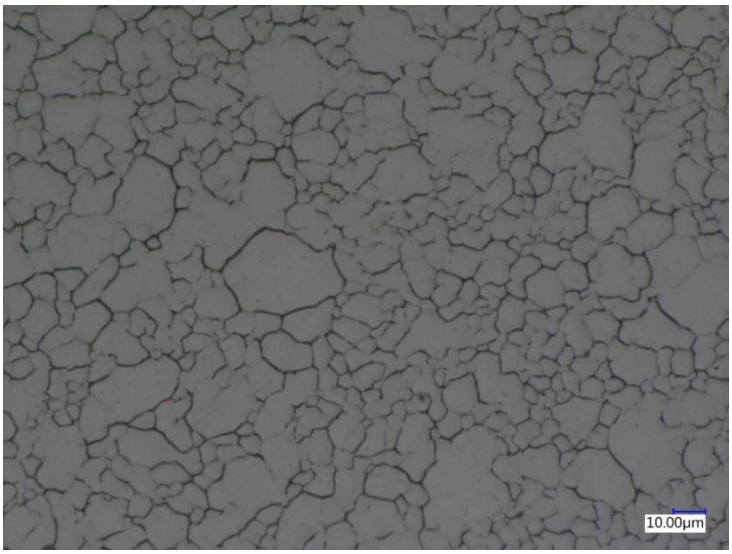

Fig. 1 Optical images of graphene grains growth on Cu_xNi_{1-x} alloy on Si/SiO_2 substrate

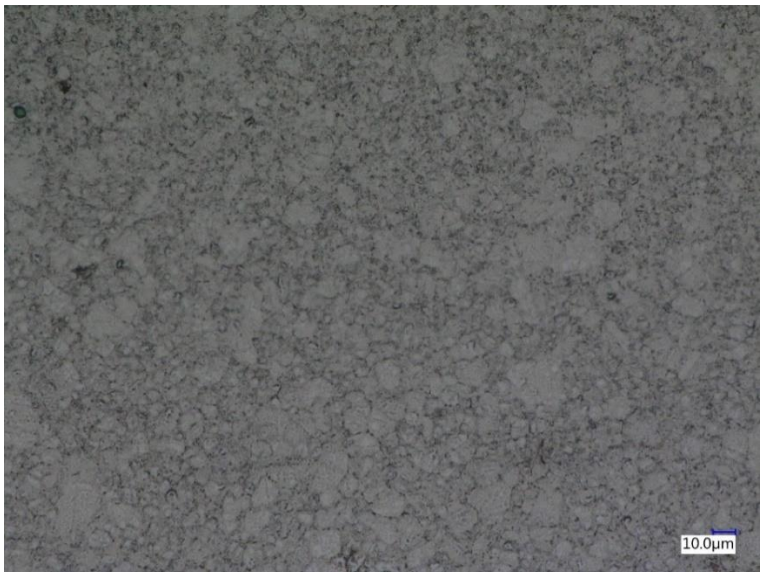

Fig. 2 Optical image of graphene grains growth in regions of high Cu at.% of Cu_xNi_{1-x} alloy film on Si/SiO_2 substrate showing discoloration and small sized grains-silicide formation

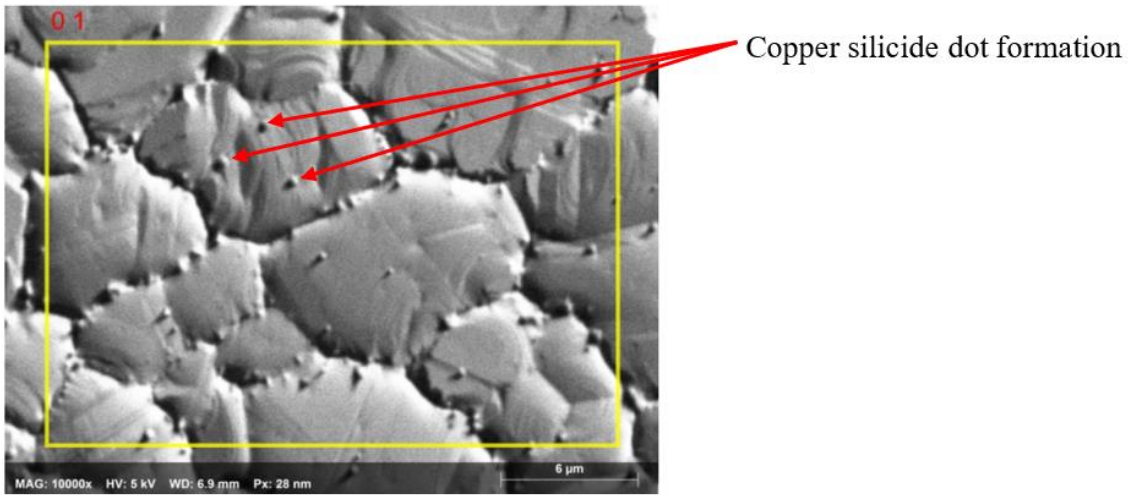

Fig. 3 EDS analysis (area) for silicide dot formation on graphene layer deposited on Cu_xNi_{1-x} alloy film on Si/SiO_2 substrate in regions of high Cu at.%

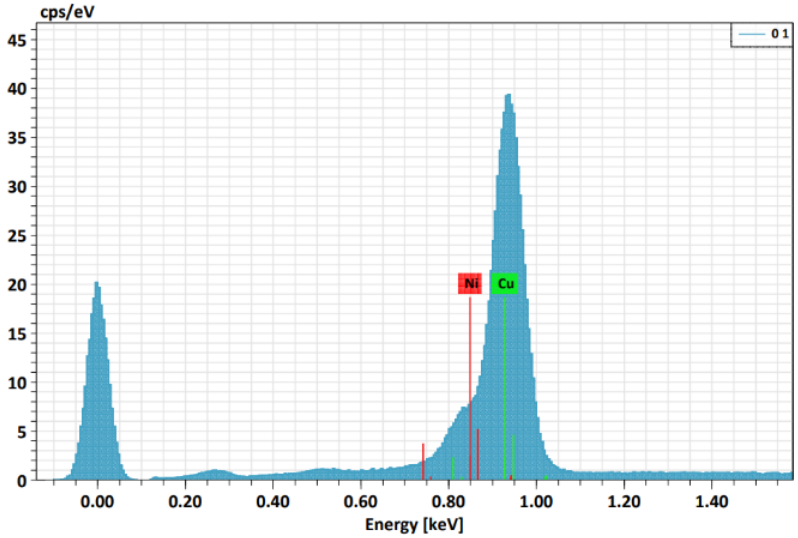

Fig. 4 EDS analysis spectrum of at.% Ni and Cu in the region of silicide particles formation

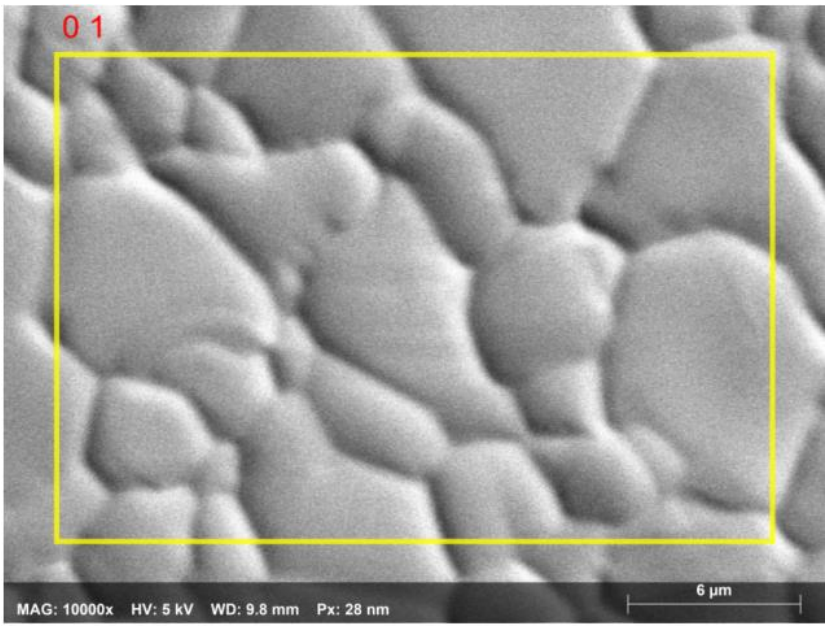

Fig. 5 SEM-EDS analysis for CVD graphene growth on Cu_xNi_{1-x} alloy on Si/SiO_2 without any dots

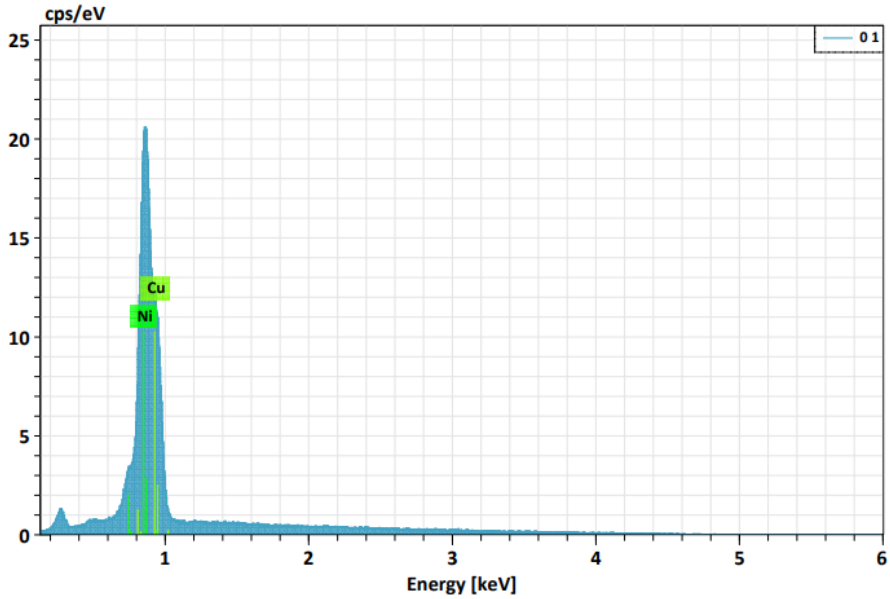

Fig. 6 EDS spectra for cvd graphene growth on Cu_xNi_{1-x} alloy on SiO_2/Si without any dots

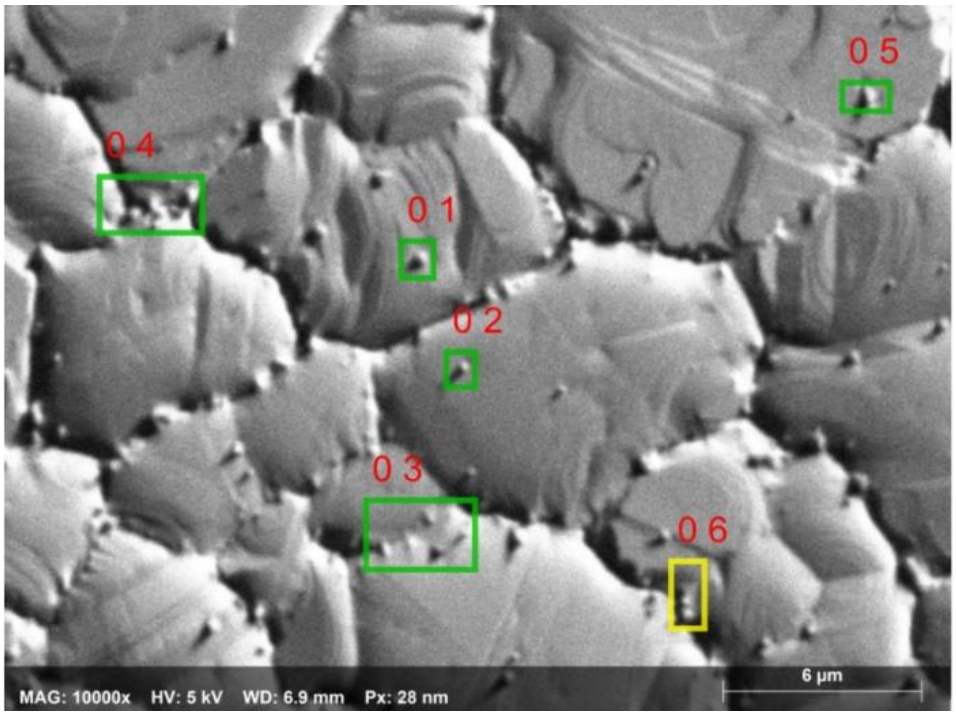

Fig. 7 EDS analysis for Cu silicide dot (area across single dot) formation on graphene layer deposited on Cu_xNi_{1-x} alloy film on Si/SiO_2 substrate in regions of high Cu at.%

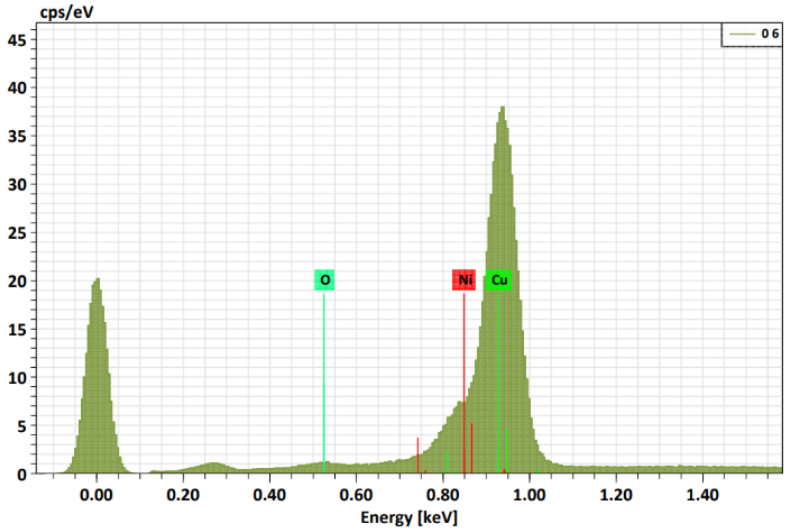

Fig. 8 EDS analysis for Cu silicide dot (area across single dot) formation on graphene layer deposited on Cu_xNi_{1-x} alloy film on Si/SiO_2 substrate in regions of high Cu at.%

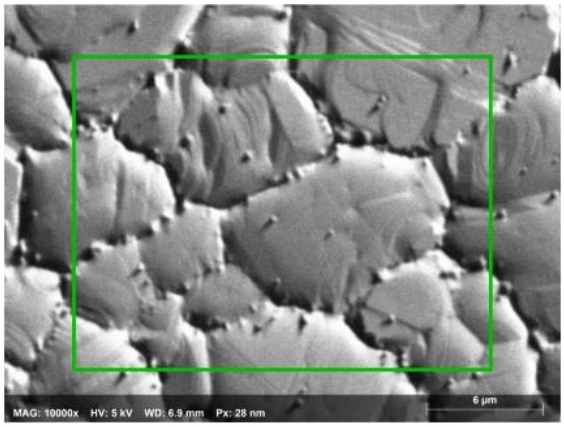

Fig. 9 EDS analysis (mapping) of Cu silicide formation on graphene layer deposited on Cu_xNi_{1-x} alloy film on Si/SiO_2 substrate

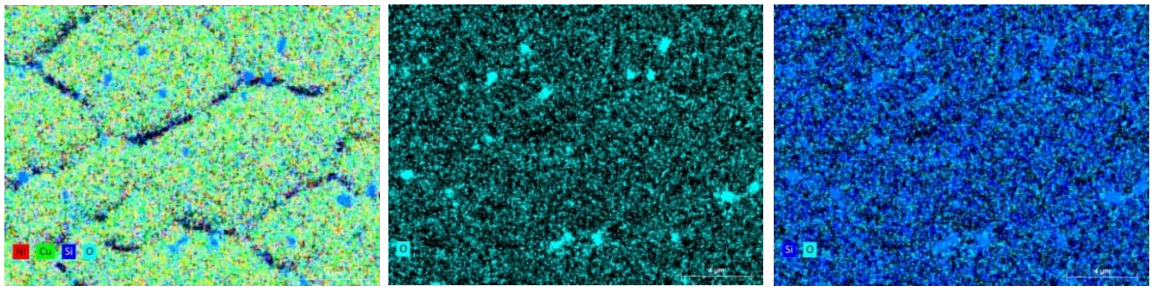

EDS mapping (a) NiCuSiO, (b) O, (c) SiO

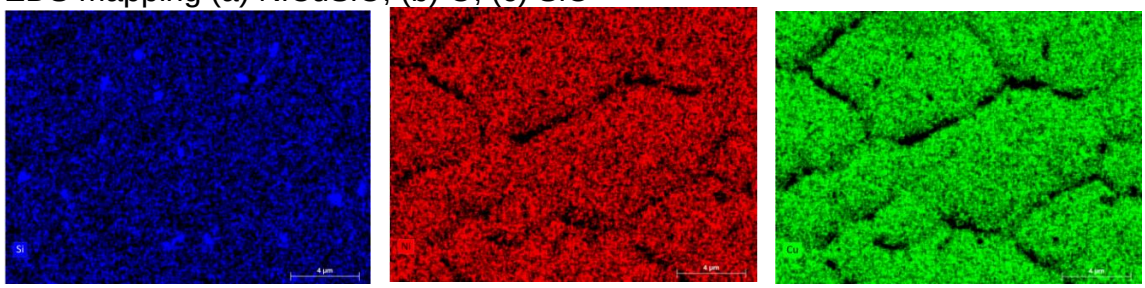

EDS mapping (d) Si, (e) Ni, (f) Cu

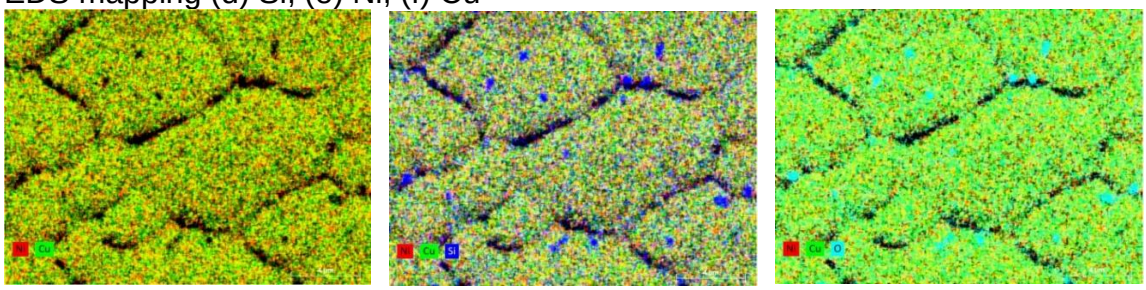

Fig. 10 EDS mapping (g) NiCu, (h) NiCuSi, (i) NiCuO

II. Dewetting issues in graphene layer in regions of very high Cu at. %

As discussed in results, we observe dewetting and steadiness problems hindering growth of uniform graphene islands especially monolayer graphene domains in regions predominantly high in Cu at. %, where the Cu_xNi_{1-x} alloy catalyst is essentially behaving as a thin Cu film. The as-deposited Cu_xNi_{1-x} alloy catalyst films are transient in nature and ~30% of them tend to disappear during the growth process due to thermal heating (evaporate out). Consequently, rupturing (void development) of these metal alloy films occurs because of dewetting from the Si/SiO_2 surfaces. Over a period, formation (cumulation) of small separate domains of this alloy occurs, if the dewetting process persists for a longer scale. Additionally, this impedes the graphene source nucleation process and subsequent development of long chains of C-C atom layers into graphene due to lack of coherent structure (morphology) of alloy thin film surface at the base.

The capillary forces lead to generation of voids in the catalyst alloy region and tend to decrease the free energy at boundary of this alloy film. The high energy at the boundary of alloy film and Si/SiO_2 substrate provides impetus to accumulation of cavities. The total energy of metal film, Si/SiO_2 substrate and their interface can be decreased by reordering of metal atoms in the Cu_xNi_{1-x} alloy catalyst layer which is typically driven by enhancement of thermal energy (increasing temperature) into thermal CVD chamber.

Subsequently, due to much higher energy at the interface of alloy catalyst layer and Si/SiO_2 substrate compared to that of surface energies of individual catalyst layer and Si/SiO_2 substrate, the metal films restructure themselves to diminish the area of interaction between the catalyst film and Si/SiO_2 substrate. As a result, void formation takes place in the thin film of alloy catalyst layer which is followed by total dewetting of alloy catalyst layer into small separate islands. Generally, the surface diffusion during the thermal CVD growth process can generate dewetting at temperatures below the melting point of alloy catalyst layers. Thus, alloy catalyst layers of higher thickness can prevent dewetting to occur by decreasing the total energy present at the interface between the alloy catalyst layer and Si/SiO_2 substrate. Additionally, due to the lack of Ni present in this region, there is no Ni diffusion into the Cu regions to avoid this formation of voids by dissolution of more C atoms in Ni liquid solution [1].

The generation of void can be related mathematically to average grain size (radius R), angle of wetting (θ) of Cu_xNi_{1-x} alloy catalyst layer to substrate and thickness of catalyst film (t). It is under the following conditions that void formation will take place [81].

$$\left(\frac{R}{t}\right) > \frac{3\sin^2\theta}{2 - 3\cos\theta + \cos^3\theta}$$

Particle dot formation (aggregates) in regions of very high Cu at. % is reported during the graphene CVD growth process i.e. accretion of particle dots development in regions of very high Cu at. % $\geq$ 85%. As per our initial assumption, formation of copper silicide ($SiCu_x$) or silicide oxide (SiO_x) is hypothesized. On further analysis by EDS mapping over the dots, the particle aggregation is attributed to diffusion of oxygen atoms from the SiO_2 oxide film due to its low thickness. Thus, the thickness of SiO_2 layer deposited on Si is an important process parameter. On increasing thickness of SiO_2 from 100 nm to 285 nm, this particle aggregation is reduced.

III. Raman spectroscopy and mapping after improving SiO_2 thickness

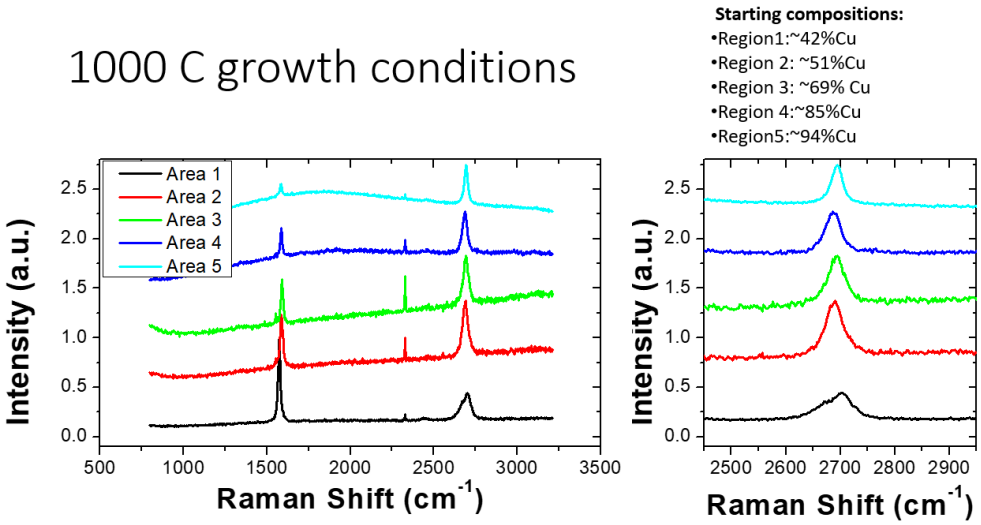

Fig. 11 Raman spectra of CVD graphene growth on Cu_xNi_{1-x} alloy deposited on high quality ~285 nm SiO_2 layer for 5 regions at 1000 °C

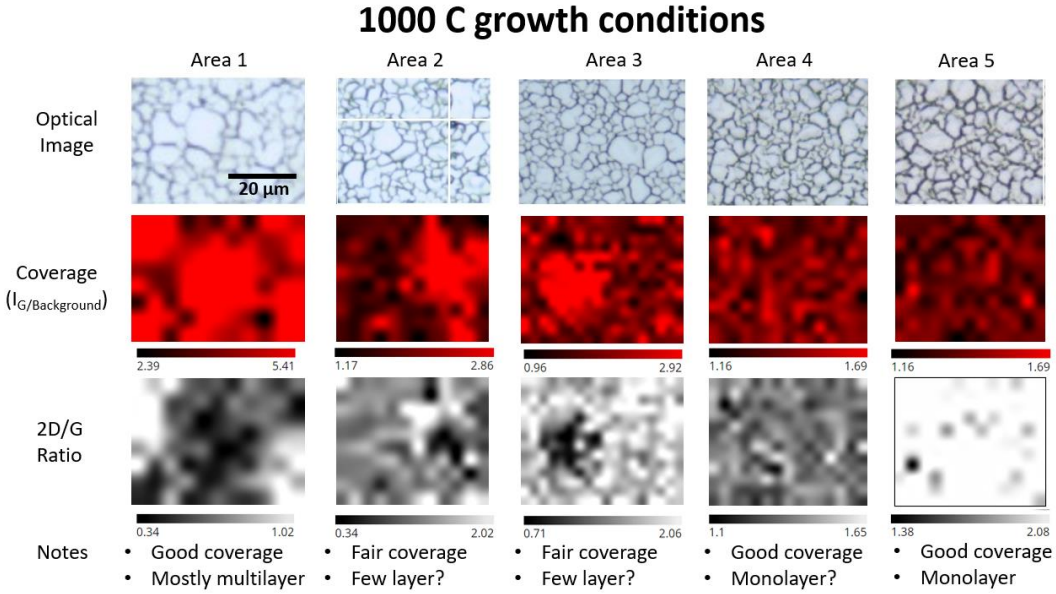

Fig. 12 Raman mapping of CVD graphene growth at 1000°C on Cu_xNi_{1-x} alloy thin film deposited on high quality ~285 nm SiO_2 layer on Si wafer-(a) optical image of 5 regions, (b) coverage-intensity ratio of G peak to that of background ($I_{G/background}$), (c) intensity ratio of 2D to G peaks

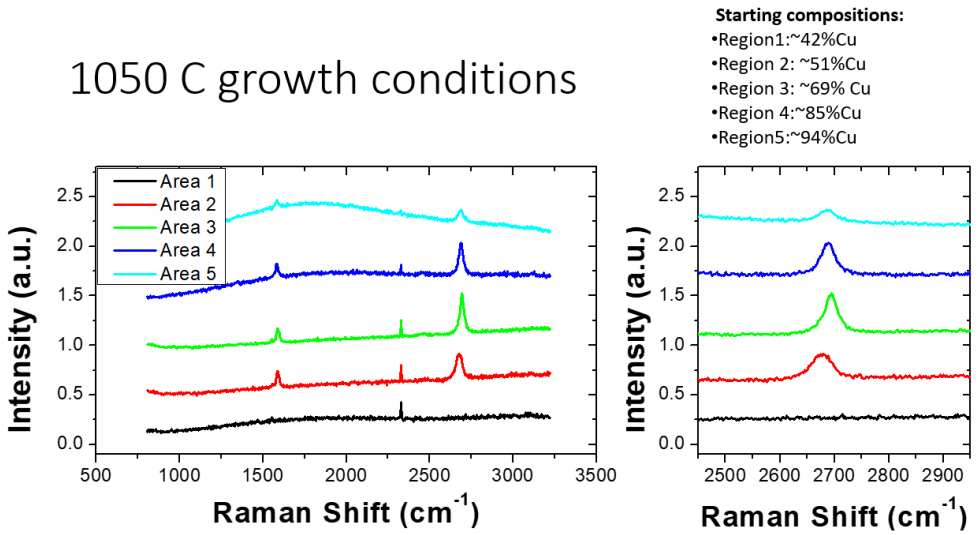

Fig. 13 Raman spectra of CVD graphene growth on high quality ~285 nm SiO_2 layer on Si wafer for 5 regions at 1050 °C

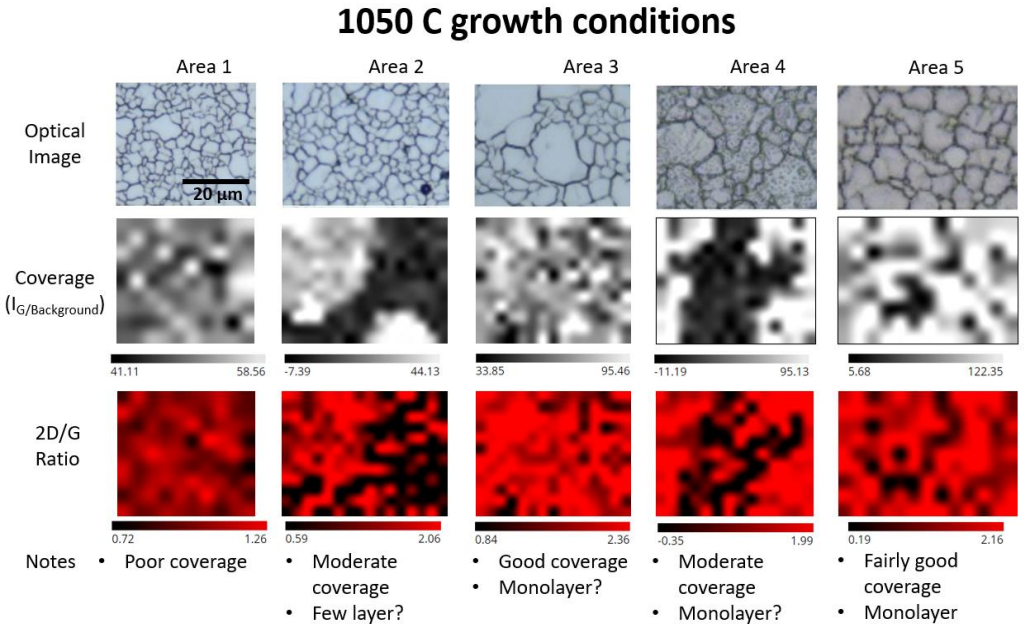

Fig. 14 Raman mapping of CVD graphene growth at 1050°C on Cu_xNi_{1-x} alloy thin film deposited on high quality ~285 nm SiO_2 layer on Si wafer-(a) optical image of 5 regions, (b) coverage-intensity ratio of G peak to that of background ($I_{G/background}$), (c) intensity ratio of 2D to G peaks

VITA

Sumeer Khanna received his bachelor's degree in metallurgical and materials engineering from the Faculty of Technology and Engineering at the Maharaja Sayajirao University of Baroda, India. After undergraduate studies, he pursued master's degree in mechanical engineering from University of Maryland, College Park, where he worked as a graduate research assistant in the Center for Advanced Life Cycle Engineering (Calce) lab. The focus of this study was on integrating novel thin film thermoelectrics by innovative 3-D nanostructures for dissipating high density hotspot heat flux (upto 5 kW/cm^2) in 200μm x 200μm regions in Gallium Nitride (GaN) device layer on Silicon Carbide (SiC) and GaN on diamond substrates based high-power military electronics used in RADAR, nanophotonics (laser, nanoantenna) and energy applications. In this work, he contributed to interchip/intrachip enhanced cooling (ICECool) and near junction thermal transport (NJTT) programs of US Department of Defense (DoD)'s Defense Advanced Research Project Agency (DARPA) under their Microsystem Technology Office (MTO). After receiving this degree, he continued researching at Univ of Maryland, College Park and then taught fundamental engineering courses in materials engineering to undergraduate and graduate level students. After this, he was really encouraged to focus deeper on how these novel nanomaterials can be fabricated and integrated into innovative 2D and 3D device structures. At University of Tennessee, Knoxville he investigated on the nanosynthesis of high crystalline quality 2D materials like bi-layer graphene by chemical vapor deposition (CVD) process on copper-nickel gradient thin films sputtered on Si/SiO_2 substrates. These layers can be integrated with other 2D materials as heterostructures for studying quantum physics and applications in field effect transistors (FET), plasmonic sensors and spintronics. The project work at UTK was supported by US Department of Energy (DoE) Oak Ridge National laboratory (ORNL) user facility.